The Pennsylvania State University

The Graduate School

Department of Civil and Environmental Engineering

KINETIC AND MECHANISTIC STUDY FOR THE ABIOTIC OXIDATION OF Fe(II) CATALYZED AT THE FERRIC (OXYHYDR)OXIDE AND SOLUTION INTERFACE

A Dissertation in

Environmental Engineering

by

Yuan-Liang Tai

Submitted in Partial Fulfillment
of the Requirements
for the Degree of

Doctor of Philosophy

December 2009

The thesis of Yuan-Liang Tai was reviewed and approved* by the following:

Brian A. Dempsey
Professor of Environmental Engineering
Dissertation Advisor
Chair of Committee

William D. Burgos
Professor of Environmental Engineering

James D. Kubicki
Professor of Geosciences

Richard C. Stehouwer
Associate Professor of Environmental Soil Science

Peggy A. Johnson
Professor of Civil Engineering Professor's Name
Head of the Department of Civil and Environmental Engineering

*Signatures are on file in the Graduate School

ABSTRACT

This research dealt with the heterogeneous oxidation of Fe(II) by some environmentally significant contaminants including nitrite, uranium, and arsenate using Hydrous Ferric Oxide (HFO) as the catalytical solid phase in anoxic soil medium and sediments. It is the first study of the Fe(II)/Fe(III)/HFO system in which mass balance has been performed for both Fe(II) and all the oxidant species using a strictly anoxic environment at circumneutral pH. Fe(II) and HFO were used as the electron donor and catalytical solid phase because Fe(II)/Fe(III) redox couple is often dominant in controlling the redox potential in anoxic groundwater system and HFO is ubiquitous in soils and sediments, and it is an important adsorbent for a wide range of chemicals. The results showed that the reaction between Fe(II) and either NO_2^- or U(VI) was fast in the presence of HFO. The rate for the oxidation of Fe(II) and the reduction of either NO_2^- or U(VI) was found to be a function of dissolved Fe(II), solid-bound Fe(II) and oxidant concentration, and can be described by Rate = - $k_{overall}$ • [$Fe(II)_{diss}$] • [$Fe(II)_{solid\text{-}bound}$] • [Oxidant]. However, the reaction rate for Fe(II)/HFO/U(VI) was an order of magnitude faster than for nitrite, possibly due to high affinity of U(VI) to the HFO surface which could provide a shorter pathway for electron-transfer. Conservation of solid-bound Fe(II) was observed for either oxidant throughout the reaction with Fe(II)/HFO, therefore solid-bound Fe(II) functioned as a catalyst for the reduction of either oxidant by Fe(II). In experiments with nitrite or no oxidant in Fe(II)/HFO, concentration of $Fe(II)_{solid\text{-}bound}$ first increased less than 100% and then decreased coincident with partial conversion of HFO to goethite. When U(VI) was used as an oxidant, $Fe(II)_{solid\text{-}bound}$ increased and then remained constant such that solid-bound Fe(II) density was increased by 3 to 5 times compared to absence of U(VI). The significant increase of solid-bound Fe(II) in Fe(II)/U(VI) reaction could be due to the newly formed sorption sites created by the sorption and reductive precipitation of U(VI) and oxidative precipitation of Fe(II). The characterization of Fe(II)/Fe(III)

systems from this study is consistent with several other recent studies that have supported the hypothesis that Fe(II) is incorporated into the bulk phase of Fe(III) oxides, rather than remaining at the interface, and that this unusual behavior results in apparently unique redox reactivity. Interestingly, overall rate constants declined when $Fe(II)_{solid\text{-}bound}$ exceeded 0.02 mol Fe(II) per mol Fe(III), similar to results from previous studies using O_2 and NO_2^- as oxidants.

We also investigated the effectiveness of two extractants, bicarbonate and phosphoric acid, on the quantification of U(VI) species during Fe(II)/U(VI) reaction in HFO suspension. Higher phosphate extractable U(VI) ($U(VI)_{phosphate}$) than bicarbonate extractable U(VI) ($U(VI)_{bicarbonate}$) was observed in all experiments. Interestingly, consumed $U(VI)_{bicarbonate}$ /consumed $U(VI)_{phosphate}$ ratios were about 2 in all the experiments. Using H_3PO_4 as an extracting reagent could increase U(VI) extractability from HFO suspension due to high solubility of HFO at pH 1.5. It is also possible that carbonate ligand stabilize U(V) species which was formed as a intermediate product of U(VI) reduction to U(IV), consistent with the mechanism that U(VI) reduction is an one-electron-transfer reaction followed by disproportionation of U(V) to U(VI) and U(IV) species. It was also found that when freshly prepared HFO was used as the solid phase in Fe(II)/U(VI) reaction, multiple stages reaction and a lag phase was observed. This study showed that the presence of reducing agents and dynamic mineral phases could increase the complexity of both uranium removal processes and operational procedures for quantifying uranium reduction.

Fe(II)/NO_2^- reaction was simulated using quantum mechanical calculation in both homogeneous and heterogeneous system to identify the favorable reaction pathway for electron transfer. Molecular orbital/density function theory (MO/DFT) calculation showed that Fe(II)/NO_2^- redox reaction in aqueous phase without the presence of solid phase was thermodynamically favorable in contrast to the wet chemistry result. The absence of the spontaneous reaction could be due to the difficulty in forming inner-sphere Fe – O – N – O – Fe

complexes in dilute solution in batch study. In heterogeneous system, the result showed that direct electron transfer pathway was more thermodynamically favorable than indirect electron transfer pathway for Fe(II)/NO_2^- reaction in the presence of Fe(III) (oxyhydr)oxide. However, due to the limitation on simulation of Fe(III) (oxyhydr)oxide cluster with Gaussian 03, density functional theory (DFT) calculation of Fe(II)/NO_2^- redox reaction on periodic Fe(III) (oxyhydr)oxide structure using Vienna Ab Initio Simulation Package (VASP) is under way to justify thermodynamic data of indirect pathway. NBO population analysis showed sorbed Fe(II) became more oxidized than dissolved Fe(II) in the model product in heterogeneous system indicating that sorbed Fe(II) could be the electron donor in Fe(II)/NO_2^- redox reaction.

Catalytical effect of solid-bound Fe(II) on Fe(II)/As(V) reaction using HFO as the solid phase was not observed in our study. The inertness of redox reaction between As(V) and Fe(II) could be due to the requirement of two-electron transfer for As(V) reduction to As(III), whereas it is possible for O_2, nitrite, and uranyl to undergo one electron transfer with Fe(II) in the presence of HFO.

TABLE OF CONTENTS

LIST OF FIGURES viii

LIST OF TABLES x

ACKNOWLEDGEMENTS xi

Chapter 1 Introduction 1

1.1 Background of this study 1
1.2 Problem Statement and Hypotheses 2
1.3 Objectives of Study 4

Chapter 2 Nitrite Reduction with Hydrous Ferric Oxide and Fe(II): Stoichiometry, Rate, and Mechanism 6

Abstract 6
2.1 Introduction 7
2.2 Materials and Methods 9
2.2.1 Chemicals 9
2.2.2 Anoxic environment 9
2.2.3 Analyses 10
2.2.4 Experimental procedure 10
2.3 Results and Discussion 11
2.3.1 Homogeneous and heterogeneous results 11
2.3.2 Solid-bound Fe(II) as a catalyst 13
2.3.3 Overall rate equation 14
2.3.4 Reaction mechanism 14
2.4 Conclusions 15

Chapter 3 Rate and Mechanism of Uranium Reduction in Fe(II)/HFO/U(VI) system 22

Abstract 22
3.1 Introduction 23
3.2 Materials and Methods 25
3.2.1 Chemicals 25
3.2.2 Anoxic Environment 26
3.2.3 Analyses 26
3.2.4 Experimental Procedure 27
3.3 Results and Discussions 27
3.3.1 Fe(II)/U(VI) redox kinetics 27
3.3.2 Pseudo-first-order rate law 28
3.3.3 Pseudo-second-order rate law 30
3.3.4 Effect of Fe(II) surface coverage on reaction rate 31
3.3.5 Variation of solid-bound Fe(II) in Fe(II)/U(VI) reaction 32
3.3.6 Stoichiometry of Fe(II)/U(VI) reaction 34
3.3.7 Reaction mechanism 35

3.4 Conclusions 36

Chapter 4 A Comparison of Extraction Techniques for U(VI) and Implications for Speciation and Immobilization of Uranium in the Fe(II)/HFO/U(VI) System 47

Abstract 47
4.1 Introduction 48
4.2 Materials and Methods 51
4.2.1 Chemicals and Reagents 51
4.2.2 Anoxic environment 51
4.2.3 Analyses 52
4.2.4 Experimental Procedure: 52
4.3 Results and Discussions: 53
4.3.1 Fe(II)/U(VI) redox kinetics 53
4.3.2 $U(VI)_{bicarbonate}$ versus $U(VI)_{phosphate}$ 54
4.3.3 XPS analysis 57
4.4 Conclusions 58

Chapter 5 Simulation of Redox Reaction between Nitrite Ion and Ferrous Ion Mediated by Goethite (010) Surface – a Quantum Mechanical Study 64

Abstract 64
5.1 Introduction 65
5.2 Materials and Methods 66
5.3 Results and Discussions 67
5.3.1 Modeling of homogeneous Fe(II)/NO_2^- reaction 67
5.3.2 Modeling of heterogeneous Fe(II)/NO_2^- reaction at solid-water interface 68
5.3.3 Comparison of homogeneous and heterogeneous Fe(II)/NO_2^- reaction 69
5.3.4 NBO population analysis 70
5.4 Conclusions 71

Chapter 6 Conclusions 78

6.1 Conclusions 78
6.2 Recommendations for Future Study 81

Appendix A: Kinetic Modeling Procedures 83

Appendix B: A Study of Fe(II)/HFO/As(V) Reaction 88

Appendix C: NBO Population Analysis Output 93

REFERENCES 97

LIST OF FIGURES

Figure 1- 1 Schematic of direct electron pathway (a) and indirect electron pathway (b) between Fe(II) and NO_2^- at Fe(III) (oxyhydr)oxide-water interface. 5

Figure 2- 1 Experimental setup 18

Figure 2- 2 Oxidation of dissolved Fe(II) (◇) and reduction of nitrite (□) were insignificant in the absence of HFO at pH 6.8 in 24 hours (solid lines). Decreases of total Fe(II) (▲),dissolved Fe(II) (◆), and nitrite (■) were rapid in the presence of HFO (experiment 6). Error bars refer to replicate analyses and were smaller than the symbol size. Dashed lines show the predicted concentrations of dissolved Fe(II) and nitrite based on k_{obs}. 19

Figure 2- 3 A stoichiometric excess of Fe(II) compared to nitrite was used in experiment 15. Solid-bound Fe(II) was still present after almost all nitrite was consumed. Error bars are smaller than the symbol size. 19

Figure 2- 4 Dissolved Fe(II) (open symbols and light lines) and solid-bound Fe(II) (closed symbols and heavy lines) for experiments with HFO > 2.5mM as Fe(III). Dissolved Fe(II) decreased to close to zero within 10 hours. Solid-bound Fe(II) increased initially, decreased between 2 and 6 hours, and then remained relatively constant. These changes in the concentration of solid-bound Fe(II) are similar to earlier observations in the absence of oxidant (36). 20

Figure 2- 5 Cumulative stoichiometric ratio of consumed Fe(II)/nitrite (experiment 15, see Figure 3 for details). Final stoichiometric ratios for all experiments are reported in Table 2-1. 20

Figure 2- 6 Experiments with variable HFO concentration showed that k_{obs} was proportional to the total concentration of solid-bound Fe(II) (μM) rather than to the "sorption density" of solid-bound Fe(II) (mol Fe(II)/mol Fe(III), 7500X). 21

Figure 2- 7 A linear relation between k_{obs} and [$Fe(II)_{solid\text{-}bound}$] indicated the reaction was 1st order with respect to $Fe(II)_{solid\text{-}bound}$. Filled symbols and the solid line (R^2=0.94) are for $Fe(II)_{solid\text{-}bound}$/Fe(III) ≤ 0.26 mol/mol. The linear relation failed for $Fe(II)_{solid\text{-}bound}$/Fe(III) ≥ 0.39 mol/mol (open symbols). A similar decrease in k_{obs} with high surface density was reported for Fe(II)/HFO/O_2 (26). 21

Figure 3-1. Kinetic results for the experiments described in Table 3.1: (a) focus on Fe(II) speciation with (Exp 2) and without (control) addition of U(VI) - no significant changes in $Fe(II)_{total}$ (x) or $Fe(II)_{solid\text{-}bound}$ (+) without the addition of U(VI), but there was a decrease in $Fe(II)_{total}$ (▲) and $Fe(II)_{diss}$ (◆) and an increase in $Fe(II)_{solid\text{-}bound}$ (■) after U(VI) was added; (b) Exp 2 - decrease in $U(VI)_{total}$ (Δ) is compared with modeled $U(VI)_{total}$ using 1st order (solid line) and 2nd order (dashed line) rate laws - $U(VI)_{diss}$ (□) remained very low and total U(◇) was constant; (c) Exp. 1; (d) Exp 3; (e) Exp.4; (f) Exp.5; (g) Exp.6; (h) Exp. 7. All experiments were at pH 6.8 and 26ºC. Error bars show one "standard deviation" for two duplicate experiments. 41

Figure 3- 2 Pseudo-first-order rate constant k_{obs-1} for uranium reduction was in proportion to the concentration of solid-bound Fe(II) concentrations. Inhibition was observed for >0.02 mole $Fe(II)_{solid-bound}/Fe(III)$ (Exp.1, open symbol). 44

Figure 3- 3 Pseudo-second-order rate constant k_{obs-2} for uranium reduction (solid line and symbols) was greater than k_{obs-2} for nitrite reduction (dashed line (22)).....44

Figure 3- 4 Conceptual model for Fe(II)/U(VI) redox reaction occurring at Fe(III) (oxyhydr)oxide-water interface.....46

Figure 4- 1 (a) XRD pattern of freshly prepared HFO solution. (b) XRD pattern of stock HFO solution.....60

Figure 4- 2 Results for Fe(II)/HFO/U(VI) experiments: pH=6.8, 26-28ºC, (▲) $U(VI)_{bicarbonate}$, (Δ) $U(VI)_{phosphate}$, (+)$U(VI)_{diss}$, (●) $Fe(II)_{total}$, (◆) $Fe(II)_{diss}$. Panels show experiments using (a) 2.5mM HFO, (b) 5mM HFO, (c) 7.5mM HFO, (d) 10mM HFO. Solid line shows modeling of $U(VI)_{bicarbonate}$ and dashed line shows modeling of $U(VI)_{phosphate}$ both with 1st order rate law. Error bars show one standard deviation of two duplicate experiments. 61

Figure 4- 3 $\Delta U(VI)_{bicarbonate}$ versus $\Delta U(VI)_{phosphate}$ diagram during disproportionation of U(V) 63

Figure 4- 4 XP spectra of the U4f region for uranyl standard(▼), samples collected at t=3 hr(■) and t=7 hr (♦). Satellite features at about 6.7 eV on the higher binding energy sides indicate the increase of U(IV) component in the samples. Binding energies were adjusted to C1s at 285 eV.....63

Figure 5- 1 Configurations (optimized structure) of reactants, intermediate product, and products used in simulation of electron transfer process between Fe(II) and NO^- in homogeneous system: (a) reactants; (b) intermediate product; (c) products.....75

Figure 5- 2 Configurations (optimized structure) of reactants, intermediate product, and products used in simulation of *direct* electron transfer process between Fe(II) and NO^- in heterogeneous system: (a) reactants; (b) intermediate product; (c) products. 76

Figure 5- 3 Configurations (optimized structure) of reactants, intermediate product, and products used in simulation of *indirect* electron transfer process between Fe(II) and NO^- in heterogeneous system: (a) reactants; (b) intermediate product; (c) products. 77

LIST OF TABLES

Table 2- 1 Conditions and results in heterogeneous experiments. All experiments were performed in a strictly anoxic reactor at 26°C at pH 6.8. Nitrite was added 25 min after addition of Fe(II) and HFO concentration was 2.5 mM as Fe(III) unless otherwise indicated. 17

Table 3- 1 Initial conditions and results for the Fe(II)/Fe(III)/U(VI) system. Experiments were performed in a strictly anoxic reactor at 26ºC at pH 6.8. HFO was aged for 24 hr prior to addition of Fe(II). U(VI) was added 25 min after addition of Fe(II). 39

Table 3- 2 Rate equations reported by previous researchers and this study in Fe(II)/Fe(III)/oxidant reactions. 39

Table 3- 3 Potential primary reactions in each stage of Fe(II)/HFO/NO_2^- reaction. 40

Table 4- 1 Conditions and results in Fe(II)/Fe(III)/U(VI) experiments. All experiments were performed in a strictly anoxic reactor at 26°C at pH 6.8. U(VI) was added 25 min after addition of Fe(II). 59

Table 5- 1 Configurations of reactants, intermediate products, and products used in simulation of electron transfer process between Fe(II) and NO_2^- 73

Table 5- 2 Reaction energies and energies of reactants, intermediate products, and products calculated using B3LYP functionals and all-electron 6-31G(d) basis set for H, N, and O atoms and CEP-121G basis set for Fe atoms. 73

Table 5- 3 NBO charges of reactant, intermediate product, and product configurations for direct electron transfer pathway. 74

Table 5- 4 NBO charges of reactant, intermediate product, and product configurations for indirect electron transfer pathway. 74

ACKNOWLEDGEMENTS

I am heartily grateful to my advisor, Dr. Brian Dempsey, whose guidance, patience, and support from the beginning to the final stage of this study allow me to develop a better understanding on this subject. It is my great pleasure and honor to work with him again for my doctoral study. I would like to thank Dr. James Kubicki for his guidance in molecular modeling which I was not familiar with. He has made available his time and resource for me which is critical for my research. I am indebted to many of my colleagues, especially Fenglong and Morgan, who kindly offer their help in a number of ways at times when I desperately need it.

I want to dedicate this thesis to my father, who never stopped believing me and gave me all the caring and love he could offer since the day I was brought to this world. I thank my wife, Shu-Chuan, for her understanding, support and great faith in me. I would like to thank my sister Tsu-Ling. This thesis would not have been possible without her dedication to our family during the period I studied abroad.

Chapter 1 Introduction

1.1 Background of this study

The main objective of this study was to investigate the rates and mechanisms of heterogeneous oxidation of Fe(II) at the mineral-water interface with the reduction of some environmentally significant or toxic elements in groundwater. Hydrous ferric oxide (HFO) was used as solid phase in this study because it is ubiquitous in soils and sediments it is a good adsorbent for a wide range of chemicals. Therefore HFO plays a significant role in controlling the solubility, mobility, and reactivity of many toxic trace elements in groundwater and surface water systems. The Fe(II)/Fe(III) redox couple is often dominant in controlling the redox potential in anoxic groundwater systems, due to ubiquity and due to the fast one-electron transfer. Fe(II)/Fe(III) cycling and transformation of iron species can occur over almost the entire range of E_h in natural water system (1). Fe(II) reacts with Fe(III) (oxyhydr)oxides and other minerals in many ways, forming ferric hydroxide through autocatalytical reaction in oxic environments, affecting transformations of Fe(III) (oxyhydr)oxides (e.g.,into semiconductor ferric oxide species), and enhancing electron transfer reactions with a variety of oxidants. Heterogeneous oxidation of Fe(II) with a variety of organic and inorganic compounds has been extensively studied and a broad range of kinetic data for many solid phases and reductants have been published. The reactions themselves are critically important, since the redox reaction associated with iron solid phases can be used to trigger the degradation and reduction of a wide variety of organic and inorganic contaminants in groundwater remediation(2-9). However, the existing mechanistic explanations for the electron transfer processes have been diverse, and with few exceptions the experimental procedures have lacked sufficient rigor and detail to accurately describe the order of the reaction with respect to both solid-associated and dissolved Fe(II).

Nitrite, arsenate, and uranium were the candidate oxidants in this study due to their increasing environmental significance. The abiotic reduction of nitrite results in the loss of fertilizer nitrogen in agricultural land uses and is considered an important pathway that can contribute to NO and N_2O gas production, which are linked to the greenhouse effect and to stratospheric ozone destruction (8, 10-14). Arsenic and uranium are toxic and are often quite mobile in surface and ground waters, impacting the drinking water safety and resulting in acute and chronic the human health effects (15-19)**.**

1.2 Problem Statement and Hypotheses

The oxidation of Fe(II) and reduction of nitrite, arsenate, or uranyl are all spontaneous reactions at neutral pH (20, 21). However, it has been demonstrated that the rates of homogeneous redox reactions between Fe(II) and these oxidants are insignificant in the absence of solid phases (2, 8, 20-22). Iron (oxyhydr)oxides including goethite, hematite, and magnetite are among a variety of minerals that have been used as the solid phases in the study of heterogeneous redox reactions of nitrite, arsenic, and uranium with Fe(II) as the reductant (2, 7, 8, 12, 19-21, 23-25). However, few studies have investigated the abiotic redox reactions involving these constituents in groundwater systems in the presence of hydrous ferric oxide(HFO). Particularly, no rate equations for heterogeneous oxidation of Fe(II) in the presence of HFO involving these three constituents have been reported probably due to the difficulty to maintain a strictly anoxic experimental condition required for the observation of the reaction kinetics.

The kinetic and mechanistic study of the redox reaction at the mineral-water interface has been the objective of many researches. Although many redox reactions involving the Fe(II)/Fe(III) redox couple and a variety of oxidants in surface and ground waters have been explored and

kinetic data were presented, the results and the proposed reaction mechanisms have been diverse and many conclusions remain in debate.

Park and Dempsey (26) have made progress in identifying general mechanisms for heterogeneous reactions involving Fe(II)/HFO/oxidant. Previously, Jeon et al. (27) developed strategies and techniques to maintain strictly anoxic environments for rate experiments. Substantial evidence that electrons form surface-associated Fe(II) are delocalized within the bulk Fe(III) (oxyhydr)oxide phase have been provided using a wide range of techniques including wet chemistry, analytical methods, and molecular modeling (26, 28-30). These studies have provided support for a reaction mechanism for the heterogeneous oxidation of Fe(II) with a variety of organic and inorganic oxidants, in which a more complicated solid-bound Fe(II) (not just adsorbed at the interface) is required for reaction, along with dissolved Fe(II) and the oxidant.

Our research team has also identified some anomalies in the rate of the Fe(II)/HFO/oxidant reactions, e.g., the reaction is almost completely inhibited by surface coverage of HFO by U(VI) (25) and Fe(II)/HFO/O_2 redox reaction rate fails to follow third-order rate law at high concentration of solid-bound Fe(II) (26).

The work that is proposed herein was designed to test the following hypotheses.

1) Redox reactions between Fe(II) and nitrite, arsenate or uranyl at neutral pH are catalyzed by HFO.
2) The rate of reaction in Fe(II)/HFO/oxidant systems depends on the activity of both dissolved and solid-bound Fe(II), and in fact both are required for the redox reaction to proceed at a significant rate.
3) The heterogeneous oxidation rate of Fe(II)/HFO/oxidant also depends on the activity of nitrite, arsenate or uranyl.
4) Both reductants and oxidants can become attached to the surface of HFO and form surface complexes with one or more bridging atoms or ligands. Thus, the electron

transfer in redox reaction at the solid-water interface can be achieved through two types of mechanisms: direct and indirect electron transfer as shown in Figure 1-1. In the direct-electron-transfer mechanism, reductant and oxidant form ternary or quaternary surface complexes with structural Fe(III) and the formation of surface complexes facilitates the subsequent electron transfer. In the indirect-electron-transfer mechanism, the oxidation and reduction occur at different surface sorption sites.

5) Hydrous ferric oxide is a dynamic mineral phase. When Fe(II) is introduced to a HFO suspension, Fe(II) atoms or electrons could be incorporated into the bulk phase of Fe(III) oxides, rather than remaining at the solid-water interface. This unusual behavior results in apparently unique redox reactivity.
6) Surface coverage of Fe(II) on ferric oxide is an essential factor for the heterogeneous oxidation of Fe(II). Excessive surface coverage of Fe(II) or of the oxidants on solid phases results in a decreased reaction rate.

1.3 Objectives of Study

The objectives of this study are the following: (1) measure the extent and rates of heterogeneous oxidation of Fe(II) with the reduction of nitrite, arsenate, or U(VI) in the presence of HFO; (2) define rate equations for the above reactions if applicable; (3) identify the mechanisms of the above reactions; (4) model redox reactions using both conventional rate expressions and molecular modeling; and (5) use analytical techniques to identify the solid phases and interfacial species at molecular scale.

Figure 1- 1 Schematic of direct electron pathway (a) and indirect electron pathway (b) between Fe(II) and NO_2^- at Fe(III) (oxyhydr)oxide-water interface.

(a)

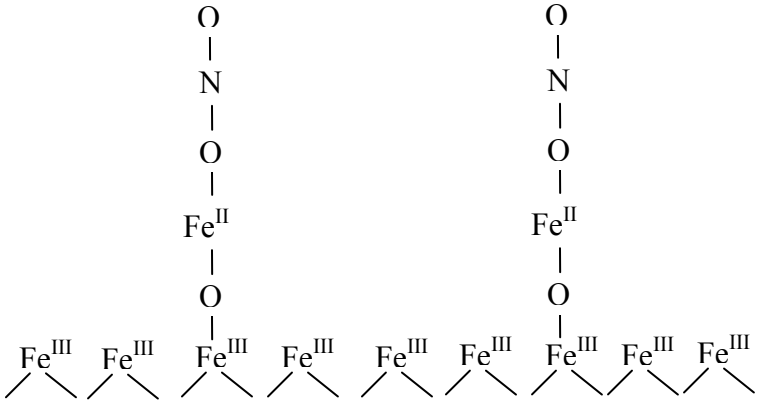

(b)

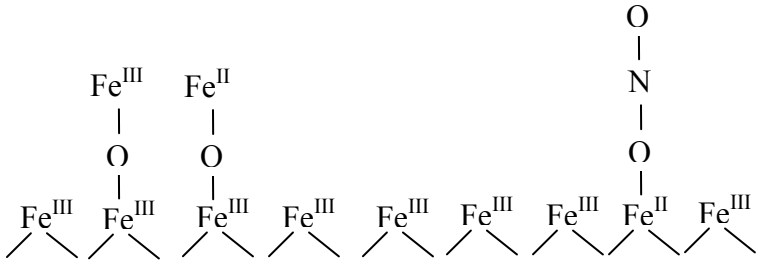

Chapter 2 Nitrite Reduction with Hydrous Ferric Oxide and Fe(II): Stoichiometry, Rate, and Mechanism

Abstract

Fe(II)/Fe(III) oxide is an important redox couple in environmental systems. Recent studies have revealed unique characteristics of Fe(II)/Fe(III) oxide and reactions with oxidizing or reducing agents. Nitrite was used as an oxidizing agent in this study in order to probe details of these reactions and hydrous ferric oxide (HFO) was used as the Fe(III) oxide phase. Abiotic nitrite reduction is a significant global producer of nitric oxide (a catalyst for production of tropospheric ozone) and nitrous oxide (a greenhouse gas and contributor to stratospheric ozone depletion). All experiments were conducted at pH 6.8 using a strictly anoxic environment with mass-balance measurements for Fe(II). Oxidation of Fe(II) was negligible in the absence of HFO. The reaction was fast in the presence of HFO and was described by $d[Fe(II)]/dt = -k_{overall}$ $[Fe(II)_{diss}]$ $[Fe(II)_{solid\text{-}bound}]$ $[NO_2^-]$ ($k_{overall}$ = 2.59x10-7 μM^{-2} min^{-1}) for Fe(II)/Fe(III) molar ratios less than 0.026. The reaction was inhibited for higher Fe(II)/HFO ratios. The concentration of solid-bound Fe(II) was constant after an initial equilibration period and the reaction stopped when dissolved Fe(II) was depleted even though substantial solid-bound Fe(II) and nitrite remained. The results regarding rate-dependence and conservation of solid-bound Fe(II) and inhibition of reaction at high Fe(II)/FeIII) ratios were similar to our earlier results for the Fe(II)/HFO/O_2 system (26).

2.1 Introduction

The objectives of this research were to investigate the kinetics and mechanisms of reactions involving Fe(II), nitrite (NO_2^-), and hydrous ferric oxide (HFO). The Fe(II)/HFO/nitrite reaction is significant *per se*. Nitric oxide (NO) catalyzes production of tropospheric ozone while nitrous oxide (N_2O) is a greenhouse gas and contributes to stratospheric ozone depletion (10, 11). We were also motivated to investigate this system in order to test observations from earlier work on Fe(II)/HFO/O_2, especially regarding first-order dependence of reaction on both dissolved Fe(II) and solid-bound Fe(II), conservation of solid-bound Fe(II) in the presence of residual oxidant, and inhibition of the reaction for high solid-bound Fe(II)/Fe(III) molar ratios (26). Nitrite was a convenient chemical probe for this work because it is reduced in one-electron steps to NO and then N_2O.

Nitrite reduction in soils proceeds by both biologically-catalyzed and abiotic pathways (13, 31, 32). Venterea and Rolston(2000) showed a strong correlation between NO_2^- accumulation and abiotic NO/N_2O production for several agricultural soils. Venterea (2007) estimated that 31-75% of total N_2O emission came from abiotic processes in an agricultural soil.

Nitrite is abiotically reduced in the presence of Fe(II)/Fe(III) oxide (8, 12). It was reported that the reaction rate for Fe(II)/lepidocrocite/nitrite increased from pH 7 to 8.5 (8), while the reaction rate for Fe(II)/Fe(III)(hydr)oxide/nitrite decreased with increasing pH (12). The concentration of solid-bound Fe(II) was not measured in either study. Rate expressions have not been reported for these reactions.

HFO is ubiquitous in the environment and in engineered systems. HFO is also known as amorphous ferric hydroxide or, 2-line or 6-line ferrihydrite (dried forms). It is a poorly crystalline ferric oxide, formed by Fe(II) oxidation or Fe(III) hydrolysis (33, 34). Primary particles (~2 nm) aggregate into larger flocs (35), resulting in high specific surface area and reactivity. HFO

transformation to goethite is catalyzed by Fe(II) (26, 34) and this results in decreases in specific surface area, uptake of Fe(II)(36), and rates of some redox reactions (26, 33).

Fe(II)/Fe(III) is an environmentally important redox couple that can affect the speciation and mobility of many organic and inorganic contaminants in soils and groundwater (37). Solid-bound Fe(II) is a more reactive reducing agent than dissolved Fe(II) (6, 8, 38-40). The rate for heterogeneous oxidation of Fe(II) by O_2 and some other oxidizing agents has been reported to be first-order with respect to solid-bound Fe(II) concentration and first-order with respect to activity of the oxidizing agent (26, 39, 41). Others have reported second-order dependence on solid-bound Fe(II) for reduction of carbon tetrachloride (3) and RDX (6) with goethite or magnetite, respectively. Park and Dempsey (2005) found that rate of reduction of O_2 was first-order with respect to both solid-bound and dissolved Fe(II), and that solid-bound Fe(II) was conservative during the reaction. Williams and Scherer (2004) similarly reported that nitrobenzene was reactive with goethite/Fe(II) only when both solid-bound Fe(II) and dissolved Fe(II) were present. Shao and Butler (42) found that the rate of reduction of carbon tetrachloride by Fe(II) correlated with the concentration of weakly-bound Fe(II).

Fe(II)/Fe(III)(hydr)oxide systems have been characterized using a range of analytical and modeling techniques. Luther (43)and Wehrli (44) used molecular orbital theory to predict transfer of electron density to adsorbed Fe(II) through both π and σ orbitals, with increased reducing power. Williams and Scherer (2004) used isotopic studies to demonstrate that electrons transfer from sorbed Fe(II) into bulk Fe(III)(hydr)oxide. Kerisit and Rosso (2007) used *ab initio* modeling to demonstrate long-range migration of electrons away from the surface sites. The expression "solid-bound" Fe(II) is used in this paper, rather than "adsorbed" Fe(II), to be consistent with evidence that electrons from surface-associated Fe(II) are delocalized within the bulk Fe(III)(hydr)oxide phase (28-30).

2.2 Materials and Methods

2.2.1 Chemicals

Chemicals were reagent grade or better. Glass and plasticware were submerged in 10% nitric acid, rinsed several times with distilled and deionized (DI) water and air-dried. Solutions were prepared using O_2-free DI water, made by purging DI water with N_2 for at least four hours followed by transfer into the anaerobic chamber and open-stirring for at least 3 days. Stock 250 mM Fe(II) was prepared with $FeCl_2 \cdot 4H_2O$ in the chamber, acidified to pH<1, calibrated with primary standard $K_2Cr_2O_7$ to a ferroin end point (45), and stored in an amber glass bottle wrapped with aluminum foil. Stock 1M nitrite was prepared in the chamber and calibrated by back-titration of excess permanganate with sodium oxalate (45). HFO was prepared according to the procedures described by Park and Dempsey (26). Briefly, $FeCl_3 \cdot 6H_2O$ was dissolved and then precipitated at controlled pH6.8 by slow addition of NaOH during 1 hour. HFO contained 2.5 mM Fe(III) and 0.01 M sodium PIPES (piperazine-1,4-bis-2-ethanesulfonic acid) at pH 6.8. PIPES pH buffer does not significantly affect speciation and complexation of transition metal ions (41, 46) and is commonly used to control pH in systems containing Fe(II)/Fe(III) (oxy)hydroxide. The pH was measured at the end of each experiment.

2.2.2 Anoxic environment

Experiments were performed at 26~28ºC inside an anaerobic chamber (Coy Laboratory Products, Inc.) equipped with two heated boxes for temperature control, containing palladium catalyst for O_2 removal and desiccant. The chamber contained 97% N_2/3% H_2. Reactors were additionally isolated from the chamber gas by an O_2-trap, a series of reactor bottles containing 93.2mM Fe(III) as HFO and 0.9mM Fe(II) buffered at pH 8.1 as shown in Figure 2-1, to protect

against trace O_2 that is present even in well-operated anaerobic chambers (27). This system has been used successfully in a number of laboratories.

2.2.3 Analyses

Dissolved Fe(II) was determined using 1,10-phenanthroline (APHA et al., 2005) after filtration (25-mm syringe filter holder with 0.2μm Pall membrane disc filter). Solid-bound Fe(II) was defined as Fe(II) retained on the membrane filter and extracted into 0.5 N HCl in 20 hours (36). All HFO dissolved in the acid extraction. The extract was filtered and the solid-bound Fe(II) was determined using 1,10-phenanthroline with ammonium fluoride added to overcome interference from Fe(III) (47). Nitrite was determined colorimetrically with sulfanilamide and *N*-(1-naphthyl)-ethylenediamine dihydrochloride (APHA et al., 2005). Filtered Fe(II) and nitrite samples were removed from the chamber after addition of reagents and prior to measuring absorbance.

2.2.4 Experimental procedure

The experimental setup is shown in Figure 2-1. Experimental conditions and initial reactant concentrations are listed in Table 2-1. A 1-liter HFO suspension at pH 6.8 was prepared inside the anaerobic chamber in a glass bottle that was then connected to the O_2 trap, placed on a magnetic stirrer, and aged for 24 hours. After 24 hours, Fe(II) was injected, and either 25min or 24 hours (experiments 3, 5, and 12) was allowed for pre-equilibration prior to injection of nitrite. Samples were withdrawn by syringe, filtered, and analyzed as described above.

2.3 Results and Discussion

2.3.1 Homogeneous and heterogeneous results

Experimental conditions and some results for the heterogeneous experiments are reported in Table 2-1. In the absence of HFO, less than 1% of initial nitrite and Fe(II) reacted within 24 hours at pH 6.8 (Figure 2-2). Sørensen and Thorling (1991) reported about 8% decrease of Fe(II) concentration during 10 hours with nitrite at pH 8.0 in the initial absence of solid phase.

The reaction proceeded rapidly in the presence of HFO, as illustrated in Figure 2-2 (experiment 6, stoichiometric excess of nitrite) and in Figure 2-3 (experiment 15, stoichiometric excess of Fe(II)). These figures also show that solid-bound Fe(II) did not react with nitrite in the absence of dissolved Fe(II) during the time of observation. We observed similar conservation of solid-phase Fe(II) after depletion of dissolved Fe(II) for Fe(II)/HFO/O_2 (26). The concentration of HFO was increased in experiments 8 to 11, so that solid-bound Fe(II) could be measured with greater accuracy. The initial concentrations of dissolved Fe(II) and solid-bound Fe(II) were about equal in experiments 10 and 11 (Table 2-1). The ratio of solid-bound to dissolved Fe(II) was slightly lower in experiments 8 and 9. Results for concentrations of dissolved and solid-bound Fe(II) versus time are shown in Figure 2-4. Dissolved Fe(II) decreased rapidly and was almost completely eliminated within 10 hours, while solid-bound Fe(II) increased during the first hour, decreased from 2 to 6 hours, and then remained relatively constant for the remainder of the experiments. Solid-bound Fe(II) was conserved in all of our experiments after the initial increase and decrease, i.e., solid-bound Fe(II) did not rapidly re-partition from the solid phase back into the dissolved phase during the observation time in these experiments, although it is noted below that some re-partitioning may have occurred. The initial increase, subsequent decrease, and then stability in the concentration of solid-bound Fe(II) were similar to observations for Fe(II)/HFO

without any oxidant (36), attributed to partial conversion to goethite in the presence of Fe(II)(26, 48) and consequent decreased specific surface area (note lower solid-bound Fe(II) for 24 hr pre-equilibration, i.e., experiments 3, 5, and 12 in Table 2-1). Solid-bound Fe(II) became relatively constant in concentration at about the same time that dissolved Fe(II) was close to zero, and it is possible that these observations were related. Conservation of solid-bound Fe(II) during the first stage of the redox reaction is consistent with other evidence about the delocalization and migration of electrons from surface-bound Fe(II) to bulk Fe(III)(hydr)oxide (29, 30).

For data fitting, we assumed two moles of Fe(II) were oxidized for every mole of NO_2^- reduced based on the reaction mechanism that was proposed by Sørensen and Thorling (1991).

$$4\ Fe^{2+} + 2\ NO_2^- + 5\ H_2O \rightarrow\ 4\ FeOOH + N_2O + 6\ H^+ \quad (1)$$

$$6\ Fe^{2+} + 2\ NO_2^- + 5\ H_2O \rightarrow\ 2\ Fe_3O_4 + N_2O + 10\ H^+ \quad (2)$$

Sørensen and Thorling (1991) used lepidocrocite and may have produced magnetite, which does not completely dissolve during acid extraction (36). Sørensen and Thorling (1991) reported four Fe(II) removed for every mole of nitrite in their Figure 2-4; they attributed the apparent anomaly to the formation of new phases containing Fe(II). Our results were generally consistent with the proposed stoichiometry as shown in Table 2- 1. Typically the removal stoichiometry for Fe(II)/nitrite increased during the course of the experiment; Figure 2-5 illustrates this trend for experiment 15.

We initially evaluated rates of reaction using the following second order rate expression.

$$d[Fe(II)]/dt = -\ k_{obs}[Fe(II)_{diss}]\ [NO_2^-] \quad (3)$$

Values for k_{obs} were obtained for each experiment using an integrated equation

$$k_{obs}t = \frac{1}{[Fe(II)_{diss}]_o - 2[NO_2^-]_o} \ln \frac{[NO_2^-]_o([Fe(II)_{diss}]_o - 2x)}{[Fe(II)_{diss}]_o([NO_2^-]_o - x)} \quad (4)$$

where *x* denotes the disappearance in nitrite. The observed rate constant for each experiment, k_{obs}, was derived as the slope of the right-hand side of Equation (4) versus t. Fits are illustrated by lines in Figures 2-2 and 2-3. The dashed lines represent the predicted concentrations of dissolved Fe(II) and NO_2^- calculated. R^2 values for observed versus predicted concentrations of nitrite and dissolved Fe(II) are reported in Table 2-1. Although R^2 values are good, the predictive curves underestimated dissolved Fe(II) after substantial removal of dissolved Fe(II), indicating a possible slow re-partitioning between solid-bound and dissolved Fe(II).

2.3.2 Solid-bound Fe(II) as a catalyst.

Figure 2-6 (experiments 7 to 11 with variable HFO concentrations) shows that k_{obs} ($\mu M^{-1}.min^{-1}$) was proportional to the volumetric concentration of solid-bound Fe(II) ($\mu mol\ L^{-1}$), but was inversely proportional to the "sorption density" of Fe(II), i.e., the solid-bound Fe(II)/Fe(III) molar ratios. Some investigators have reported that rate constants for the Fe(II)/ferric oxide/oxidant system increased with "sorption density", e.g., for reduction of hexahydro-1,3,5-trinitro-1,3,5-triazine (RDX), polyhalogenated methanes (PHMs), and oxamyl (6, 40, 41). The ferric oxide concentration was held constant in all of these studies. Amonette et. al.(3) studied Fe(II)/goethite/CCl_4 and used variable concentrations of ferric oxide. They observed (as we did) that k_{obs} was directly proportional to solid-bound Fe(II) and inversely proportional to "sorption density" of Fe(II) (their Figure 2-5).

2.3.3 Overall rate equation

Values of k_{obs} are plotted against concentrations of solid-bound Fe(II) in Figure 2-7. The slope in Figure 2-7 represents the 3rd order rate constant, $k_{overall}$ ($\mu M^{-2}\ min^{-1}$), for the reaction Fe(II)/HFO/NO_2^- at pH 6.8.

$k_{obs} = k_{overall}\ [Fe(II)_{solid\text{-}bound}]$ ………………………………………………………….(5)

$Rate = -\ k_{overall}\ [Fe(II)_{diss}]\ [Fe(II)_{solid\text{-}bound}]\ [NO_2^-]$ …….…………...…………………(6)

The dashed line is the linear best fit for all experiments and results in $k_{overall}$ (slope) = $2.30 \times 10^{-7}\ \mu M^{-2}\ min^{-1}$ and R^2=0.76. The solid line is the linear best fit for experiments 1-12 only (filled symbols) and results in $k_{overall} = 2.59 \times 10^{-7}\ \mu M^{-2}\ min^{-1}$ and R^2=0.94. We previously observed that $k_{overall}$ for Fe(II)/HFO/O_2 decreased when $Fe(II)_{solid\text{-}bound}$ exceeded 0.022 mol Fe(II) per mol Fe(III) (26). Experiments 13-16 had high density of $Fe(II)_{solid\text{-}bound}$, i.e., 0.039-0.046 $Fe(II)_{solid\text{-}bound}$/Fe(III) (mol/mol), compared to 0.007-0.026 $Fe(II)_{solid\text{-}bound}$/Fe(III) for experiments 1-12. The break-point of ~0.026 mol/mol for the nitrite experiments is in good agreement with the break-point of ~0.022 mol/mol for the earlier O_2 experiments. We do not know the reason for the decrease in rate constant for very high $Fe(II)_{solid\text{-}bound}$/Fe(III) ratios, but it seems a fertile area for further study.

2.3.4 Reaction mechanism

A mechanism for Fe(II)/HFO/nitrite reaction must be consistent with the experimental observations, i.e., (i) the reaction is catalyzed by HFO, (ii) both dissolved and solid-bound Fe(II) are required for the reaction to proceed, (iii) the rate is first-order with respect to both solid-bound as well as dissolved Fe(II), and (iv) dissolved Fe(II) is lost while solid-bound Fe(II) is relatively conservative. These observations are identical to those reported for the Fe(II)/HFO/O_2 system(26).

Two mechanisms are proposed here. First, it was previously suggested (26) that oxidation and reduction might occur at separate sites, so that dissolved Fe(II) is oxidized at electron-poor anodic sites and nitrite is reduced at electron-rich cathodic patches of solid-bound Fe(II). This mechanism is consistent with recent progress in characterizing Fe(II)/Fe(III) systems by means of wet experimental (26, 42), analytical (29, 49), and molecular modeling techniques (28, 30). These studies have demonstrated that electrons from "adsorbed" Fe(II) can be delocalized into the bulk Fe(II)/Fe(III)(oxyhydr)oxide phase. Alternatively, electrons could be transfered within an inner-sphere Fe(II)-nitrite-Fe(II) complex at the Fe(II)/ Fe(III)(oxyhydr)oxide surface. We are further investigating these mechanistic hypotheses with wet experimental techniques using uranyl as oxidant. We are also using molecular modeling tools to estimate the energetics of the alternative mechanisms.

2.4 Conclusions

These results provide both qualitative and quantitative description for abiotic reactions that can result in production of NO and N_2O. The results support the previously proposed (26) general rate expressions and proposed reaction mechanisms for Fe(II)/HFO/oxidant systems. The results also provide additional wet-experimental support for emerging concepts about the nature of Fe(II)/Fe(III)(hydr)oxide systems, especially regarding the delocalization of electrons. The following conclusions were made.

- Reduction of nitrite at pH 6.8 was catalyzed by HFO. Reaction was not observed in the absence of the solid phase.
- The heterogeneous reaction was fast for the experimental conditions and resulted in greater than 90% depletion of Fe(II) in the presence of excess nitrite or 75% depletion of nitrite in the presence of excess Fe(II) and HFO within 10 hours.

- Solid-bound Fe(II) was conservative after the depletion of dissolved Fe(II) or nitrite. The initial increase and then decrease of solid-bound Fe(II) was similar to that previously observed in Fe(II)/HFO systems without oxidant present.
- Approximately two moles of Fe(II) were consumed for every mole of NO_2^- produced, consistent with the theoretical stoichiometry. This is the first experimental demonstration of this stoichiometry.
- A second-order rate equation, $d[Fe(II)]/dt = - k_{obs}[Fe(II)_{diss}] [NO_2^-]$, accurately predicted the concentrations of dissolved ferrous iron and nitrite versus time in the each of the individual experiments.
- Values for k_{obs} were proportional to the concentration of solid-bound Fe(II), resulting in a rate equation $d[Fe(II)]/dt = - k_{overall} [Fe(II)_{diss}] [Fe(II)_{solid\text{-}bound}] [NO_2^-]$.
- The reaction was inhibited when the solid-bound Fe(II) to Fe(III) molar ratio exceeded 0.026. This result was similar to our earlier observations for the Fe(II)/HFO/O_2 system.
- The results were consistent with at least two possible reaction mechanisms, an anode/cathode electron transfer process or a ternary surface complexation reaction. We are investigating these mechanisms by using molecular modeling techniques.

Table 2- 1 Conditions and results in heterogeneous experiments. All experiments were performed in a strictly anoxic reactor at 26°C at pH 6.8. Nitrite was added 25 min after addition of Fe(II) and HFO concentration was 2.5 mM as Fe(III) unless otherwise indicated.

Exp. No.	Initial NO_2^-, µM	Initial Fe(II), µM	Average Solid-bound Fe(II), µM	Cumulative ΔFe(II)/ΔN	k_{obs}, $\mu M^{-1} \cdot min^{-1}$	R^2 for Fe(II) and NO_2^- fits	"Sorption Density", mole Fe(II)/ mole Fe(III)
1	629	261	51	1.69	1.73E-05	1.00/0.99	0.020
2	360	265	40	1.91	1.16E-05	1.00/1.00	0.016
3*	726	269	31	1.47	6.73E-06	1.00/0.98	0.012
4	1062	270	43	1.67	1.65E-05	1.00/0.97	0.017
5*	454	351	16	2.20	6.07E-06	1.00/1.00	0.007
6	379	376	64	2.01	1.85E-05	1.00/0.99	0.026
7#	372	381	120	1.98	3.06E-05	1.00/0.96	0.024
8#	378	357	144	1.79	3.76E-05	1.00/0.91	0.019
9#	346	353	159	1.36	4.12E-05	1.00/0.95	0.016
10#	318	356	176	1.37	4.44E-05	0.99/0.94	0.014
11#	320	341	188	1.07	4.59E-05	0.99/0.94	0.011
12*	515	517	17	2.10	1.30E-05	1.00/1.00	0.007
13	492	518	97	2.65	1.91E-05	1.00/1.00	0.039
14	621	622	105	2.04	1.38E-05	1.00/1.00	0.042
15^	262	717	111	2.31	1.73E-05	1.00/1.00	0.044
16	809	817	115	1.84	1.18E-05	1.00/1.00	0.046

^Fe(II) was in stoichiometric excess in experiment 15; nitrite was in excess in other experiments.

* Nitrite was added 24 hr after addition of Fe(II) in experiments 3, 5, and 12.

HFO was 5.0, 7.5, 10.0, 12.5, and 17.5 mM in experiments 7 to 11, respectively.

Figure 2- 1 Experimental setup

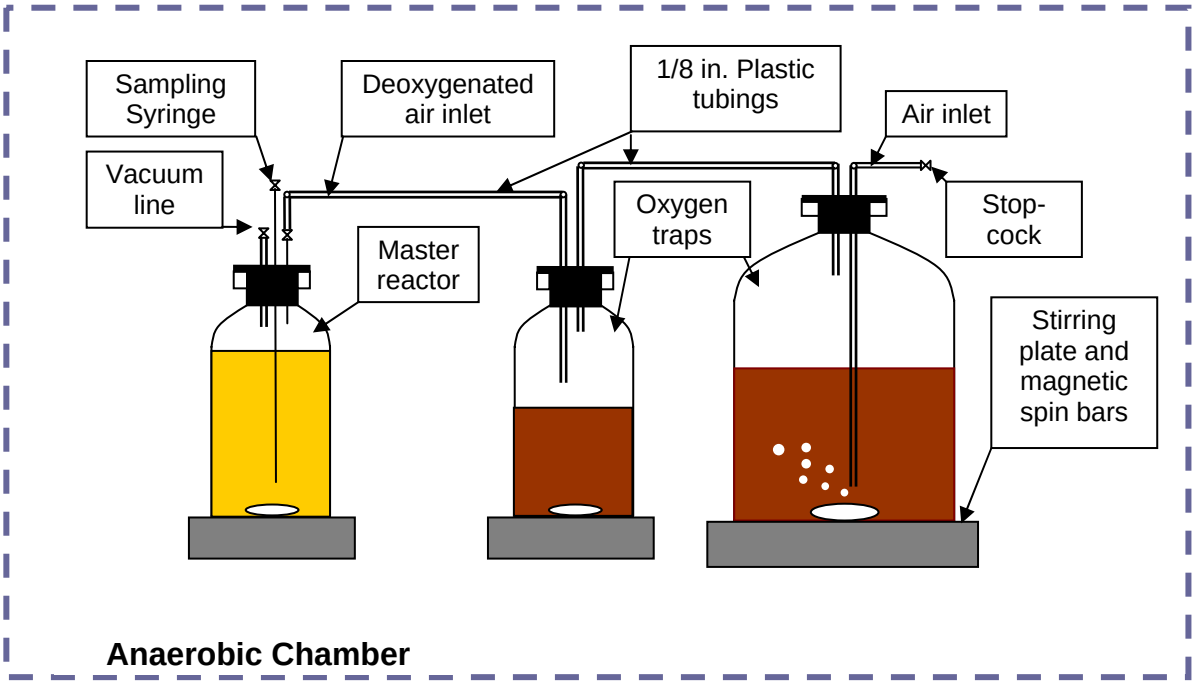

Figure 2- 2 Oxidation of dissolved Fe(II) (◇) and reduction of nitrite (□) were insignificant in the absence of HFO at pH 6.8 in 24 hours (solid lines). Decreases of total Fe(II) (▲),dissolved Fe(II) (◆), and nitrite (■) were rapid in the presence of HFO (experiment 6). Error bars refer to replicate analyses and were smaller than the symbol size. Dashed lines show the predicted concentrations of dissolved Fe(II) and nitrite based on k_{obs}.

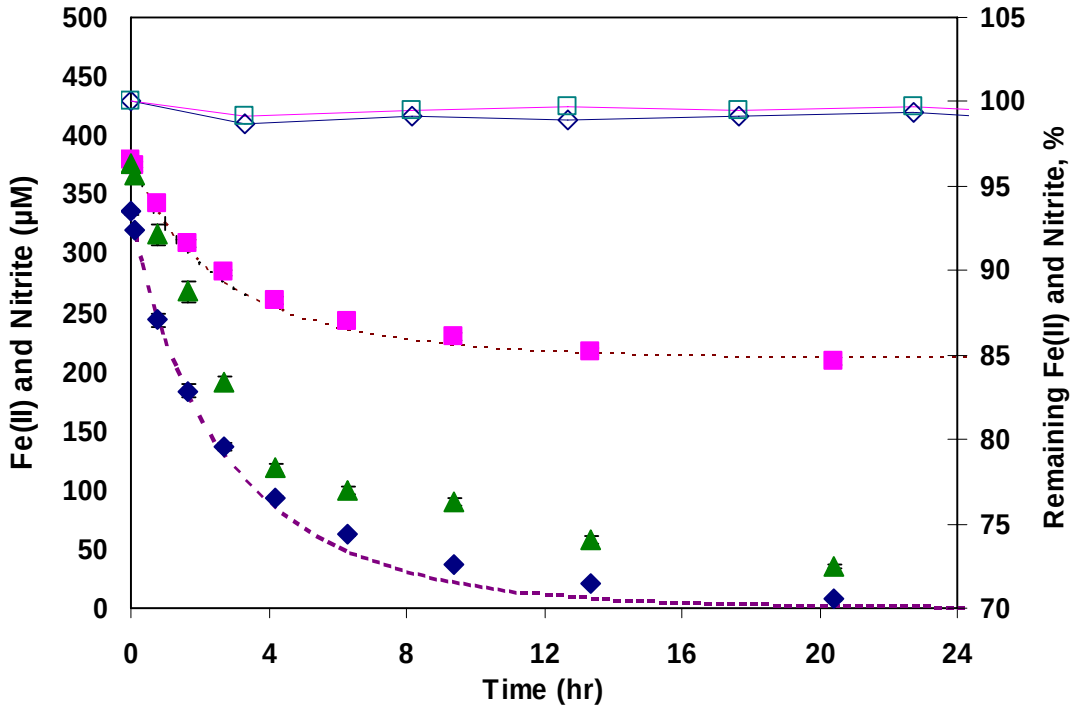

Figure 2- 3 A stoichiometric excess of Fe(II) compared to nitrite was used in experiment 15. Solid-bound Fe(II) was still present after almost all nitrite was consumed. Error bars are smaller than the symbol size.

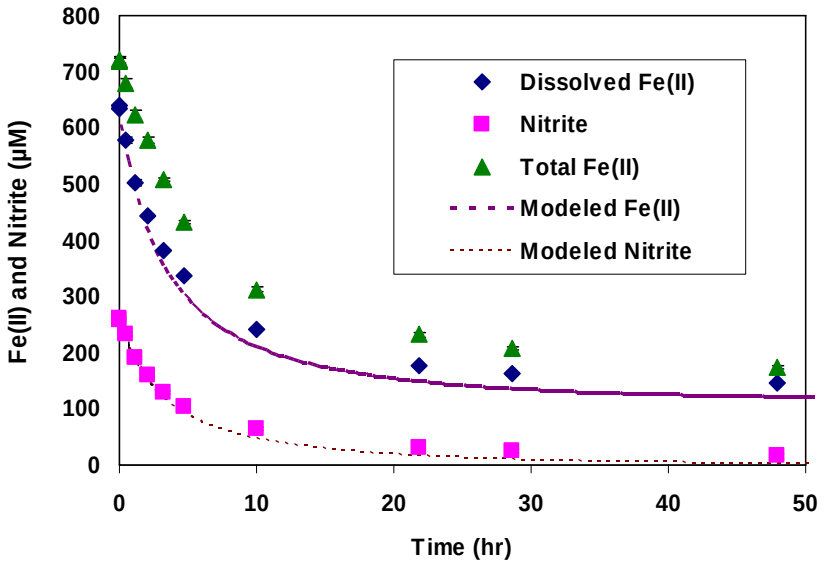

Figure 2- 4 Dissolved Fe(II) (open symbols and light lines) and solid-bound Fe(II) (closed symbols and heavy lines) for experiments with HFO > 2.5mM as Fe(III). Dissolved Fe(II) decreased to close to zero within 10 hours. Solid-bound Fe(II) increased initially, decreased between 2 and 6 hours, and then remained relatively constant. These changes in the concentration of solid-bound Fe(II) are similar to earlier observations in the absence of oxidant (36).

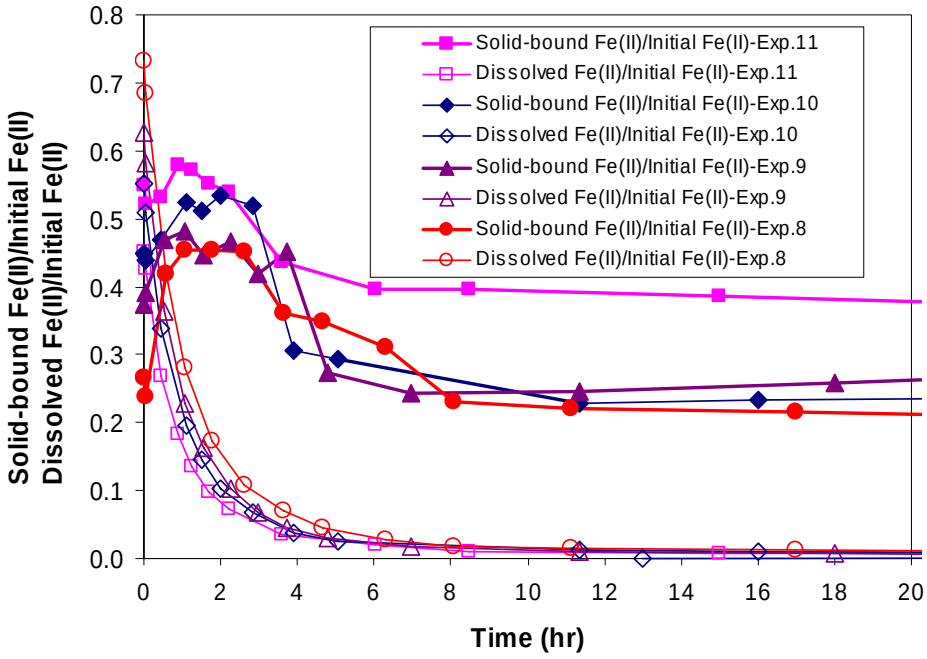

Figure 2- 5 Cumulative stoichiometric ratio of consumed Fe(II)/nitrite (experiment 15, see Figure 3 for details). Final stoichiometric ratios for all experiments are reported in Table 2-1.

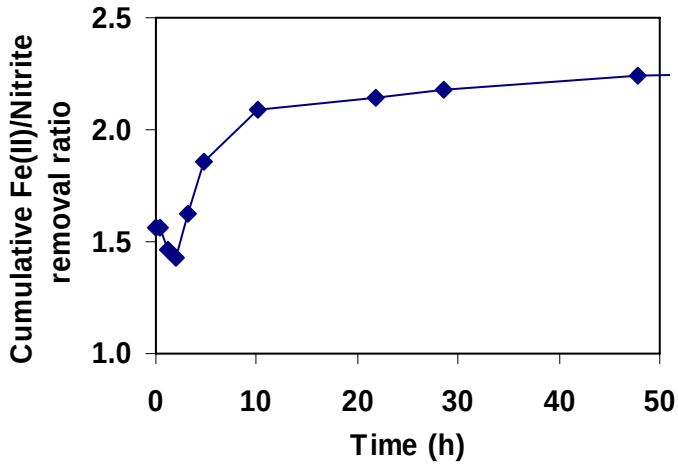

Figure 2- 6 Experiments with variable HFO concentration showed that k_{obs} was proportional to the total concentration of solid-bound Fe(II) (μM) rather than to the "sorption density" of solid-bound Fe(II) (mol Fe(II)/mol Fe(III), 7500X).

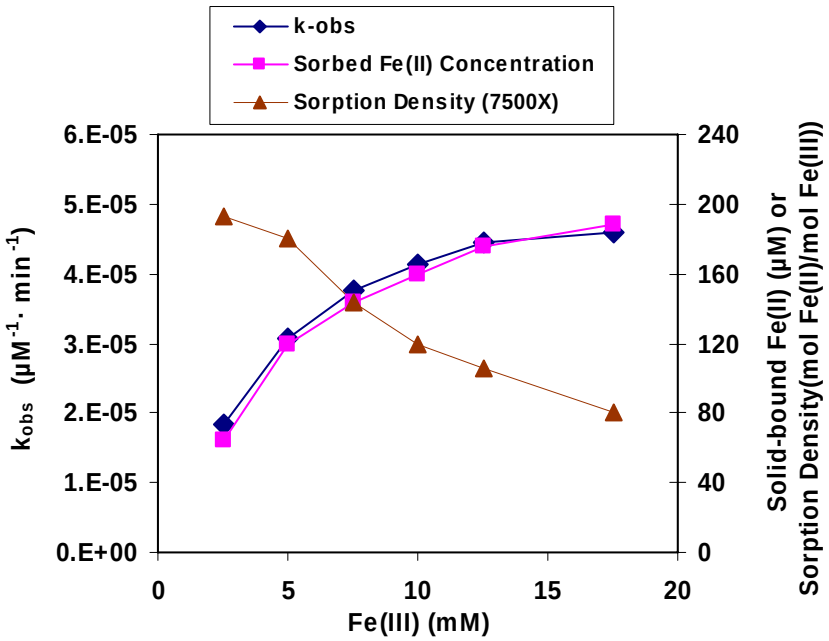

Figure 2- 7 A linear relation between k_{obs} and $[Fe(II)_{solid\text{-}bound}]$ indicated the reaction was 1st order with respect to $Fe(II)_{solid\text{-}bound}$. Filled symbols and the solid line (R^2=0.94) are for $Fe(II)_{solid\text{-}bound}/Fe(III) \leq 0.26$ mol/mol. The linear relation failed for $Fe(II)_{solid\text{-}bound}/Fe(III) \geq 0.39$ mol/mol (open symbols). A similar decrease in k_{obs} with high surface density was reported for Fe(II)/HFO/O_2 (26).

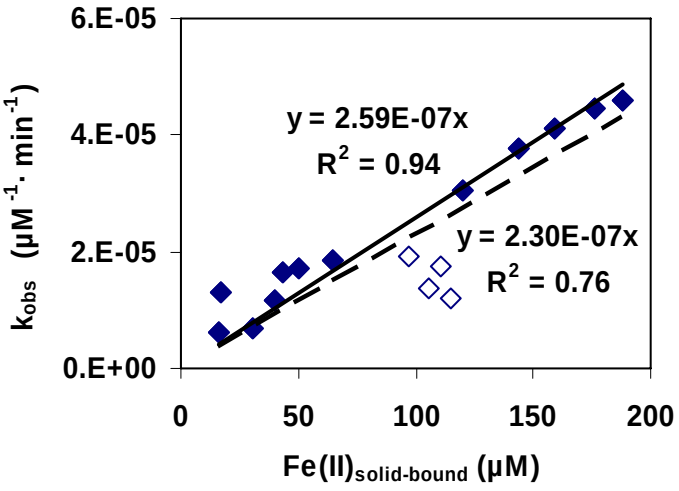

Chapter 3 Rate and Mechanism of Uranium Reduction in Fe(II)/HFO/U(VI) system

Abstract

This is the first study of the Fe(II)/Fe(III)/HFO system in which mass balance has been performed for both Fe(II) and U(VI) species. Previously we showed (also using mass balances) that the reaction rate for heterogeneous oxidation of Fe(II) by O_2 or by nitrite were first order each in $Fe(II)_{diss}$, $Fe(II)_{solid\text{-}bound}$, and oxidant. It was also discovered that $Fe(II)_{solid\text{-}bound}$ was conservative, and therefore functioned as a catalyst. The reaction rate slowed or stopped when $Fe(II)_{diss}$ was depleted, although $Fe(II)_{solid\text{-}bound}$ was still present. In this chapter, similar results are reported using U(VI) as the oxidant. However, the reaction rate for Fe(II)/HFO/U(VI) was an order of magnitude faster than for nitrite, possibly due to high affinity of U(VI) to the HFO surface which could provide a shorter pathway for electron-transfer. Another difference was that the concentration of $Fe(II)_{solid\text{-}bound}$ increased and then remained constant in the presence of U(VI) such that solid-bound Fe(II) density was increased by 3 to 5 times compared to absence of U(VI), while with nitrite or O_2 or with Fe(II) in the absence of oxidant the concentration of $Fe(II)_{solid\text{-}bound}$ first increased less than 100% and then decreased coincident with partial conversion of HFO to goethite. This result also indicates that the extra $Fe(II)_{solid\text{-}bound}$, newly formed after addition of U(VI), also acted as a catalyst. Both second-order with respect to $U(VI)_{total}$ and $Fe(II)_{solid\text{-}bound}$ and third-order (also dependent on $Fe(II)_{diss}$) rate laws were consistent with experimental data. Overall rate constants decreased when $Fe(II)_{solid\text{-}bound}$ exceeded 0.02 mol Fe(II) per mole Fe(III), similar to results for O_2 and nitrite. The characterization of Fe(II)/Fe(III) systems from this study is consistent with several other recent studies that have supported the hypothesis that Fe(II) is incorporated into the bulk phase of Fe(III) oxides, rather than remaining at the interface, and that

this unusual behavior results in apparently unique redox reactivity. Unexpectedly, the stoichiometric ratio of reduced U to oxidized Fe was 1.0 for these experiments, based on extraction with 1M $NaHCO_3$. This could be due to meta-stability of intermediate product U(V) rather than reduction to the stable U(IV) species in Fe(II)/U(VI) redox reaction; this issue will be studied in subsequent experiments.

3.1 Introduction

Anthropogenic release of uranium into surface and subsurface environments mainly results from the mining and processing of uranium ores for nuclear fuel and material production (19, 50). U.S. DOE reported that groundwater contamination by radionuclides occurred at 70% of its facilities (51). Uranium is also found in groundwater and surface waters, typically as U(VI), due to the dissolution or erosion of naturally occurring uranium.

The mobility of U(VI) in water-rock systems is typically controlled by adsorption to mineral phases, especially iron-containing minerals such as hydrous ferric oxide and hematite due to their high sorption capacity over a wide range of pH, high surface area, and ubiquity as grain coatings (52-54). Complexing ligands such as carbonate can increase U(VI) mobility due to decreased adsorption onto mineral phases (55-57). Since the solubility of U(IV) is low, reduction of U(VI) to U(IV) has been used to decrease the mobility of uranium in groundwater (2, 7, 9). The Fe(II)/Fe(III) redox couple is often involved in either abiotic or biotic reduction of U(VI) to U(IV). In addition to U(VI) and U(IV) oxidation states, some researchers have suggested that U(V) (as UO_2^+) can persist in the sorbed state or as the carbonato complex; U(V) is unstable and can subsequently disproportionate to U(IV) and U(VI) species (2, 58).

Fe(II) can exist in either dissolved or solid-bound forms. In this paper the term “solid-bound” is used instead of “adsorbed”. Solid-bound Fe(II) is an effective agent for biotic or abiotic

reduction of various contaminants (3, 7, 8, 41, 59-61). We previously studied mechanisms and rates for abiotic reactions involving Fe(II), Fe(III) as hydrous ferric oxide (HFO), and either O_2 or nitrite (22, 26). The reactions were first-order each with respect to dissolved Fe(II), solid-bound Fe(II), and oxidant concentrations. Solid-bound Fe(II) was conservative after some early fluctuations that were associated with partial transformation to goethite or hematite. Dissolved Fe(II) disappeared completely when there was a stoichiometric excess of the oxidant and the reaction stopped when dissolved Fe(II) was depleted. The conservation of solid-bound Fe(II) in our experiments was initially a surprise, but it now seems consistent with subsequent analytical and molecular modeling evidence that electrons from surface-associated Fe(II) can be delocalized within the bulk Fe(III)(hydr)oxide phase (26, 28-30).

Various mechanisms have been proposed for Fe(II)/U(VI) reactions. With few exceptions the experimental procedures have lacked sufficient rigor and detail to accurately describe the order of the reaction with respect to U(VI), solid-bound Fe(II), and dissolved Fe(II) (7, 20, 25, 59, 62, 63). The Liger et al. (20) investigation of abiotic reduction of Fe(II)/hematite (αFe_2O_3)/U(VI) was unique in reporting both a mechanism and a rate equation. They reported that the rate was first order with respect to $U(VI)_{ads}$ and depended on pH and total Fe(II) concentration. They demonstrated a linear relationship between the pseudo-first-order reduction rate and the concentration of the surface complex ≡Fe(III)OFe(II)OH, which was estimated using a surface complexation model rather than by measurement of the real-time surface-bound Fe(II). Later work by Larese-Casanova (49) has stated that surface complexation modeling is inappropriate for describing Fe(II) speciation in the presence of Fe(III) oxides. On the other hand, Shao and Butler (42) reported that the rate of reaction was first order in Fe(II) that was weakly adsorbed, even though weakly-bound Fe(II) represented only a few percent of total solid-bound Fe(II). These reports illustrate the diversity of extant ideas regarding the speciation of Fe(II) in the presence of

Fe(III) oxides, and the significance of the various Fe(II) species for redox reactions. This work provides some additional information that can help in understanding these issues.

The goal in this study was to evaluate the redox system Fe(II)/HFO/U(VI) using a strict anoxic environment (27) and in the absence of CO_2. We measured concentrations of dissolved Fe(II), solid-bound Fe(II), dissolved U(VI), solid-bound U(VI), and total U in order to provide mass balances, determine effects of all species on reaction rate, derive insights into reaction mechanism, and determine the stoichiometry of the reaction. Finally we compared the derived mechanisms and rates with earlier results for Fe(II)/HFO/NO_2^- and Fe(II)/ferric oxide/U(VI).

3.2 Materials and Methods

3.2.1 Chemicals

Chemicals were reagent grade or better. Solutions were prepared using O_2-free DI water that was purged with N_2 for >4 hours, transferred into the anaerobic chamber, and open-stirred for >3 days. Stock 250 mM Fe(II) was prepared in the chamber with pH<1. The calibration and storage of Fe(II) stock solutions followed procedures described in Tai and Dempsey . HFO contained 1.00, 2.50, 3.75, or 5.00 mM Fe(III) and 0.01 M sodium PIPES (piperazine-1,4-bis-2-ethanesulfonic acid) at pH 6.8 (26). PIPES pH buffer does not significantly affect speciation of transition metal ions (41, 46, 64). HFO stock solution was prepared by slow titration of 1M $FeCl_3$ solution with NaOH to pH 6.8, and then the solid phase was settled and >90% of supernatant was decanted and replaced with DI water. Settling/decant was repeated seven times to reduce chloride to levels that do not interfere with analysis of U(VI) (65). Fe(III) in the HFO stock solution was determined by 1,10-phenanthroline method after reductive dissolution (45).

3.2.2 Anoxic Environment

Experiments were performed at 26~28ºC inside an anaerobic chamber (Coy Laboratory Products, Inc.). Reactors were additionally isolated from the chamber gas by an O_2-trap (27). The chamber atmosphere was continuously circulated through NaOH solution to eliminate CO_2.

3.2.3 Analyses

U(VI) concentrations were determined by kinetic phosphorescence analyzer (KPA-11, Chemchek, Richland, WA, USA). Dissolved U(VI) was determined after centrifugation (MiniSpin, Eppendorf, Westbury, NY, USA) at 14,000 rpm for 10 min. Total U(VI) was measured after extraction of the suspension with 1 M $NaHCO_3$ for 30 min at pH 8.4 followed by centrifugation. All of these separations and extractions were performed in the anaerobic chamber Total U was determined after placing the sample suspension in 20% HNO_3 and then exposing to air for >1 day, resulting in dissolution of all HFO (66). All samples for KPA analysis were measured in an identical HNO_3 matrix.

Dissolved Fe(II) and solid-associated Fe(II) was determined using previously-described techniques (22). Briefly, dissolved Fe(II) was determined using 1,10-phenanthroline (45) after filtration (0.2μm). Solid-bound Fe(II) was defined as Fe(II) retained on the membrane filter and extracted into 0.5 N HCl in 1 hour (7). This procedure removes dissolved Fe(II) and thus inhibits further redox reactions. Total Fe(II) was the sum of dissolved and solid-bound Fe(II). Extractions, filtrations, and color development were performed in the anaerobic chamber.

3.2.4 Experimental Procedure

The experimental setup is shown in Figure 2-1. The experimental conditions and initial reactant concentrations are listed in Table 3-1. An HFO suspension was prepared at pH 6.8 in a 500-mL Pyrex glass bottle in the anaerobic chamber. The reactor was connected to an oxygen trap, placed on a magnetic stirrer, and aged for 24 hours. After 24 hours, Fe(II) was injected into the reactor bottle and 25min was provided for pre-equilibration of HFO and Fe(II) prior to injection of U(VI). Samples were withdrawn by syringe, filtered for dissolved Fe(II) or U(VI), and analyzed for dissolved Fe(II), solid-bound Fe(II), dissolved U(VI), total U(VI), and total U as described above. Experiments were run in duplicate.

3.3 Results and Discussions

3.3.1 Fe(II)/U(VI) redox kinetics

Experimental results are reported in Table 3-1 and in Figure 3-1**.** A control experiment without addition of U(VI) is shown in Figure 3.1(a); more than 95% of Fe(II) was recovered and the concentration of solid-bound Fe(II) did not increase with time.

Results for experiment 2 are shown in Figure 3.1(a) and (b); more than 97% of U(VI) were immediately associated with the solid phase, total U(VI) decreased rapidly (98% removal in 5 hours), total U was conservative (>95% recovery throughout the experiment), the concentration of solid-bound Fe(II) increased by ~300%, and ΔFe(II)/ΔU(VI) was 0.97 mol/mol.

The immediate decrease in dissolved U(VI), rapid removal of total (extractable) U(VI) within hours, conservation of total U, four-fold increase in solid-bound Fe(II) upon addition of U(VI), and ΔFe(II)/ΔU(VI) $\leq$1 mol/mol (rather than the expected 2.0) were observed in all of the other experiments. Results for experiments 1, 3, 4, 5, 6, and 7 are shown in Figure 3.1(c) to (h).

U(VI) was reduced to <50% of initial in less than 2 hr except for experiment 5 that had the lowest HFO concentration and therefore the lowest concentration of solid-bound Fe(II). Total U values are not shown in these figures, for simplicity, but >95% recovery was achieved for every experiment, indicating adsorption to the reactor bottle and sampling set was minimal.

In previous work we used a 2nd order rate law for the initial k_{obs} value and a 3rd order overall (including $Fe(II)_{solid\text{-}bound}$) to model Fe(III)/Fe(II)/oxidant reactions in the presence of HFO (22). Liger et al.(20) proposed that reduction rate of U(VI) in Fe(II)/hematite solution was 1st order with respect to U(VI) concentration. Rate equations and rate orders reported by previous researchers using O_2, NO_2^-, and U(VI) as oxidants are summarized in Table 3-2. We modeled Fe(II)/U(VI) reaction with both pseudo-1st-order and pseudo-2nd-order rate laws in this study using rate equations listed in Table 3-2. The calculated rate constants for each experiment are listed in Table 3.1 and the predicted U(VI) concentrations using 1st and 2nd rate expressions for all experiments are shown in Figure 3-1(b) to (h). The modeling results using the 1st order rate law demonstrated good fits on real data except in experiments 3 and 4, 2nd order fits were better for experiment 1, and neither 1st nor 2nd order rate equations accurately predicted total U(VI) results for initial changes in experiments 3 and 4. Both of these two hypotheses of reaction order will be discussed in the following sections and detailed kinetic modeling procedures including support data will be described in Appendix A.

3.3.2 Pseudo-first-order rate law

In hypothesis 1, the reaction rate of U(VI) reduction with Fe(II) can be modeled as a function of total U(VI) concentration in the system:

$$d[U(VI)]/dt = - k_{obs\text{-}1} \bullet [U(VI)] \quad \text{.....(1)}$$

The only rate equation and rate constant for Fe(II)/U(VI) redox reaction catalyzed by ferric

(oxyhydr)oxides was reported by Liger et. al. (20). They studied abiotic uranyl reduction kinetics with Fe(II) in hematite suspension. A 1st order rate constant of 0.02 min^{-1} for U(VI) reduction was reported with 3.32 mM hematite and 160 mM Fe(II) at pH 7.5. The lower 1st order rate reaction rate constant reported in our study could be due to the lower pH (pH 6.8) which results in a decrease of hydrolytic surface complex ≡Fe(III)OFe(II)OH (20, 59). It has been suggested that the formation of hydroxo complexes transfer electron density from OH-surface-bonded ligands to sorbed Fe(II), thus increasing the reducing power of Fe(II) (43, 67). Additionally, a higher redox potential of HFO/Fe(II) couple than αFe_2O_3 /Fe(II) couple due to the higher solubility of HFO contributed to the lower reaction rate in Fe(II)/HFO/U(VI) system despite equal or larger Fe(II) sorption densities in this study compared with 0.015 mol Fe(II)/mol Fe(III) surface coverage in Liger's study.

We previously demonstrated that the reduction of nitrite at pH 6.8 was catalyzed by solid-associated Fe(II) and reduction rate was first order with respect to the solid-bound Fe(II) concentration (22). In this study, HFO concentrations were varied from 1mM to 5 mM in order to investigate the dependency of uranium reduction rate on solid-bound Fe(II). As shown in Figure 3-2, k_{obs-1} increased linearly with increasing solid-bound Fe(II) with a r-squared value of 0.99. The relationship between k_{obs-1} and solid-bound Fe(II) concentration can be expressed as:

$$k_{obs-1} = k_1 \cdot [Fe(II)_{solid\text{-}bound}] - k_2 \quad \ldots\ldots (2)$$

Where $k_1 = 0.018\ \mu M^{-1} \bullet hr^{-1}$ and $k_2 = 0.318\ hr^{-1}$ in this study. k_1 is the 2nd order reaction rate constant for uranium reduction and k_2 accounts for the minimum solid-bound Fe(II) pool that was required for the reaction to proceed. I will further discuss this finding in section 3.3.5.

3.3.3 Pseudo-second-order rate law

For experiments with 2.5 mM Fe(III) solid concentration, the removal stoichiometry for Fe(II)/U(VI) was about 1 as shown in Tabel 3-1. In a previous study on Fe(II)/NO_2^- heterogeneous reaction, we reported that the reaction rate of NO_2^- reduction was first order with respect to both [$Fe(II)_{diss}$] and [NO_2^-] (22). When we assume that uranium reduction is one-electron transfer process and the reaction follows 2nd rate law in which:

$$d[U(VI)]/dt = -k_{obs\text{-}2} \bullet [U(VI)] \bullet [Fe(II)_{diss}] \quad \text{.....(3)}$$

Pseudo-second-order rate constant $k_{obs\text{-}2}$ were obtained for each experiment by calculating $k_{obs\text{-}2} \cdot t$ with the following equation:

$$k_{obs-2}t = \frac{1}{[Fe(II)_{diss}]_o - [U(VI)]_o} \ln \frac{[U(VI)]_o([Fe(II)_{diss}]_o - x)}{[Fe(II)_{diss}]_o([U(VI)]_o - x)} \quad \text{.....(4)}$$

and $k_{obs\text{-}2}$ was derived as the slope of $k_{obs\text{-}2} \cdot t$ versus t plot. *x* denotes the disappearance in U(VI) in Equation (4). Good fitting results by using 2nd order rate law might have confirmed the existence of one-electron-transfer reduction of U(VI) to U(V) as proposed by Charlet et at. (2).

The pseudo-second-order rate constant $k_{obs\text{-}2}$ also exhibited a strong correlation with solid-bound Fe(II) (Figure 3-3). The relationship can be expressed as:

$$k_{obs\text{-}2} = k_1' \cdot [Fe(II)_{solid\text{-}bound}] - k_2' \quad \text{.....(5)}$$

using linear regression with $k_1' = 1.6 \times 10^{-4}\ \mu M^{-2} \bullet hr^{-1}$ and $k_2' = 3.05 \times 10^{-3}\ \mu M^{-1} \bullet hr^{-1}$. k_1' is the 3rd order reaction rate constant for uranium reduction and k_2' accounts for the minimum solid-bound Fe(II) pool that was required for the reaction to proceed. Both pseudo-first-order rate constant ($k_{obs\text{-}1}$) and pseudo-second-order rate constant ($k_{obs\text{-}2}$) exhibited linear relationships with solid-bound Fe(II) concentrations and the x-axis intercepts are fairly close (19.06 μM and 17.67 μM).

When using NO_2^- as the oxidant (22), we reported linear correlation between k_{obs} and $Fe(II)_{solid\text{-}bound}$ as:

$$k_{obs} = k_{overall} \cdot [Fe(II)_{solid\text{-}bound}] \quad (6)$$

The dashed line in Figure 3-3 represents the linear regression line determined for the reduction of NO_2^- by Fe(II)/HFO. When compared with pseudo-second-order rate constant for U(VI) reduction, the trendline for nitrite reduction has a much flatter slope than the trendline for U(VI) reduction. Previous research (25) and this study showed instantaneous removal of over 97% U(VI) from carbonate-free solution at circumneutral pH. Since practically all of the U(VI) is associated with solid phase, the reduction of U(VI) must have occurred at the solid-water interface (20). Our study implies that electron transfer through a sorbed oxidant (U(VI)) is more efficient than through a dissolved oxidant (NO_2^-). Previously we demonstrated the conservation of solid-bound Fe(II) during the first redox reaction stage and evidence for the delocalization and migration of electrons from surface-bound Fe(II) to bulk Fe(III) (hydr)oxide(22, 29, 30). Electron transfer from this pool of electrons to the surface-bound oxidant could be a kinetically shorter pathway for redox reactions involving Fe(II)/HFO. This pathway is also consistent with the anode/cathode mechanism proposed by Park and Dempsey (26) for Fe(II)/O_2 redox reaction with reduction and oxidation occurring on separate sorption sites of Fe(III) (hydr)oxides.

3.3.4 Effect of Fe(II) surface coverage on reaction rate

Park and Dempsey (26) reported that Fe(II)/O_2 heterogeneous reaction rate decreased at high Fe(II) surface coverage on HFO. Jang et al. (25) demonstrated inhibition of uranium reduction at high uranium surface coverage on HFO. Surface sorption density could affect surface coordination between sorbates and sorbents and efficiency of subsequent electron transfer processes (68). Previously we reported a decrease in the Fe(II)/NO_2^- reaction rate when Fe(II) coverage of HFO was above the breakpoint of 0.026 mol Fe(II)/mol Fe(III)(22). Park and Dempsey also reported a breakpoint of 0.022 mol Fe(II)/mol Fe(III) above which the Fe(II)/O_2

reaction rate was observed to decrease (26). In this study, both pseudo-first-order and pseudo-second-order rate constants in experiments 2~7 appeared to increase linearly with increasing solid-bound Fe(II) concentrations. A highest surface coverage (0.0253 mol Fe(II)/mol Fe(III)) among all experiments were used in experiment 1, which led to a drastic drop of reaction rate as shown in open symbols in Figure 3-2 and Figure 3-3. The Fe(II) surface coverage where we observed a decrease of U(VI) reduction rate was in good agreement with previous studies.

3.3.5 Variation of solid-bound Fe(II) in Fe(II)/U(VI) reaction

Figure 3-4 (a) shows the variation $Fe(II)_{solid\text{-}bound}$ up to 15 hours for all experiments with 2.5 mM Fe(III) in solid concentration either with or without U(VI) addition. Without the presence of uranium an averaged solid-bound Fe(II) density of 0.0073 mol Fe(II)/ mol Fe(III) was measured with HFO in 1 day, which is in good agreement with Jeon's study (0.0065 mol Fe(II)/ mol Fe(III)) on HFO sorption kinetics (36). However, upon addition of U(VI), solid-bound Fe(II) density was increased by a factor of 3-5 as shown in both Figure 3-1 and 3-4(a). Solid-bound Fe(II) reached the highest point in about 5 hours at about the same time when most of the U(VI) was depleted. After reaching maximum solid-bound Fe(II) density, the amount of solid-bound Fe(II) stayed almost constant for up to 48 hours in some experiments.

Figure 3-4 (b) shows the variation of solid-bound Fe(II) density using NO_2^- as an oxidant in Fe(II)/HFO solution with similar experimental conditions as Fe(II)/U(VI) experiments. All the experiments reported in Figure 3-4 (a) and (b) were conducted with 2.5 mM Fe(III) in solid concentration at pH 6.8. Possibly three stages for the Fe(II)/HFO/NO_2^- reaction could be identified as shown in Figure 3-4 (b). In the first stage, an rapid sorption of Fe(II) was observed within 1~2 hours. The rapid increase in Fe(II) sorption was followed by desorption of Fe(II) in the second stage. The initial increase and then significant decrease in concentration of solid-

bound Fe(II) was consistent with Jeon's Fe(II)/Fe(III) oxide study (36) in which rapid uptake of Fe(II) onto HFO in the first hour was followed by a decrease of solid-bound Fe(II), concurrent with partial conversion of HFO to goethite. In stage III, solid-bound Fe(II) concentration became relatively constant at about the same time that dissolved Fe(II) was close to depletion. Table 3-3 lists the probable primary reactions in each stage. Lowest solid-bound Fe(II) density was observed in experiment without addition of NO_2^-. This could be due to low Fe(II) dosage used in no-oxidant experiment or due to new sorption sites created by the oxidative precipitation of Fe(II) in experiments with the addition of NO_2^-. Different behaviors in sorption kinetic were observed for each control experiment (no oxidant) shown in Figure 3-4 (a) and 3-4 (b). The fast increasing pattern of solid-bound Fe(II) density in first 2 hours in no-nitrite experiment (Figure 3-4 (b)) was not as significant in no-uranium experiment (Figure 3-4 (a)). This could be due to the different procedures used in HFO preparation. For Fe(II)/NO_2^- experiment, freshly prepared HFO was used, whereas in Fe(II)/U(VI) experiment HFO was prepared from a stock solution. Aging of HFO stock solution could lead to change in crystallinity as well as its sorption characteristics. This issue will be further discussed in section 4.3.1.

Consistent with Fe(II)/HFO/NO_2^- in the first stage of reaction, Fe(II)/HFO/U(VI) experiment also exhibited a rapid sorption of Fe(II) within 1 hour. The initial fast sorption of Fe(II) was followed by a lag phase or/and tapering Fe(II) sorption increase. After that, level-off and conservation of solid-bound Fe(II) was observed in about 5 hr reaction, approximately consistent with stage III of Fe(II)/HFO/NO_2^- reaction. A couple of mechanisms were possibly involved for the significant increase in solid-bound Fe(II) in the Fe(II)/HFO/U(VI) reaction. The initial increase in solid-bound Fe(II) could be due to the formation of Fe(II)-UO_2^{2+}-ferrihydrite ternary complex with a possible electron transfer between Fe(II) and U(VI) as reaction proceeded. The newly formed sorption sites could also be created by the reductive precipitation of U(VI) and oxidative precipitation of Fe(II). Electron-donating Fe(II) after oxidation could form a coating of

Fe(III) (hydr)oxides on HFO surface (autocatalytical reaction). Reductive precipitation of U(VI) leading to a film of UO_2 coating on mineral or cell surfaces have been observed by previous researchers (63, 69). These precipitates could generate new sorption sites for Fe(II) on HFO surface even when partial transformation of HFO could have happened. Regeneration of solid-bound Fe(II) suggested by other researchers (3, 61) involving ion-exchange, reduction, and hydrolysis of structural and surface-bound Fe(III) could also contribute to the continuous increase and conservation of solid-bound Fe(II).

3.3.6 Stoichiometry of Fe(II)/U(VI) reaction

In experiments with 2.5 mM HFO, the stoichiometric ratio for ΔFe(II)/ΔU(VI) were about 1. There were two possibilities for this finding. First, only one electron transfer occurred in Fe(II)/U(VI) reaction. This would result in the appearance of U(V) as the intermediate product for Fe(II)/U(VI) reaction. We further investigated the Fe(II)/U(VI) reaction mechanism using alternate extraction reagent in the next chapter. Alternately, if two-electron transfer did occur and Fe(II) was the sole electron donor (U(V) might have been the electron source in disproportionation reaction), uranium could be involved in reactions other than Fe(II)/U(VI) redox reaction. One possibility is the inclusion of U(VI) within the unextracted HFO phase. Reductive precipitation, oxidation precipitation, and Fe(III)/U(VI) co-precipitation could lead to the incorporation U(VI) into the bulk mineral phases. The formation of Fe(III) (oxyhydr)oxides either through autocatalytical reaction or Fe(III)/U(VI) co-precipitation could occlude U(VI) and thus reduce its extractability (70-72). Fredrickson et al. (69) reported that Formation of UO_2 precipitates on microbial surface inhibited further bio-reduction of U(VI). ΔFe(II)/ΔU(VI) ratios substantially decreased in experiments with higher HFO concentration than 2.5mM as shown in Table 3-1. This could be due to the high solid concentrations that accelerated the occlusion of

U(VI) by Fe(III) (oxyhydr)oxide mineral. The occlusion of U(VI) could also have occurred in experiment 5 in which the uptake and incorporation of U(VI) by mineral phases could prevail due to the slow reduction of U(VI) at low HFO concentration (1mM).

3.3.7 Reaction mechanism

In this study we've shown that (i) both dissolved and solid-bound Fe(II) are required for the Fe(II)/HFO/U(VI) reaction to proceed, (ii) the rate is first order with respect to dissolved Fe(II) and U(VI) concentrations, (iii) the reduction rate is a function of solid-bound Fe(II) concentration, and (iv) between 25~45% of initially doped Fe(II) was preserved with HFO solids. Based on these observations, we proposed that solid-bound Fe(II) is composed of two Fe(II) pools: the strongly bound Fe(II) and the weakly bound Fe(II). Strongly bound Fe(II) is incorporated into the Fe(III) bulk structure due to electron delocalization from dissolved or surface associated Fe(II) into structural Fe(III) or occlusion of Fe(II) by mineral precipitates such as Fe(III) (oxyhydr)oxide and uraninite. Evidence of electron migration from surface-associated Fe(II) into the bulk Fe(III) (oxyhydr)oxide phase have been demonstrated using Mössbauer spectroscopy (29, 49), molecular modeling (28, 30), and wet chemistry (22, 26). Weakly bound Fe(II) refers to the pool of solid-bound Fe(II) that is outer-spercially complexed with the bulk Fe(III) surface. Larese-Casanova and Scherer (49) reported that under monolayer coverage density of Fe(II) on hematite, transient sorbed Fe(II) exhibited quick interfacial electron transfer with structural Fe(III) in hematite, whereas at higher Fe(II) concentrations, formation of a stable sorbed Fe(II) phase was observed. Their study has provided spectroscopic evidence for two distinct phases in solid-bound Fe(II). Shao and Butler (42) demonstrated a better correlation between reduction rate of carbon tetrachloride and weakly bound Fe(II) than strongly bound Fe(II) in a sulfide-treated goethite suspension. We proposed that weakly-bound Fe(II) that is much lower in concentration

than strongly-bound Fe(II), is in dynamic equilibrium with dissolved Fe(II) and is changing in concentration with decrease in dissolved Fe(II) in the presence of U(VI). Strongly-bound Fe(II) affects the redox capability of the Fe(III) (oxyhydr)oxide but is conservative and is not oxidized during the short term. A conceptual model for Fe(II)/U(VI) redox reaction occurring at Fe(III) (oxyhydr)oxide-water interface is shown in Figure 3-5. This mechanism is consistent with the overall rate equation for Fe(II)/HFO/U(VI) reaction:

$$\text{Rate} = -k_{overall} \bullet [Fe(II)_{diss}] \bullet [Fe(II)_{solid\text{-}bound}] \bullet [U(VI)]$$

3.4 Conclusions

This study was performed in order to determine environmentally significant reactions involving U(VI) in the environment, and more generally in order to investigate the important redox couple HFO/Fe(II). We made the following observations and conclusions.

- Adsorption of U(VI) by HFO is very fast. For the experimental conditions, more than 97% adsorption of U(VI) occurred within 2 minutes at pH6.8.
- HFO/Fe(II) is a very effective redox couple for the abiotic reduction of U(VI). The $t_{½}$ for reduction of U(VI) was less than 2 hr for our typical experimental conditions.
- Reduction of U(VI) in individual experiments was reasonably described by either first-order $k_{obs\text{-}1} \cdot [U(VI)_{total}]$ or second-order $k_{obs\text{-}2} \cdot [U(VI)_{total}] \cdot [Fe(II)_{diss}]$ rate expressions.
- Both 1st order and 2nd order k_{obs} values were directly proportional to solid-bound Fe(II) concentrations, i.e., solid-bound Fe(II) was a catalyst for the reaction. This result is consistent with results from our earlier investigations of Fe(II)/HFO/O_2 (26) and Fe(II)/HFO/NO_2^- (22).
- Although solid-bound Fe(II) was conservative after the early phase of the experiment, changes in solid-bound Fe(II) was different than for other experimental systems. In prior experiments with Fe(II)/Fe(III) only or with Fe(II)/Fe(III)/ NO_2^-, solid-bound Fe(II) initially increased and

then decreased before remaining constant for the remainder of the experiment and this was attributed to reduced surface area due to partial conversion to goethite. In the presence of uranium, solid-bound Fe(II) increased and remained at the higher concentration during the rest of the experiment.

- Solid-bound Fe(II) density was increased by a factor of 3-5 after the addition of U(VI) into Fe(II)/HFO solution compared with Fe(II)/HFO solution without U(VI). The significant increase in solid-bound Fe(II) could be due to the increases of sorption sites resulting from the oxidative precipitation of Fe(II) and the reductive precipitation of U(VI) or occlusion of Fe(II) by uraninite and ferric hydroxide precipitates.
- Surprisingly, the stoichiometric ratio for oxidation of Fe(II) versus reduction of U(VI) was about one when extracting with 1M $NaHCO_3$. This could be due to meta-stability of U(V) or it could be due to inclusion of U(VI) within the unextracted HFO phase. Others have reported both of these phenomena for other experimental systems, but this is the first report of Fe(II)/U(VI) stoichiometry during redox experiments. This issue will be further investigated in subsequent experiments.
- Surface coverage of Fe(II) greater than about 0.02 mol Fe(II) per mole Fe(III) in the Fe(II)/HFO/U(VI) system resulted in decreased rate of reaction. This observation is consistent with Park and Dempsey (26) and Tai and Dempsey (22).
- $Fe(II)_{solid\text{-}bound}$ –initiated reduction of U(VI) exhibited higher reaction rate compared with reduction of NO_2^-. This could be due to the high affinity of U(VI) to HFO surface which could provide a shorter pathway for the electron-transfer process.
- Base on our observations, we proposed that solid-bound Fe(II) can be divided into two Fe(II) pools: the strongly bound Fe(II) and weakly bound Fe(II). Strongly-bound Fe(II) affects the redox capability of the Fe(III) (oxyhydr)oxide but is conservative and is not oxidized, whereas weakly-bound Fe(II) with much lower concentration than strongly-bound Fe(II) is in dynamic

equilibrium with dissolved Fe(II) and is changing in concentration with decrease in dissolved Fe(II) in the presence of U(VI). This mechanism is consistent with the overall rate equation for Fe(II)/HFO/U(VI) reaction in which the reaction rate is a function of solid-bound Fe(II), dissolved Fe(II) and U(VI) concentrations.

Table 3- 1 Initial conditions and results for the Fe(II)/Fe(III)/U(VI) system. Experiments were performed in a strictly anoxic reactor at 26ºC at pH 6.8. HFO was aged for 24 hr prior to addition of Fe(II). U(VI) was added 25 min after addition of Fe(II).

Exp. No.	Initial Fe(II) (μM)	Initial U(VI) (μM)	k_{obs-1} (hr^{-1})	k_{obs-2} $(\mu M \cdot hr)^{-1}$	HFO as Fe(III) (mM)	Solid-bound Fe(II) (μM)	Sorption Density mol Fe(II)/ mol Fe(III)	ΔFe(II)/ ΔU(VI) (mol/mol)
Control	304	0	-	-	2.50	18.4	0.0073	-
1	395	35.0	0.54	0.00149	2.50	63.2	0.0253	1.10
2	314	37.6	0.58	0.00340	2.50	47.8	0.0191	0.97
3	153	38.2	0.42	0.00310	2.50	40.2	0.0161	0.97
4	240	46.4	0.51	0.00400	2.50	43.8	0.0175	0.97
5	149	66.8	0.03	0.00027	1.00	19.4	0.0194	0.61
6	155	60.0	0.59	0.00528	3.75	50.6	0.0135	0.50
7	156	61.3	0.82	0.00710	5.00	61.6	0.0123	0.31

Table 3- 2 Rate equations reported by previous researchers and this study in Fe(II)/Fe(III)/oxidant reactions.

Reference	Solid phases	Oxidants	Rate equation	Rate order
Park and Dempsey (26)	HFO	O_2	$d[Fe(II)]/dt = - k \cdot [Fe(II)_{diss}] \cdot [Fe(II)_{sorbed}] \cdot [DO]$	3rd
Tai and Dempsey (22)	HFO	NO_2^-	$d[Fe(II)]/dt = -k_{overall} \cdot [Fe(II)_{diss}] \cdot [Fe(II)_{solid-bound}] \cdot [NO_2^-]$	3rd
Liger (20)	Hematite	U(VI)	$d[U(VI)]/dt = - k_{obs} \cdot [U(VI)]_{ads}$	Pseudo -1st
This study	HFO	U(VI)	$d[U(VI)]/dt = - k_{obs-1} \cdot [U(VI)]_{total}$	Pseudo -1st
This study	HFO	U(VI)	$d[U(VI)]/dt = -k_{obs-2} \cdot [U(VI)]_{total} \cdot [Fe(II)_{diss}]$	Pseudo -2nd

Table 3- 3 Potential primary reactions in each stage of Fe(II)/HFO/NO_2^- reaction.

Reference	Primary reactions
I	Sorption of Fe(II) onto Fe(III) (oxyhydr)oxide surface; Incorporation of Fe(II) into Fe(III) texture; Migration of e^- from sorbed Fe(II) into Fe(III) structure
II	Phase transformation of Fe(III) (oxyhydr)oxide; Desorption of Fe(II) due to decrease of specific surface area
III	Recrystallization

Figure 3-1. Kinetic results for the experiments described in Table 3.1: (a) focus on Fe(II) speciation with (Exp 2) and without (control) addition of U(VI) - no significant changes in $Fe(II)_{total}$ (x) or $Fe(II)_{solid\text{-}bound}$ (+) without the addition of U(VI), but there was a decrease in $Fe(II)_{total}$ (▲) and $Fe(II)_{diss}$ (◆) and an increase in $Fe(II)_{solid\text{-}bound}$ (■) after U(VI) was added; (b) Exp 2 - decrease in $U(VI)_{total}$ (Δ) is compared with modeled $U(VI)_{total}$ using 1st order (solid line) and 2nd order (dashed line) rate laws - $U(VI)_{diss}$ (□) remained very low and total U(◇) was constant; (c) Exp. 1; (d) Exp 3; (e) Exp.4; (f) Exp.5; (g) Exp.6; (h) Exp. 7. All experiments were at pH 6.8 and 26ºC. Error bars show one "standard deviation" for two duplicate experiments.

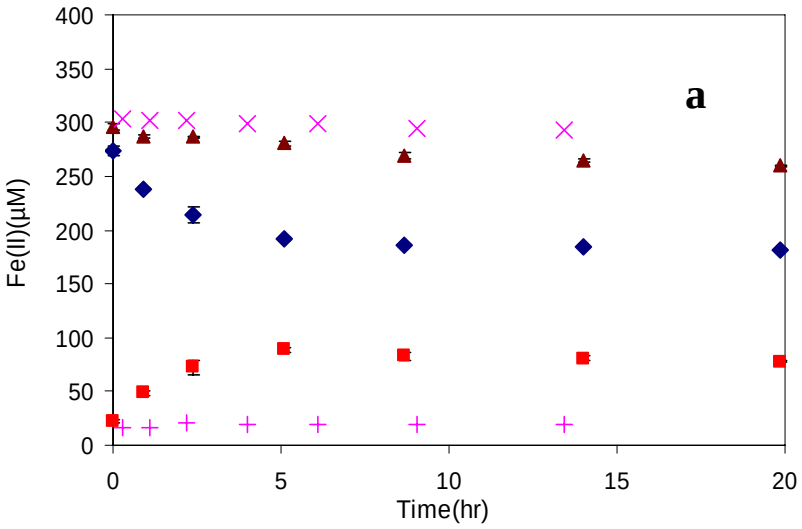

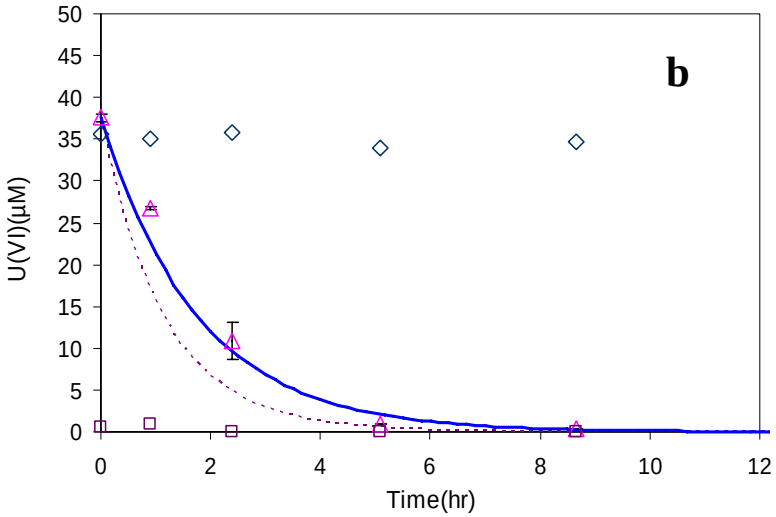

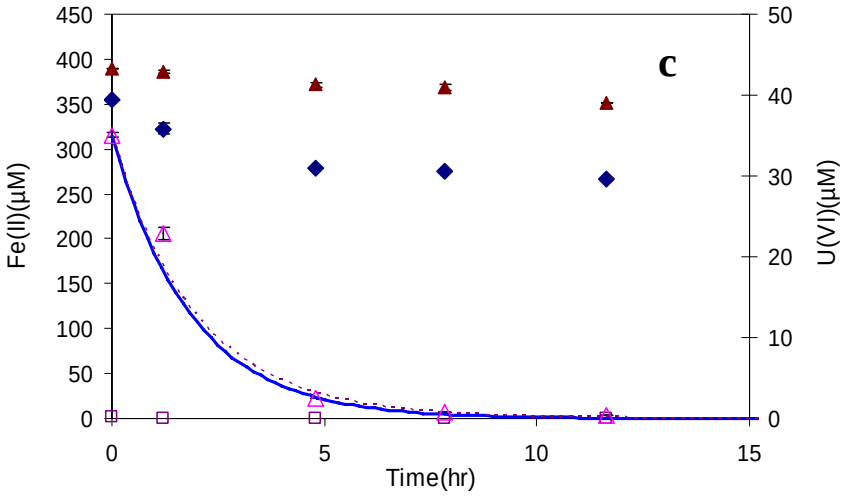
c
Fe(II)(μM)
U(VI)(μM)
Time(hr)
0
50
100
150
200
250
300
350
400
450
10
20
30
40
5
15

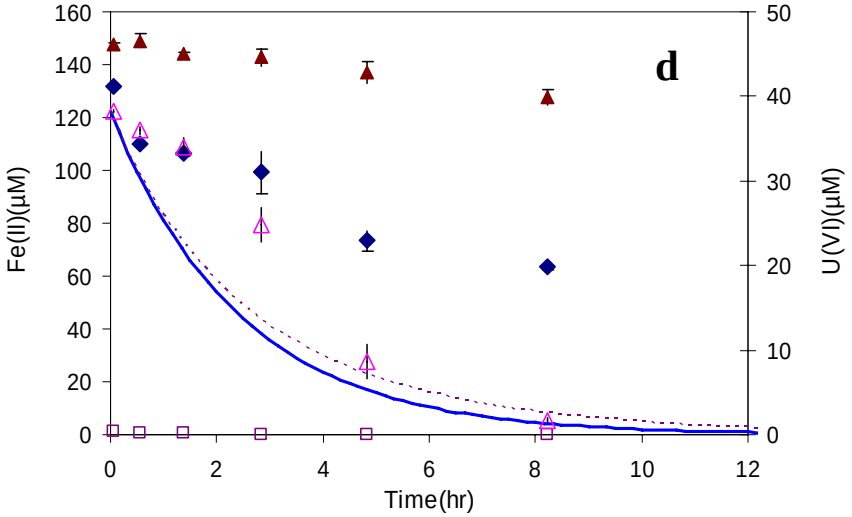
d
Fe(II)(μM)
U(VI)(μM)
Time(hr)
0
20
40
60
80
100
120
140
160
10
30
2
4
6
8
12

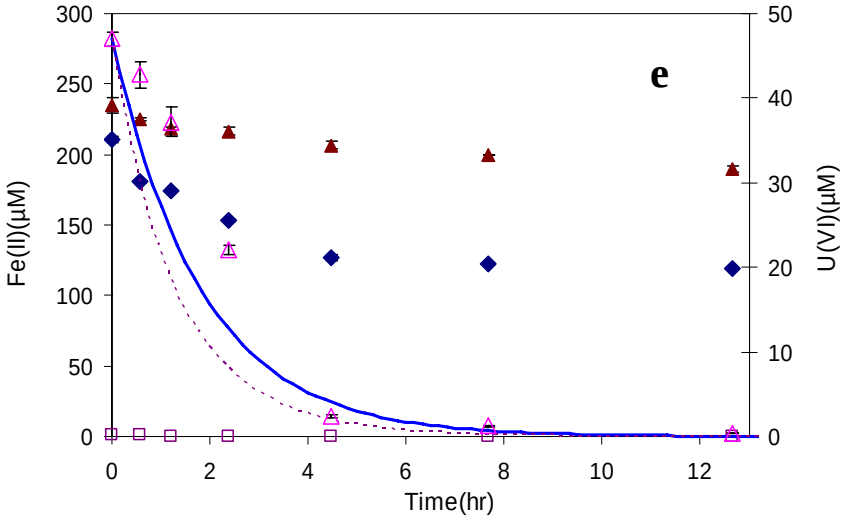
e
Fe(II)(μM)
U(VI)(μM)
Time(hr)
0
50
100
150
200
250
300
10
20
30
40
2
4
6
8
12

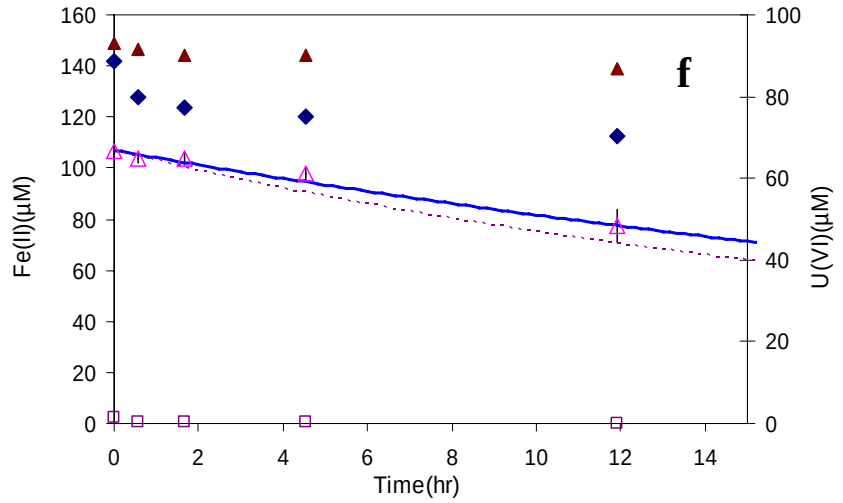
f
Fe(II)(μM)
U(VI)(μM)
Time(hr)
0
20
40
60
80
100
120
140
160
0
2
4
6
8
10
12
14
0
20
40
60
80
100

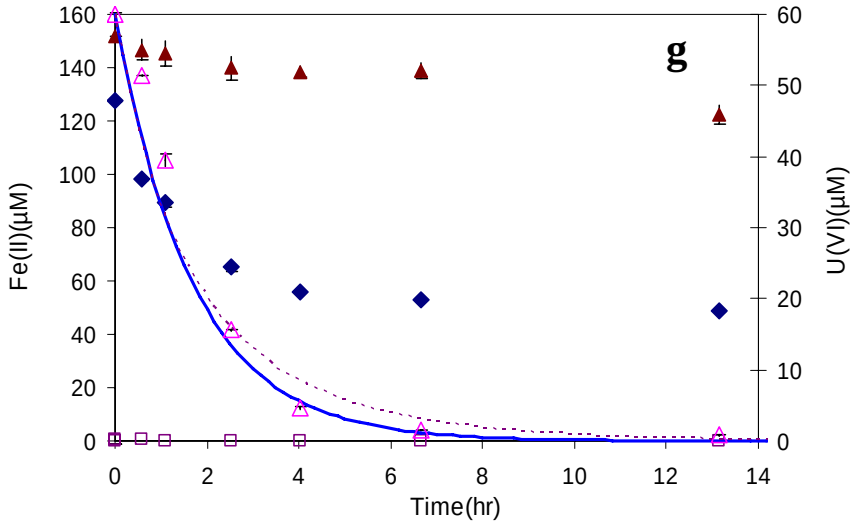
g
Fe(II)(μM)
U(VI)(μM)
Time(hr)
0
20
40
60
80
100
120
140
160
0
2
4
6
8
10
12
14
0
10
20
30
40
50
60

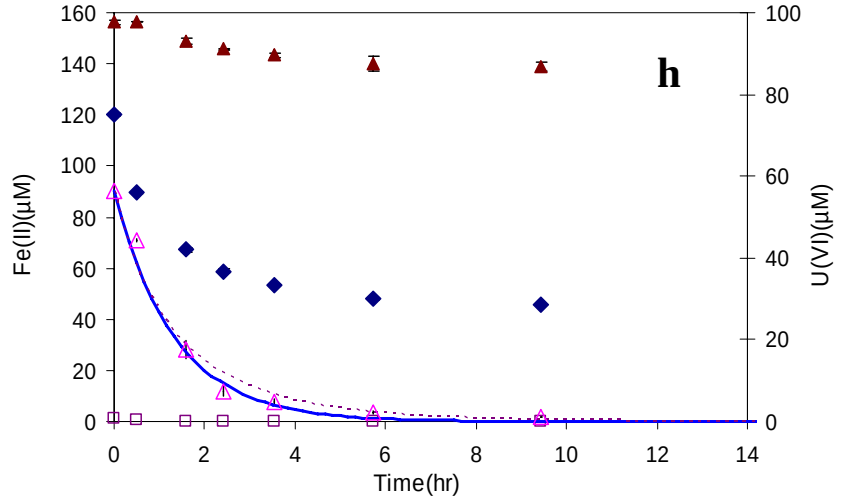
h
Fe(II)(μM)
U(VI)(μM)
Time(hr)
0
20
40
60
80
100
120
140
160
0
2
4
6
8
10
12
14
0
20
40
60
80
100

Figure 3- 2 Pseudo-first-order rate constant k_{obs-1} for uranium reduction was in proportion to the concentration of solid-bound Fe(II) concentrations. Inhibition was observed for >0.02 mole $Fe(II)_{solid-bound}/Fe(III)$ (Exp.1, open symbol).

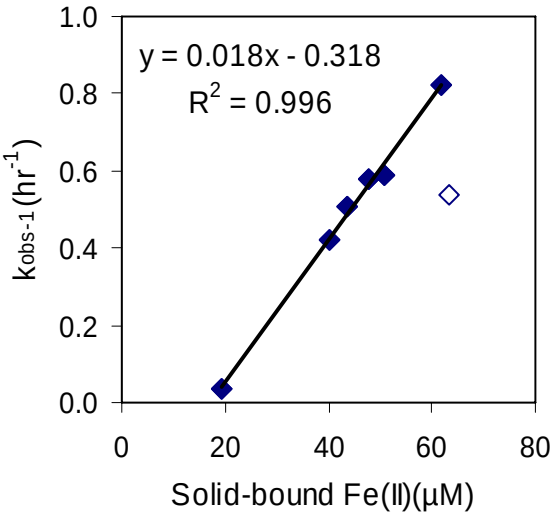

Figure 3- 3 Pseudo-second-order rate constant k_{obs-2} for uranium reduction (solid line and symbols) was greater than k_{obs-2} for nitrite reduction (dashed line (22)).

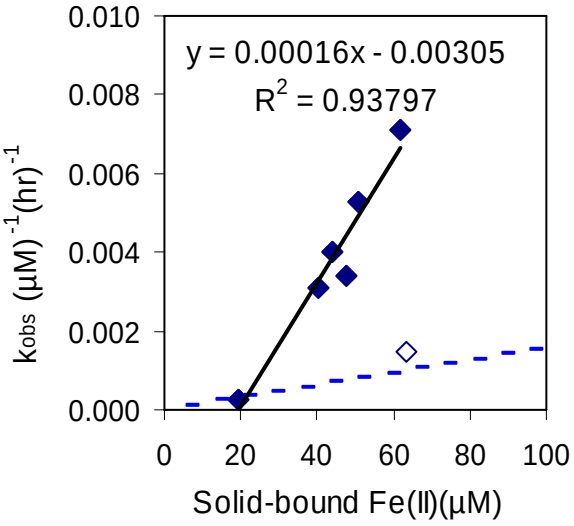

Figure 3-4. Solid-bound Fe(II) density variation using U(VI) (a) or NO_2^- (b) as oxidants with initial Fe(II)/oxidant concentrations shown in the legends. All the experiments were conducted with 2.5 mM HFO at pH 6.8. Experiment numbers in (b) are from Tai and Dempsey (22).

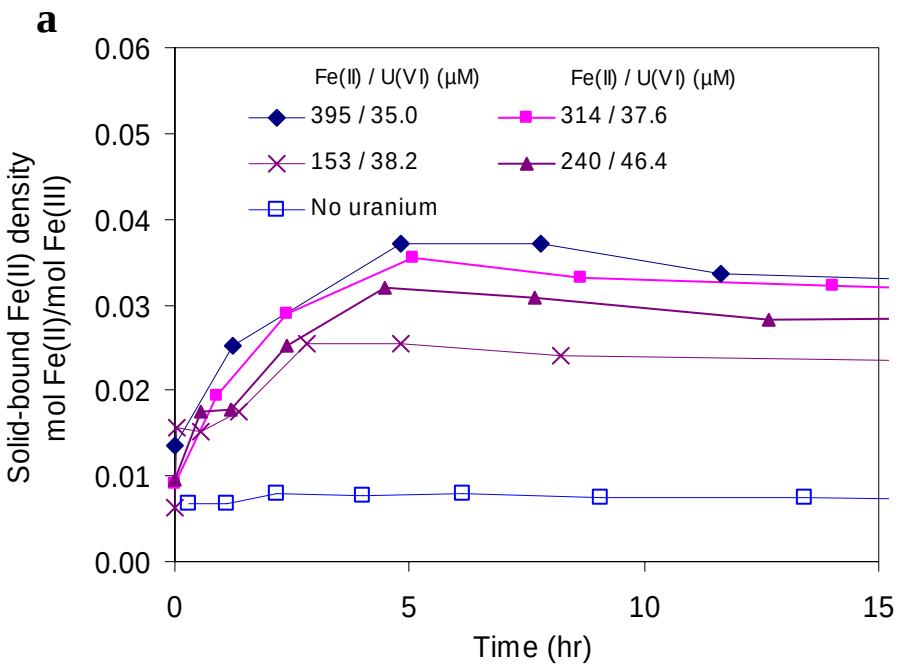

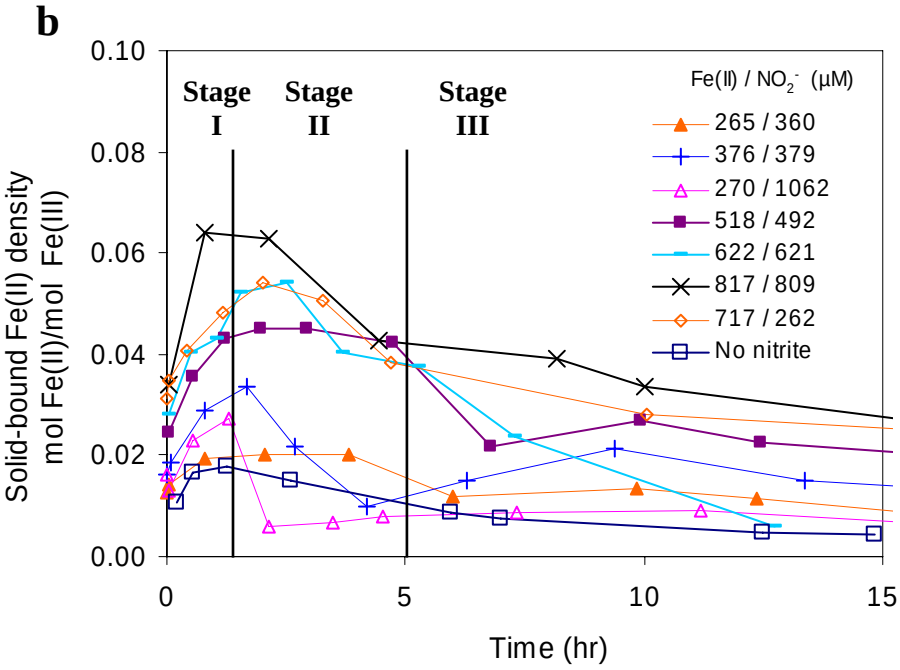

Figure 3- 4 Conceptual model for Fe(II)/U(VI) redox reaction occurring at Fe(III) (oxyhydr)oxide-water interface.

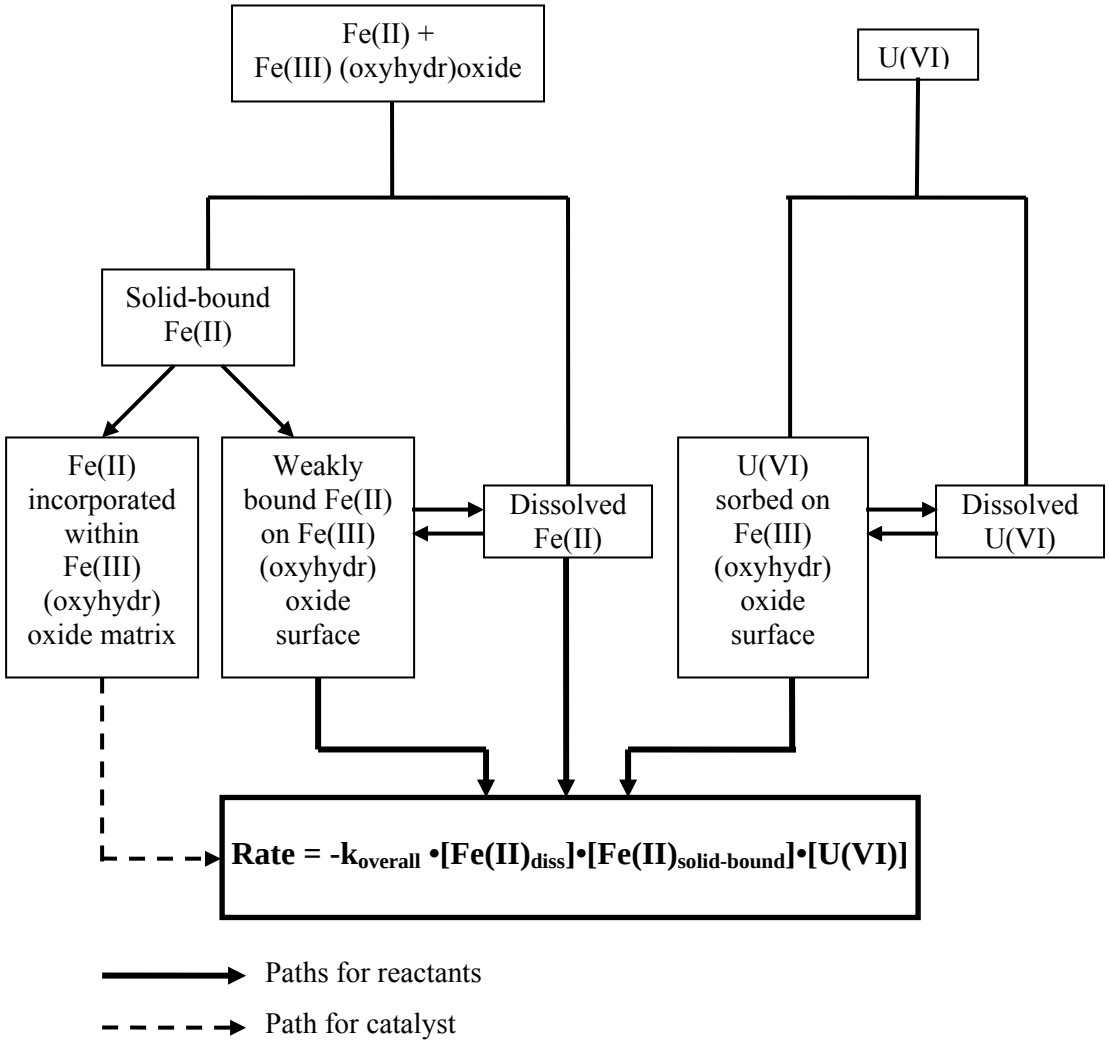

Chapter 4 A Comparison of Extraction Techniques for U(VI) and Implications for Speciation and Immobilization of Uranium in the Fe(II)/HFO/U(VI) System

Abstract

Carbonate and phosphate complexation with UO_2^{2+} has been common extraction practices in studying uranium chemistry. The presence of reducing agents and dynamic mineral phases is expected to increase the complexity of both uranium removal processes and operational procedures for quantifying reactions of uranium. We investigated the effectiveness of two extractants (bicarbonate and phosphoric acid) for characterizing the extent of uranium reduction in the presence of Fe(II) and HFO. Immediate reduction of U(VI) in freshly prepared HFO in the presence of Fe(II) was observed followed by a lag phase before continuing reaction in the second phase. Reaction in the first stage could be approximately modeled with pseudo-first-order rate equation, rate= k_{obs} [U(VI)]. The subsequent lag phase and/or second phase reaction slower than the first phase reaction could be caused by multiple reactions including phase transformation of Fe(III) solids, co-precipitation of iron and uranium, and occlusion of U(VI) by UO_2 or iron oxide coating.

Consumed $U(VI)_{bicarbonate}$ /Consumed $U(VI)_{phosphate}$ ratios were about 2 in all the experiments. We provided two explanations for this finding. First, inclusion of U(VI) within the unextracted HFO phase might decrease the apparent $\Delta Fe(II)/\Delta U(VI)$ ratios. Using H_3PO_4 as an extraction reagent could increase U(VI) extractability from HFO due to high solubility of HFO at pH 1.5. It's also possible that carbonate ligand stabilize U(V) which was formed as a intermediate product of U(VI) reduction to U(IV) consistent with the mechanism that U(VI) reduction is one-electron transfer followed by disproportionation of U(V). XPS measurement confirmed the

reduction of U(VI) in Fe(II)/HFO. XP spectra shifted to the lower binding energies as reaction proceeded indicating decrease of U valence state and occurrence of uranium reduction.

4.1 Introduction

Uranium was present at 35% of NPL sites and listed as the most serious hazardous element in radioactively contaminated NPL sites by EPA (73). Dissolution or erosion of naturally occurring uranium, mainly as U(VI), also post immediate threat to the quality of groundwater and surface waters. Uranyl ion, UO_2^{2+}, is the most dominant uranium species in aerated aqueous phase under pH6. UO_2^{2+} readily complexes with anionic ligands including CO_3^{2-}, OH^-, PO_4^{3-}, F^-, and SO_4^{2-}, and the complexation greatly increases the solubility and mobility of uranium in natural water system (74). Under anoxic and reducing environments uranium forms insoluble uraninite (UO_2), which was proposed to be a remediation technique to decrease the mobility of uranium in groundwater (2, 75, 76).

Ferric (oxyhydr)oxides are ubiquitous mineral phases in soils and sediments. Hydrous ferric oxide (HFO) is produced during rapid precipitation in engineered and natural systems and is commonly observed as a weathering product of iron minerals. HFO is highly porous and poorly crystalline, and is an important sorbent for organic and inorganic compounds, especially trace metals, phosphate and other ligands, and some organic compounds (1, 35, 77). HFO occurs as ~2 nm primary particles that aggregate into larger flocs. HFO is a meta-stable solid phase and subject to Ostwald ripening effect and transformation with or without the presence of other transition metals (34, 48, 78-80). Pedersen et al. considered HFO a dynamic phase, and reported exchange of structural Fe(III) for aqueous Fe(II) along with the transformation of HFO into lepidocrocite and goethite (77).

Various extraction methodologies have been used to recover uranium species from HFO or other mineral lattices, to provide evidence for detemining the nature of interactions between uranium and minerals, and to characterize transformation of the mineral phases. Both bicarbonate ions and phosphate ions are known to form strong complexes with actinides (74, 81, 82), and both ligands are commonly used as reagents for uranium extraction (65, 66). Recently, bicarbonate extraction has been used more often. Bicarbonate is a strong complexing agent for U(VI), resulting in formation of anionic complexes and dramatic reduction in the activity of UO22+ and other hydrolysis species including polymers, and this change in speciation results in effective extraction of sorbed U(VI). U(VI) extraction efficiency as high as 97.9% was reported by Elias et al.(66), using bicarbonate extraction in their study on uranium quantitation procedure. However, the presence of reducing agents and dynamic mineral phases in more complex systems is expected to increase the complexity of both uranium removal processes and operational procedures for quantifying reactions of uranium. The extraction efficiency of uranium from HFO-uranium co-precipitates has been found to decrease due to mineral ripening, surface reductive and oxidative precipitation, occlusion by mineral and oxide coatings, and other solid-water interfacial reactions (24, 72, 81). At low pH, as occurs during extraction using phosphoric acid, increasing solubility of HFO might lead to the exposure of uranium that was occluded by the Fe(III) (oxyhydr)oxide structure. We are not aware of any previous study that has compared the extractability of uranium in carbonate and phosphoric acid solutions.

Uranium is usually identified with U(VI) and U(IV) valence states in minerals; only a few studies reported the potential existence of U(V) in mineral structures (83-85). Aqueous U(V) species are generally considered to be unstable and subject to rapid disproportionation into U(VI) and U(IV) (2, 85-89). Langmuir (74) reported that UO_2^+ could persist in an intermediate Eh range between -0.1V and 0.2V and pH 1-7. However, later researchers (86, 89-91) demonstrated that

acidity tends to destabilize U(V) and trigger disproportionation as described in the following equation:

$$2UO_2^{+} + 4H^{+} \rightarrow UO_2^{2+} + U^{4+} + 2H_2O \quad \text{.....(1)}$$

Homogeneous reduction of uranyl with oxidation of Fe(II) is thermodynamically favorable. It has been reported that Fe(III) (oxyhydr)oxides and other solid phases catalyze the disproportionation reaction (2, 20). However, the second electron-transfer seems to be the rate limiting step for U(VI) reduction. Burns and Finch (84) reported that the reduction of uranyl to U(IV) could be kinetically hindered due to the requirement of two-electron-transfer and the increasing electron-transfer distance resulting from the change of the geometry from U(VI) to U(V) to U(IV). Using molecular dynamics simulation and density functional theory, Wander et al. (92) demonstrated that U(V) is a meta-stable product for triscarbonato uranyl reduction with Fe(II) due to the significant energy barrier of the second electron transfer U(V) to U(IV), and implied that disproportionation of U(V) could be the main pathway for uranyl reduction to U(IV). Renshaw et al. (58) studied the kinetics and mechanism for bioreduction of U(VI). They also showed that disproportionation of U(V) was the main pathway leading to U(IV) final product by testing their hypothesis with NpO_2^{+}, a U(V) analogue but stable with respect to disproportionation. As a intermediate or end product of uranium reduction, until recently U(V) was greatly ignored due to its instability and rare occurrence in uranium minerals. However, U(V) could play a important role in uranium reduction kinetics and deserves more discussion in studying the migration and transformation of uranium species in soil medium and groundwater system.

The objective of this research was to investigate the effectiveness of two extractants (phosphoric acid and bicarbonate) for characterizing the extent of reduction of U(VI) in the presence of Fe(II) and HFO This study is unusual in that mass balance was performed on all reactants, allowing calculation of stoichiometry between U(VI) and Fe(II). Solid phases were probed using various analytical techniques. Results were used to identify redox speciation of

uranium in the Fe(III) (oxyhydr)oxide lattice and at the solid/water interface and to provide insights into the mechanism of abiotic reduction of U(VI) by Fe(II)/HFO .

4.2 Materials and Methods

4.2.1 Chemicals and Reagents

Chemicals were reagent grade or better. Solutions were prepared using O_2-free DI water, made by purging DI water with N_2 for at least four hours followed by transfer into the anaerobic chamber and open-stirring for at least 3 days. Stock 250 mM Fe(II) was prepared with $Fe(NH_4)_2(SO_4)_2 \cdot 4H_2O$ in the chamber, acidified to pH<1. The calibration and storage of Fe(II) stock solution followed procedures described in Section 2.2.1. HFO was prepared according to the procedures described by Park and Dempsey (26). Briefly, $FeCl_3 \cdot 6H_2O$ was dissolved and then precipitated at pH 6.8, controlled by slow addition of NaOH during 1 hour. HFO contained 2.5, 5.0, 7.5 or 10.0 mM Fe(III) and 0.01 M sodium PIPES (piperazine-1,4-bis-2-ethanesulfonic acid) at pH 6.8. PIPES pH buffer does not significantly affect speciation and complexation of transition metal ions (41, 46) and is commonly used to control pH in systems containing Fe(II)/Fe(III) (oxyhydr)oxide. The pH was measured at the end of each experiment.

4.2.2 Anoxic environment

All experiments were performed at 26 to 28ºC inside an anaerobic chamber (Coy Laboratory Products, Inc.). Reactors were additionally isolated from the chamber gas by an O_2-trap to protect against trace O_2 as described in Chapter 2. In order to eliminate CO_2 in the

chamber air and CO_3^{2-} in the reactor, the chamber atmosphere was continuously circulated through a NaOH solution.

4.2.3 Analyses

Procedures for handling U(VI) stock solutions, sample handling,and analysis of uranium concentrations are described in Section 3.2.3. Both 0.17M $NaHCO_3$ and 0.5N phosphoric acid were used as extraction reagents. All samples for measurement of U(VI) were diluted to keep chloride less than 1mM to avoid interference in the KPA measurement.

Dissolved Fe(II) and solid-associated Fe(II) were determined using techniques described in Section 3.2.3.

X-ray photoelectron spectroscopy (XPS) analysis was performed using a Kratos Axis Ultra spectrometer with Monochromatic Al K-alpha as the X-ray source. System pressure during analysis was set at mid 10^{-8} torr and the charge neutralizer was set at the "on" position. All analyses used 80 eV pass energy for surveys and 20 eV pass energy for high-resolution scans.

X-ray diffraction (XRD) analysis was performed using a Scintag PAD V diffractometer with CuKα source. Data were collected every 0.02º for 2θ with a scan rate of 2 deg/minute from 5º to 70º 2θ.

4.2.4 Experimental Procedure:

The experimental conditions and initial reactant concentrations are listed in Table 4-1. The experimental setup and procedure was similar to that used in the Fe(II)/Fe(III)/U(VI) system described in section 3.2.4. Freeze-dried samples were prepared for XRD and XPS analysis by filtering samples with 25-mm syringe filter holder/0.2μm Pall membrane disc filter. The retentate

and disc filters were then retrieved from filter holder, placed into an air-tight scintillation bottle, and stored in a -80ºC freezer. The freeze drying procedure was performed at -40ºC for 24 hours with FreeZone Freeze Dry System (Labconco Co.)

4.3 Results and Discussions:

4.3.1 Fe(II)/U(VI) redox kinetics

The freshly prepared HFO samples were analyzed by XRD and results are shown in Figure 4.1(a). The XRD pattern shows that hematite was the dominant phase followed by Fe_2O_3 and ferrihydrite. Using Mössbauser spectroscopy Park and Dempsey (26)confirmed that HFO was produced with the identical procedure. It's possible that the dehydration step during freeze drying resulted in transformation of the HFO sample. Transformation of ferrihydrite to hematite has been reported by previous researchers after heating (93, 94). The XRD pattern of the freeze-dried sample from an HFO stock solution prepared as described in Section 3.2.1 is shown in Figure 4.1(b). The HFO stock solution was aged up to 2 months, and the XRD pattern shows a much stronger characteristic peak of goethite than for freshly prepared HFO.

The experimental conditions and some overall results of the experiments in this study are reported in Table 4-1. Concentrations of reactants and products versus time of reaction are shown in Figure 4-2 for all experiments**.** Gradual disappearance of $U(VI)_{total}$, $U(VI)_{bicarbonate}$ (bicarbonate extractable U(VI)), and $U(VI)_{phosphate}$ (phosphate extractable U(VI)) and $Fe(II)_{total}$ was observed after U(VI) was added to the Fe(II)/HFO suspension. $U(VI)_{diss}$ quickly diminished as most of the U(VI) was associated with solids (>98%). $U(VI)_{bicarbonate}$ decreased in the first 6 hours of reaction and a lag period was observed before $U(VI)_{bicarbonate}$ started to decrease in a second stage of

reaction. The rate of Fe(II)/U(VI) reaction with freshly prepared HFO was an order of magnitude slower than reaction in HFO solution made with aged stock solution, as reported in Chapter 3.

The lag phase and second stage reaction was not significant for $U(VI)_{phosphate}$. Instead, $U(VI)_{phosphate}$ seemed to stay stable after first stage reaction. Both $U(VI)_{bicarbonate}$ and $U(VI)_{phosphate}$ can be approximately modeled in the first stage of reaction with a pseudo-first-order rate equation, rate = k_{obs} [U(VI)], as shown in Figure 4-2. In the first stage of reaction, we observed the simultaneous decreases of $Fe(II)_{total}$, $U(VI)_{bicarbonate}$, and $U(VI)_{phosphate}$. Therefore, it's reasonable to conclude that the Fe(II)/U(VI) redox reaction dominated in the first stage and the reaction followed 1st order rate law in our experimental conditions. The U(VI) reduction rate is slower in the second phase compared with the first phase reaction despite excessive Fe(II) present in the system. Based on above observation, the lag phase and the slower second phase reaction could be due to multiple reactions including phase transformation of Fe(III) solids, co-precipitation of iron and uranium, and occlusion of U(VI) by UO_2 or iron oxide coating. Transformation of Fe(III) (oxyhydr)oxides leads to change in redox potential and surface reactivity (1, 48). Co-precipiatation of U(VI) and Fe oxide, and occlusion of U(VI) by UO_2 or $Fe(OH)_3$ coating has also been reported by previous researchers (69, 72).

4.3.2 $U(VI)_{bicarbonate}$ versus $U(VI)_{phosphate}$

Three additional observations from these experiments are as follows: (1) the ΔFe(II)/ ΔU(VI) molar ratio was close to 2, and therefore consistent with reduction of uranium from +VI to +IV, only for phosphoric acid extraction for experiment 1 with 2.5mM HFO; (2) the apparent removal of U(VI) using bicarbonate extraction ($\Delta U(VI)_{bicarbonate}$) was twice that observed with the phosphoric acid extraction ($\Delta U(VI)_{phosphate}$) and this was observed in all experiments; and (3),

substantial U(VI) residual remained un-reacted in experiments 2, 3 and 4 even though there was stoichiometric excess of Fe(II).

$\Delta Fe(II)/ \Delta U(VI)_{phosphate}$ ratio was about 2 in experiment 1. At first glance, this was the stoichiometry of two-electron transfer from Fe(II) to U(VI). However, for U(VI) to acquire two electrons from two Fe(II) atoms at the same time requires either a appropriate coordination of three monomeric species or direct contact between Fe(II) oligomer and U(VI) atom (68). The possibility of these formations for direct two-electron transfer could be extremely small either in solution or at solid-water interface. Therefore, several researchers have suggested the formation of U(V) species as the intermediate product for U(VI) reduction (2, 82, 84-86, 92). First U(VI) is reduced to U(V) by Fe(II) (2):

$$(\equiv FeO)_2UO_2^0 + \equiv FeO\ FeOH^0 + 3\ H_2O \rightarrow\ 3\equiv FeOH + Fe(OH)_{3(s)} + UO_2\ (OH)^0_{aq} \quad .....(2)$$

U(VI) U(V)

It has been reported that U(V) species are highly unstable in circumneutral pH and readily disproportionate into U(VI) and U(IV) (2, 85-89):

$$2UO_2\ (OH)^0_{aq} + 2 \equiv FeOH \rightarrow\ (\equiv FeO)_2UO_2^0 + UO_{2(s)} + 2H_2O \quad .....(3)$$

U(V) U(VI) U(IV)

By using analytical techniques (84, 85) and computational methods (92), previous researchers suggested that second electron transfer in U(VI) reduction to U(IV) is the rate limiting step. Along with other researcher (2, 58, 90), their results strongly suggested that one electron transfer and the subsequent disproportionation is the main pathway for U(VI) reduction to U(IV). The $\Delta Fe(II)/ \Delta U(VI)$ stoichiometric ratio for this one electron transfer and the subsequent disproportionation pathway of uranium reduction would also be 2. Lower $\Delta Fe(II)/ \Delta U(VI)$ ratios were observed with higher HFO concentrations. The increasing uranium uptake could be due to the occlusion and bonding of uranium by the Fe(III) oxyhydroxide structure.

The ratio of consumed $U(VI)_{bicarbonate}$ ($\Delta U(VI)_{bicarbonate}$) versus consumed $U(VI)_{phosphate}$ ($\Delta U(VI)_{phosphate}$) was about 2:1 for all experiments as shown in Table 4-1. There are two possible explanations for this finding. There are several reactions could have occurred in the Fe(II)/HFO/U(VI) system including but not limited to reductive precipitation, oxidation precipitation, and Fe(III)/U(VI) co-precipitation (69, 72). These reactions could lead to the formation of coating and patches of uraninite and Fe(III) (oxyhydr)oxide or incorporation of U(VI) in bulk Fe(III) that can potentially make U(VI) less accessible to the redox reaction at solid-water interface. Bicarbonate is only effective in extracting surface U species (95) and is ineffective in removing U(VI) or U(IV) bounded within Fe(III) structures (72). Therefore, it's reasonable to assume that some of the U(VI) was either occluded by ferric hydroxide and uraninite precipitates or incorporated in structural Fe(III) and was resistant to bicarbonate extraction. Solubility of HFO exceeds total Fe(III) concentration at pH 1.5 when 0.5N phosphoric acid is used as a extraction reagent and solid-associated U(VI) will be more susceptible to phosphoric acid extraction than bicarbonate extraction. Therefore, $U(VI)_{phosphate} > U(VI)_{bicarbonate}$ was observed in all our experiments.

The second scenario is based on one-electron transfer and subsequent disproportionation of U(VI) reduction. If $\Delta U(VI)_{bicarbonate}$ would represent the amount of U(V) produced from the reduction of U(VI), and $\Delta U(VI)_{phosphate}$ could represent the amount of U(V) disproportionating into U(IV). Figure 4-3 shows the mass balance and transformation of uranium species for the proposed U(VI) reduction mechanism. This scenario could happen because previous researchers have shown that U(V) could stay as stable species in carbonate solution by using electrochemical methods in basic condition (82, 96, 97) and by modeling with computational methods (92). Arland (98) suggested that by forming $UO_2^{2+}UO_2^{+}$ complexes, the presence of uranyl could inhibit the disproportionation of UO_2^{+}. In contract to bicarbonate extraction, using phosphoric

acid as a extraction reagent could destabilize U(V) and trigger disproportionation reaction at low pH (86, 89-91) as shown in equation 1.

4.3.3 XPS analysis

Figure 4-4 shows XP spectra of the U4f region for uranyl standard and the evolution of the sample specta with reaction time. XP spectra are adjusted to C1s at 285 eV. Binding energies (BE) of 4f5/2 and U4f7/2 peaks were at 392 eV and 382 eV respectively for U(VI) standard. Satellite features at 4eV above the low and high U4f peaks were also observed consistent with previous XPS studies of U(VI) compounds (99-103). The shifting of XP spectra to the lower binding energies at t=3hr and t=7hr was observed and is diagnostic of the decrease of valence state and uranium reduction. The development of satellite figures at 7 ev above BE U4f component peaks which was not observed in U(VI) standard indicates the increase of U(IV) component in the samples (100, 103, 104). Although we could not identify peaks and satellite features related to U(V) in the XP spectra, the occurrence of U(V) species in Fe(II)/U(VI) reaction cannot be excluded. The identification of U valence states using XPS depends on binding energies of U4f peaks. Previous researchers (99-103, 105) have reported the separation of peaks between U(VI) and U(IV) ranging from 1 ev to 2.1 ev and peak BE for U(V) is expected to land between U(VI) and U(IV). The quantities of the individual uranium species can only be determined by model fitting with standard spectra of all U species. The closeness of U4f peaks for U(IV), U(V) and U(VI) XP spectra and difficulty in acquisition of U(V) mineral and its standard spectrum add to the complexity of data analysis and fitting.

4.4 Conclusions

- HFO was partially transformed into more stable Fe(III) (hydr)oxide phases during storage and after addition of Fe(II) and oxidizing agents. This was consistent with results from other investigators.
- Reduction of U(VI) was initially fast, followed by a lag phase and/or a second stage of reaction which is slower than the first stage. The first stage U reduction can be approximately modeled as pseudo-first-order reaction. The lag phase and slow second stage reduction could have been caused by phase transformation of Fe(III) solids, co-precipitation of iron and uranium, and occlusion of U(VI) by UO_2 or iron oxide coatings.
- Consumed $U(VI)_{bicarbonate}$/Consumed $U(VI)_{phosphate}$ ratios were about 2 in all the experiments. This and additional results indicated that the overall Fe(II)/U(VI) reaction over hours to days could be a one electron transfer process followed by eventual disproportionation of U(V). There are more evidences indicating that higher phosphoric acid extractable U(VI) could be due to inclusion of U(VI) within the unextracted HFO phase, thus more U(VI) could be extracted with phosphoric acid at pH 1.5 compared with bicarbonate extraction.
- Multiple reactions could have occurred with Fe(II)/U(VI) in freshly prepared HFO solution including redox reaction between Fe(II) and U(VI), phase transformation of Fe(III) (oxyhydr)oxide and $UO_{2(s)}$, co-precipitation of uranium with Fe(III) (oxyhydr)oxides, occlusion of U(VI) by Fe(III) (hydr)oxide and uraninite, and other adsorption/substitution reactions.
- Amount of U species with valence states lower than U(VI) increased as Fe(II)/HFO/U(VI) reaction proceeded based on the observation of satellite features in U4f XPS spectra, which indicated the potential existence of U(IV) and U(V) species.

Table 4- 1 Conditions and results in Fe(II)/Fe(III)/U(VI) experiments. All experiments were performed in a strictly anoxic reactor at 26°C at pH 6.8. U(VI) was added 25 min after addition of Fe(II).

No	Initial Fe(II), μM	Initial U(VI) ,μM	ΔFe(II)/ ΔU(VI), bicarbonate extraction	ΔFe(II)/ ΔU(VI), phosphate extraction	ΔU(VI) carbonate vs ΔU(VI) phosphate	HFO mM Fe(III)	k_{obs-1} (hr^{-1}), carbonate extraction	k_{obs-1} (hr^{-1}) phosphate extraction
1	139	19.8	0.82	2.12	2.59	2.50	0.062	0.031
2	147	29.6	0.61	1.20	1.98	5.00	0.061	0.067
3	148	18.3	0.43	0.78	1.82	7.50	0.049	0.033
4	143	18.2	0.58	1.07	1.85	10.00	0.060	0.040

Figure 4- 1 (a) XRD pattern of freshly prepared HFO solution. (b) XRD pattern of stock HFO solution.

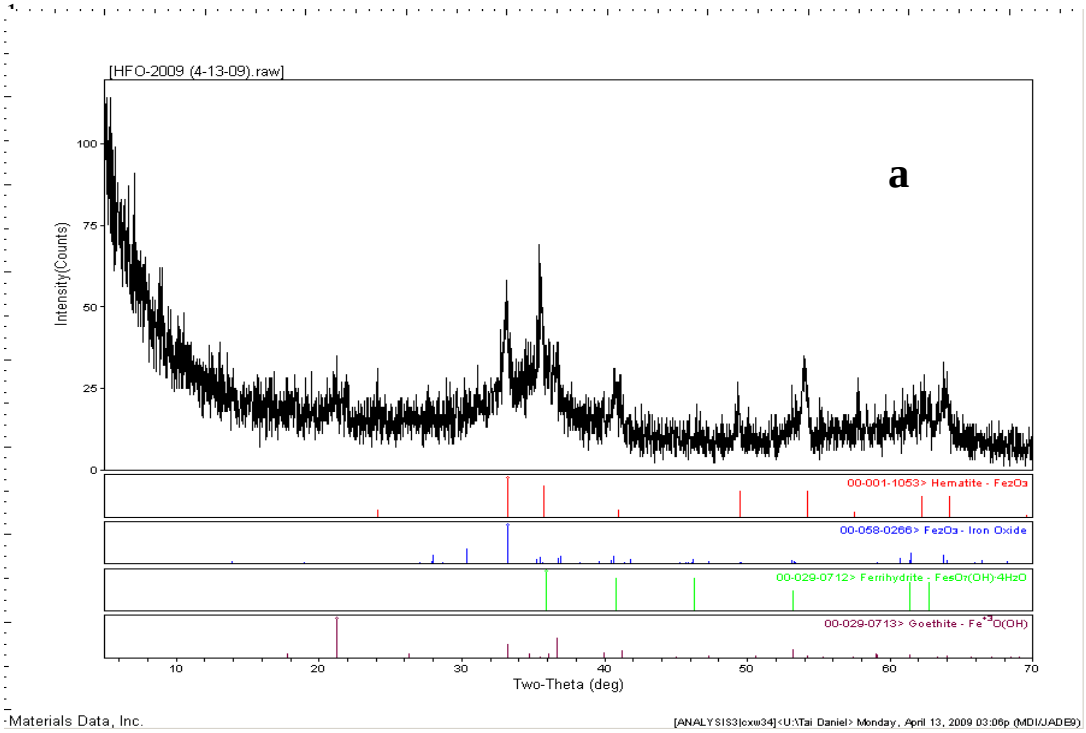

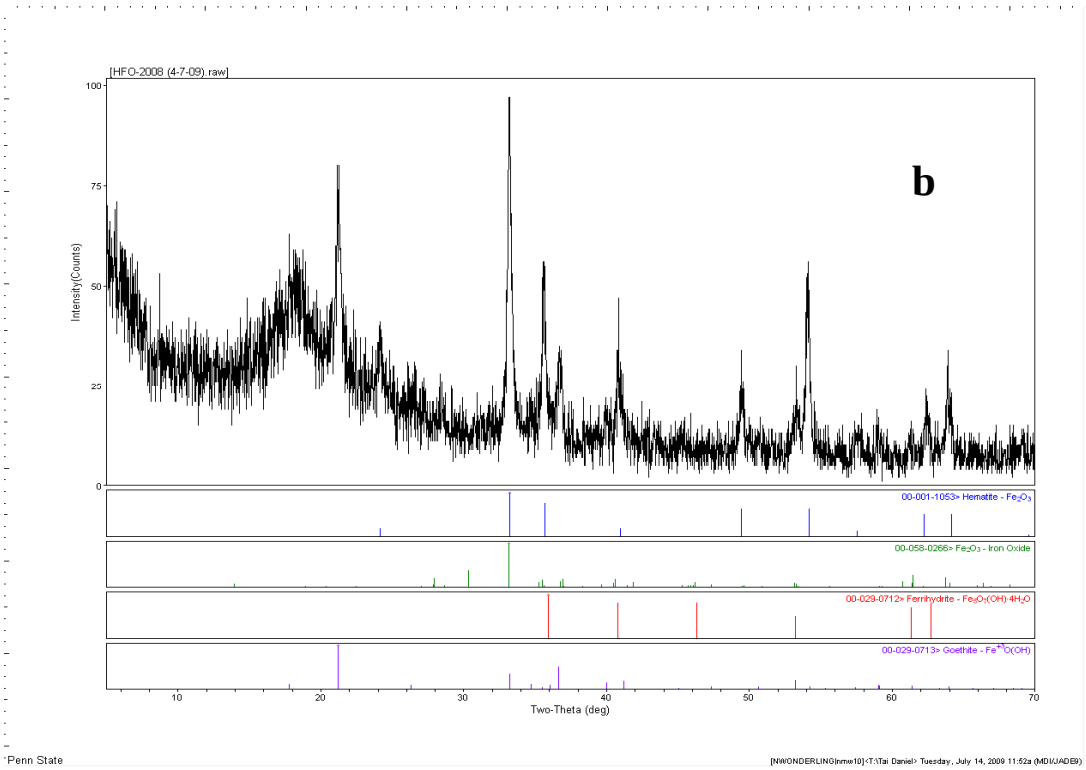

Figure 4- 2 Results for Fe(II)/HFO/U(VI) experiments: pH=6.8, 26-28ºC, (▲) $U(VI)_{bicarbonate}$, (Δ) $U(VI)_{phosphate}$, (+)$U(VI)_{diss}$, (●) $Fe(II)_{total}$, (◆) $Fe(II)_{diss}$. Panels show experiments using (a) 2.5mM HFO, (b) 5mM HFO, (c) 7.5mM HFO, (d) 10mM HFO. Solid line shows modeling of $U(VI)_{bicarbonate}$ and dashed line shows modeling of $U(VI)_{phosphate}$ both with 1st order rate law. Error bars show one standard deviation of two duplicate experiments.

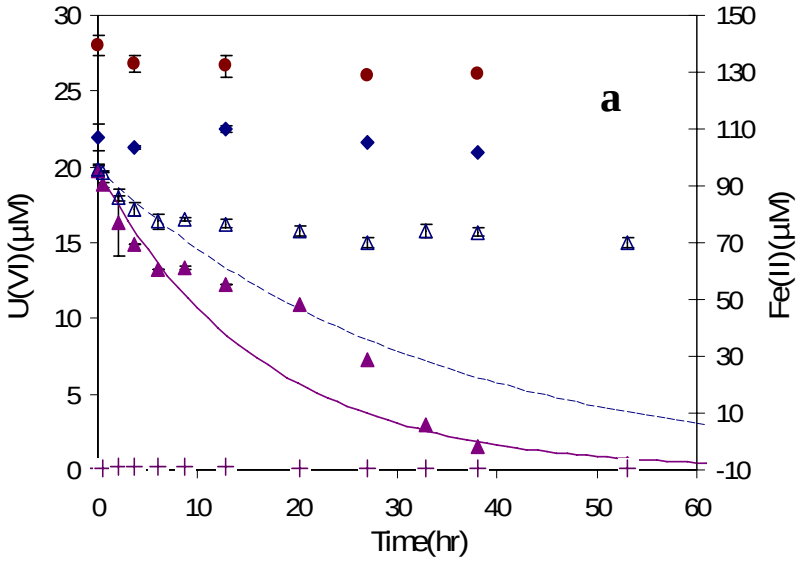

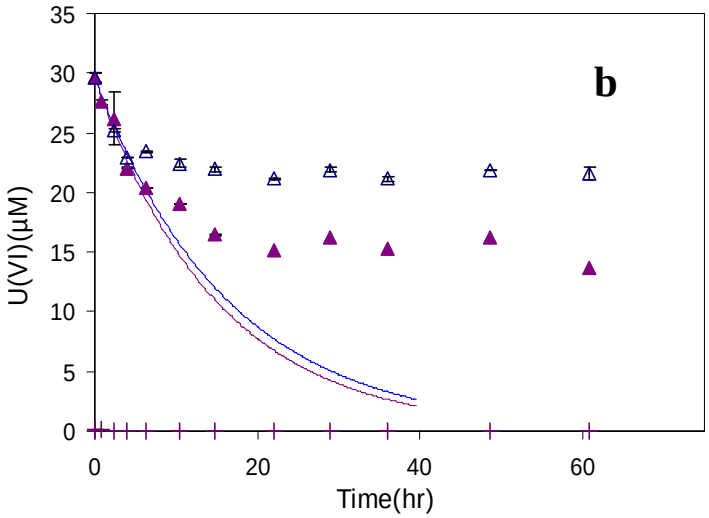

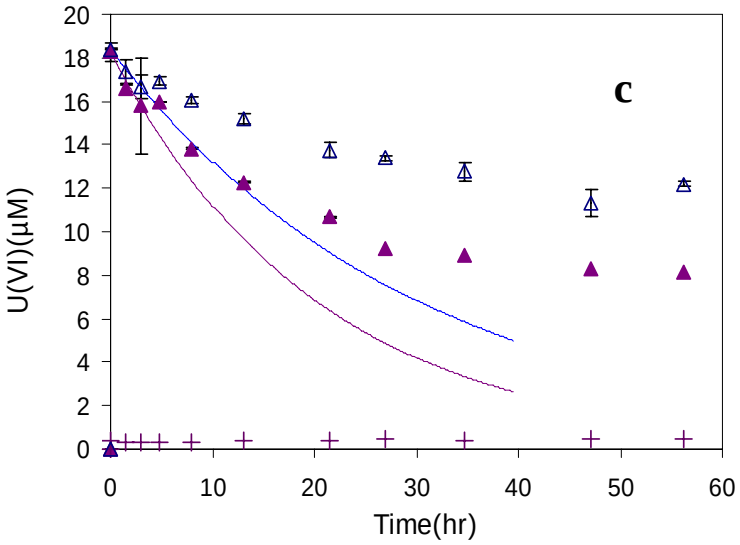
c
U(VI)(μM)
Time(hr)
0
2
4
6
8
10
12
14
16
18
20
0
10
20
30
40
50
60

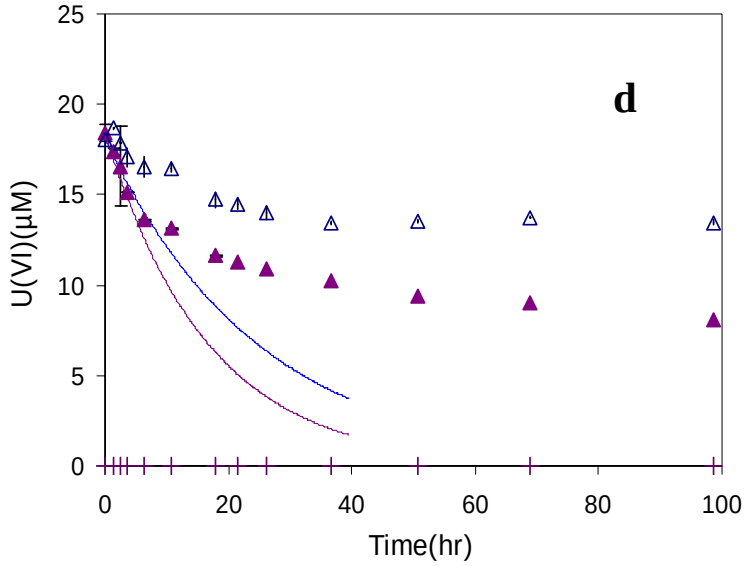
d
U(VI)(μM)
Time(hr)
0
5
10
15
20
25
0
20
40
60
80
100

Figure 4- 3 $\Delta U(VI)_{bicarbonate}$ versus $\Delta U(VI)_{phosphate}$ diagram during disproportionation of U(V)

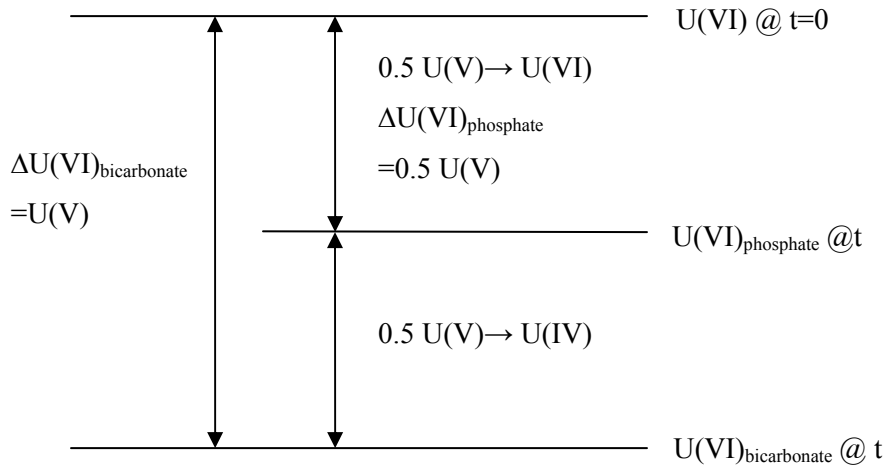

Figure 4- 4 XP spectra of the U4f region for uranyl standard(▼), samples collected at t=3 hr(■) and t=7 hr (♦). Satellite features at about 6.7 eV on the higher binding energy sides indicate the increase of U(IV) component in the samples. Binding energies were adjusted to C1s at 285 eV.

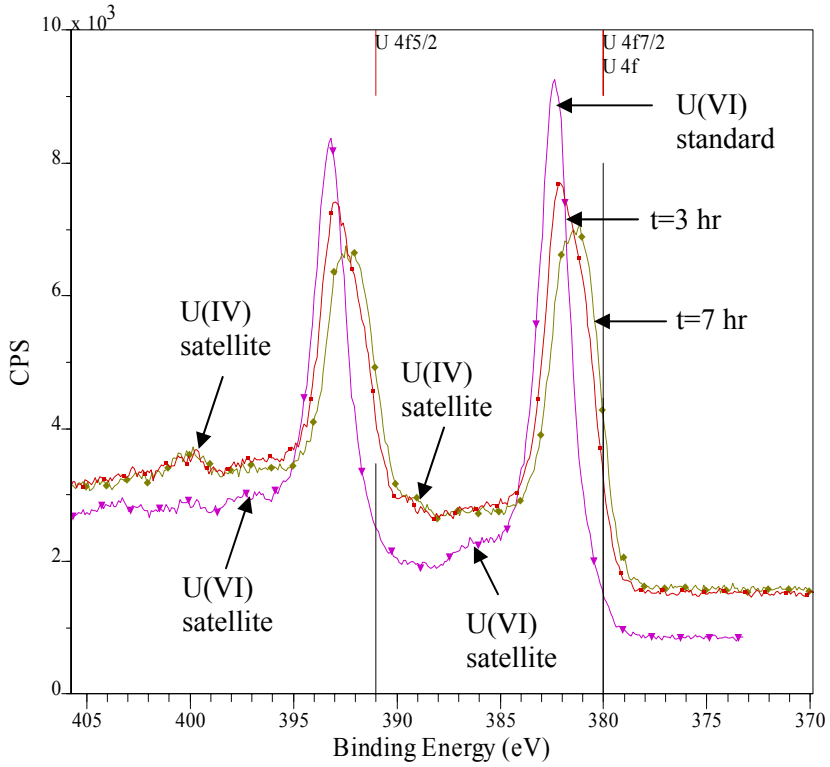

Chapter 5 Simulation of Redox Reaction between Nitrite Ion and Ferrous Ion Mediated by Goethite (010) Surface – a Quantum Mechanical Study

Abstract

Three models including homogeneous model, heterogeneous model/direct ET and heterogeneous model/indirect ET were built based on our experimental observations on Fe(II)/NO_2^- redox reaction in Fe(III) (oxy)hydroxide solution and quantum chemical calculation were performed using Gaussian 03 to determine the thermodynamically favorable pathway for the reaction. Molecular orbital/density function theory (MO/DFT) was employed using B3LYP functionals. All-electron 6-31G(d) basis set for H, N, and O atoms and effective core potential (ECP) basis set (CEP-121G) for Fe atoms was used to determine minimum potential energy structures for the reactants, intermediate products and products on the model electron transfer pathways. MO/DFT calculation showed that in homogeneous model Fe(II)/NO_2^- redox reaction in aqueous phase is thermodynamically favorable by the formation of inner-sphere Fe – O – N – O – Fe complex. By forming inner-sphere surface complexes, heterogeneous Fe(II)/NO_2^- redox reaction with direct electron transfer pathway is also thermodynamically favorable. NBO population analysis showed sorbed Fe(II) became more oxidized than dissolved Fe(II) in the model product in heterogeneous system indicating that sorbed Fe(II) could be the electron donor in Fe(II)/NO_2^- redox reaction. Heterogeneous Fe(II)/NO_2^- redox reaction with indirect electron transfer pathway is thermodynamically unfavorable with a slightly positive reaction energy. Density functional theory (DFT) calculation of Fe(II)/NO_2^- redox reaction on periodic Fe(III) (oxyhydr)oxide structure using Vienna Ab Initio Simulation Package (VASP) is under way to justify thermodynamic data of indirect pathway.

5.1 Introduction

Fe(II)/Fe(III) redox couple is of key importance in natural and engineered water environments. Fe(II)/Fe(III) cycling is relatively fast and can occur over the entire range of E_h in natural water systems, thus affecting the speciation and mobility of a wide range of natural and contaminant species in soils and groundwater (1, 37). Fe(II) in combination with Fe(III) oxyhydroxide and other iron-containing minerals often provides increased reactivity for the transformation of a variety of organic and inorganic pollutants (2, 3, 7, 8, 20, 41, 59-61). Heterogeneous oxidation of Fe(II) has been extensively studied and kinetic data for many solid phases and oxidants have been published (3, 6, 59, 61). However, the existing mechanistic explanations for Fe(II)/oxidant reactions have been diverse.

Previously we studied the stoichiometry, rate, and mechanism of heterogeneous oxidation of Fe(II) with the reduction of nitrite in the absence and presence of hydrous ferric oxide (HFO) (22). HFO is ubiquitous in natural and engineered environments. Oxidation of Fe(II) by nitrite was negligible in the absence of HFO. With HFO, solid-bound Fe(II) remained relatively constant until most of the dissolved Fe(II) had reacted, similar to previous observations by Park and Dempsey (26). We reported $d[Fe(II)]/dt = -k_{overall} \cdot [Fe(II)_{diss}] \cdot [Fe(II)_{solid\text{-}bound}] \cdot [NO_2^-]$. Two reaction mechanisms were proposed based on our experimental observations: a direct electron transfer pathway, in which a Fe(II) nitrito complex could be reduced in contact with solid-bound Fe(II) or with dissolved Fe(II) as the electron donor through inner sphere electron transfer; and an indirect electron transfer pathway in which oxidation and reduction occurred at different sites, resembling the anode-cathode effect as proposed by Park and Dempsey (26) based on their heterogeneous Fe(II) oxidation study using oxygen as oxidant.

The objective of this research was to use quantum mechanical theory to simulate homogeneous and heterogeneous oxidation of Fe(II) with the reduction of NO_2^- in order to

determine the possible and most favorable pathway for the reaction. The reactant, intermediate product and product configurations were constructed based on our wet experimental observations of Fe(II)/NO_2^- reactions in the presence of HFO. Quantum mechanical calculation of energies on model components along the proposed reaction pathways could determine the reaction direction on the electron transfer pathway. We also performed NBO population analysis on all models to determine the natural charge of all elements in order to investigate the distribution of electron density and identify electron donor/acceptor relationship on the reaction pathway. The determination of HFO (ferrihydrite after dehydration) structure is still in debate due to its low degree of order. Therefore, we created a goethite (010) surface with Fe(III) ions stacked along [010] coordinate and occupying half the octahedral interstices to simulate Fe(III) oxyhydroxide surface configuration. The Fe(III) ions are surrounded by two H_2O and four OH^- at the corners and surrounded by six OH^- at the center.

5.2 Materials and Methods

The mechanism of redox reaction is tested by comparing the thermodynamic parameters and electron distribution of reactant, intermediate product and product in the proposed redox reaction using quantum chemical calculation. Molecular structures were created sing Cerius2 (Accelrys Software Inc.). A series of models were created to simulate one-electron-transfer between NO_2^- and Fe(II) in both homogeneous and heterogeneous systems. In heterogeneous system, both direct and indirect electron transfer between Fe(II) and NO_2^- were simulated in order to investigate the probable electron transfer pathway at solid-water interface. Table 5-1 lists the components and formula for reactants, intermediate product and products in this study and Figure 5-1, 5-2, and 5-3 show all the configurations used in quantum chemical calculations. Charges of all the models are adjusted with OH^-/OH_2 functional groups terminating the models so that the

total charges are +3 for homogeneous reaction models and +1 for heterogeneous reaction models. Quantum chemical calculations do not explicitly take into account the pH parameter (106). However, the structures are set up to model reactions occurring at or below their pH of zero charge (pH_{pzc}), i.e. around neutral pH on ferric oxide cluster. Sorbed Fe(II) is attached to the ferric oxide cluster through Fe(III)-O-Fe(II) bonding.

Quantum chemical calculations were performed using Gaussian 03 (107). Molecular orbital/density function theory (MO/DFT) was employed using B3LYP functionals (108, 109). All-electron 6-31G(d) basis set for H, N, and O atoms and effective core potential (ECP) basis set (CEP-121G) for Fe atoms was used to determine minimum potential energy structures. Relativistic ECP basis set was used to increase the computational efficiency. Fe(III) atoms and the surrounding oxygen and hydrogen atoms in the ferric cluster were constrained to mimic the rigid surface of ferric oxyhydroxide. The constraint of Fe(III) and neighboring atoms helps to maintain the complete structure of the cluster and greatly increase computation efficiency. The high-spin state of Fe(III) with s=5/2 was specified for Fe(III) clusters. For the homogeneous reaction models all elements were relaxed and frequency calculations were performed to verify the potential energy minima on the optimized model configurations. Natural bond orbital (NBO) population charge analyses are carried out on all the models to determine the differences in charge distribution between reactants and products.

5.3 Results and Discussions

5.3.1 Modeling of homogeneous Fe(II)/NO_2^- reaction

Energies of reactants, intermediate products, and product in homogeneous model are shown in Table 5-2 and the energy-minimized structures are shown in Figure 5-1. Fe(II)/NO_2^-

reaction in aqueous phase is an exergonic reaction, because the energy of product is lower than that of reactant. Therefore homogeneous Fe(II)/NO_2^- redox reaction is thermodynamically a spontaneous reaction. Intermediate product in homogeneous Fe(II)/NO_2^- system was modeled as $(H_2O)_5$·Fe(II) – O – N– O – Fe(II)·$(H_2O)_5$ inner-sphere complex. The above intermediate product configuration is not a transition structure because frequency calculation of intermediate product could not find an imaginary frequency. The activation energy of this reaction pathway is about 31 kJ/mol as shown in Table 5-2.

5.3.2 Modeling of heterogeneous Fe(II)/NO_2^- reaction at solid-water interface

The direct mechanism of heterogeneous Fe(II)/NO_2^- redox reaction was tested by setting up the inner sphere quaternary surface complex, ≡Fe – O – Fe – ONO – Fe, as the intermediate product and carrying out quantum chemical calculations to derive the energies of optimized configurations for reactant, intermediate product, and product of redox reaction. All the model components on the pathway are listed in Table 5.1 and the energy-minimized structures are shown in Figure 5-2. As shown in Table 5-2, the direct mechanism follows inner sphere electon electron pathway and is thermodynamically favorable due to its negative reaction energy. We did not find a transition state intermediate product since the intermediate product being evaluated has a lower energy than reactants.

The indirect mechanism was modeled with an outer sphere electron transfer pathway. Dissolved Fe(II) and sorbed Fe(II) were positioned further away from each other than in direct electron transfer mechanism to simulate the anode-cathode electron transfer pathway. Electron transfer mechanism was studied with proton coupled electron transfer (PCET) reaction where a proton was associated with the nitrite ion as an intermediate step for the redox reaction. All the components on the pathway are listed in Table 5.1 and the energy-minimized structures are

shown in Figure 5-3. The indirect electron transfer pathway was found to be an endergonic reaction due to its positive reaction energy as shown in Table 5-2. The pathway is accompanied by a ΔE_r of 10.2 kJ/mol, which is not a huge variation in energy change between reactant and product. However, a relatively large activation energy of 74.2 kJ/mol does reflect the disadvantage of outer sphere electron transfer compared with inner sphere electron transfer.

5.3.3 Comparison of homogeneous and heterogeneous Fe(II)/NO_2^- reaction

The results of quantum mechanical calculations show that inner-sphere Fe(II)/NO_2^- electron transfer in both homogeneous and heterogeneous environments are exergoic reactions and can proceed spontaneously. It is surprising that a larger driving force for homogeneous Fe(II)/NO_2^- redox reaction was obtained using quantum mechanic calculation than heterogeneous reaction. However, in order for the redox reaction to happen in the aqueous phase, Fe(II) and nitrite ions have to encounter each other and form complexes at appropriate orientation. Hence, in dilute solution, the redox reaction is unlikely to occur at a significant rate without the presence of solids. Moreover, a high mole ratio of Fe(III)/Fe(II) (4~50) was used in our experiments. Semiconductor characteristics of Fe(III) oxide (34) and the fast transformation of Fe(III) oxyhydroxide with sorbed Fe(II) leading to a lower redox potential and stronger reducing power might facilitate the electron transfer process in a heterogeneous system.(110, 111).

Direct electron transfer is thermodynamically more favorable pathway by comparing the reaction energies of two pathways in Table 5-2. The model intermediate product in indirect mechanism is problematic since a relatively large activation energy was derived. However, a ΔEr of 10.2 kJ/mol is not thermodynamically impossible to overcome. We are also conducting quantum mechanical calculation on Fe(II)/NO_2^- reaction using Vienna Ab-initio Simulation Package (VASP) for periodic iron oxyhydroxide structure to compare the energetics of direct and

indirect mechanism. Our simulation of Fe(II)/NO_2^- reaction using Gaussian 03 on iron oxyhydroxide cluster also implies that inner-sphere electron transfer (direct mechanism) is more efficient than outer-sphere electron transfer (indirect mechanism).

5.3.4 NBO population analysis

NBO population analysis was performed for reactants, intermediate product, and product configurations in both direct and indirect electron transfer pathways to study the natural charges and valence changes for each component. The complete NBO output is attached in Appendix C. The natural charges of all the iron atoms in reactant, intermediate product and products are shown in Table 5-3 and Table 5-4. The first three Fe atoms represent the Fe(III) oxyhydroxide cluster followed by dissolved Fe(II) and sorbed Fe(II) atoms. In direct electron transfer pathway, there was an increase of the natural charge on Fe_{sorb}, whereas charge of Fe_{diss} was not significantly changed between reactant and product stages. This result showed that sorbed Fe(II) is most likely the electron donor in Fe(II)/NO_2^- redox reaction. We observed the similar trend in indirect electron transfer pathway in which Fe_{sorb} in product configuration was more oxidized than Fe_{diss}. However, NBO population analysis of indirect electron pathway could be bias since there was not clear difference on natural charges between Fe(III) cluster, dissolved Fe(II) and sorbed Fe(II). This could be due to the original set up of the indirect electron transfer pathway in which $Fe(II)_{sorb}$ was positioned at the corner of the Fe(III) cluster and therefore treated as one of the structural Fe(III) atoms by Gaussian 03. Further investigation with VASP could provide more information on the effect of sorbing Fe(II) on periodic Fe(III) oxyhydroxide structure and indirect electron transfer mechanism of Fe(II)/NO_2^- redox reaction.

The decrease of charge on N atoms reflected that nitrogen ion was the electron acceptor for direct electron transfer pathway as shown in Table 5-3. The decrease in natural charge on N

atoms from reactant to product structure in indirect electron transfer pathway was not as significant as in direct electron transfer pathway in Table 5-4. This is consistent with our result in thermodynamic calculation in previous session.

5.4 Conclusions

Our modeling of Fe(II)/NO_2^- redox reaction in both homogeneous and heterogeneous systems using quantum mechanical calculations provides an alternate way to investigate the thermodynamics and mechanism of the reaction. The models were constructed based on the results from our wet chemistry study on Fe(II)/NO_2^- redox reaction (22). Based on simulation of Fe(II)/NO_2^- redox reaction using quantum mechanical calculation, the following conclusions were made.

- Fe(II)/NO_2^- redox reaction in aqueous phase is thermodynamically favored by the formation of inner-sphere Fe – O – N – O – Fe complex. In dilute solution, the formation of inner-sphere complexes could be the rate-limiting step for homogeneous Fe(II)/NO_2^- redox reaction. Therefore, this reaction did not occur at a significant rate over hours to days in our wet experiments.
- By forming inner-sphere surface complexes, heterogeneous Fe(II)/NO_2^- redox reaction with direct electron transfer pathway is thermodynamically favorable. Solid-bound Fe(II) was conservative while dissolved Fe(II) decreased stoichiometrically with reduction of nitrite in our wet experiments. While it has been demonstrated that solid-bound Fe(II) can be distributed within the bulk Fe(III)(oxy)hydroxide phase, perhaps a fraction of solid-bound Fe(II) (or Fe(II)-nitrito complexes) are at the solid-water interface.
- Heterogeneous Fe(II)/NO_2^- redox reaction with indirect electron transfer pathway is thermodynamically unfavorable in this simulation.

- Based on the observation of our modeling on direct and indirect electron transfer pathway, inner-sphere electron transfer is more efficient than outer-sphere electron transfer mechanism.
- Sorbed Fe(II) became more oxidized than dissolved Fe(II) in the model product in heterogeneous system. Therefore, sorbed Fe(II) could be the electron donor in Fe(II)/NO_2^- redox reaction.

Table 5- 1 Configurations of reactants, intermediate products, and products used in simulation of electron transfer process between Fe(II) and NO_2^- .

Configuration	Reactants	Intermediate products	Products
Homogeneous System (AqueousPhase)	$2[Fe(II)\cdot(H_2O)_6]^{2+}$ and NO_2^-	$[Fe(II)\cdot(H_2O)_5$ ---NO_2 --- $Fe(II)\cdot(H_2O)_5]^{3+}$	$[Fe(II)(OH)\cdot(H_2O)_5]^+$, NO, $[Fe(III)(OH)\cdot(H_2O)_5]^{2+}$, and H_2O
Heterogeneuos System (direct electron transfer mechanism)	$Fe(III)_3(OH)_9$ $(OH_2)_4OFe(II)\cdot(H_2O)_5$, NO_2^-, and $[Fe(II)\cdot(H_2O)_6]^{2+}$	$[Fe(III)(OH)_9$ $(OH_2)_4OFe(II)\cdot(H_2O)_5$ ---NO_2--- $Fe(II)\cdot$ $(H_2O)_6]^+$	$[Fe(III)_3(OH)_9$ $(OH_2)_4OFe(II$ orIII) $(OH)\cdot(H_2O)_4]$, NO, [Fe(II or III) (OH)· $(H_2O)_5]$and H2O
Heterogeneuos System (indirect electron transfer mechanism)	$Fe(III)_3(OH)_9$ $(OH_2)_4OFe(II)\cdot(H_2O)_5$, NO_2^-, and $[Fe(II)\cdot(H_2O)_6]^{2+}$	$[Fe(III)(OH)_9(OH_2)_4$ $OFe(II)(OH)\cdot(H_2O)_4]^-$, NO_2H, and $[Fe(II)\cdot(H_2O)_6]^{2+}$	$[Fe(III)_3(OH)_9$ $(OH_2)_4OFe(II$ orIII) $(OH)\cdot(H_2O)_4]$, NO, [Fe(II or III) (OH) $\cdot(H_2O)_5]$ and H_2O

Table 5- 2 Reaction energies and energies of reactants, intermediate products, and products calculated using B3LYP functionals and all-electron 6-31G(d) basis set for H, N, and O atoms and CEP-121G basis set for Fe atoms.

Energy (Hartrees)	Reactants (Hartrees)	Intermediate Products (Hartrees)	Products (Hartrees)	Reaction Energy (kJ/mol)	Activation Energy (kJ/mol)
Homogeneous System	-1367.957065	-1367.945238	-1367.981904	-65.21	31.05
Heterogeneuos System (direct electron transfer mechanism)	-2726.193594	-2726.198135	-2726.203787	-26.76	
Heterogeneuos System (indirect electron transfer mechanism)	-2726.241122	-2726.212873	-2726.237237	10.20	74.17

Table 5- 3 NBO charges of reactant, intermediate product, and product configurations for direct electron transfer pathway.

Atom No.	Atom	Reactant	Intermediate Product	Product
1	$Fe_{cluster}$	1.617	1.590	1.581
7	$Fe_{cluster}$	1.616	1.611	1.598
8	$Fe_{cluster}$	1.583	1.593	1.582
17	Fe_{diss}	1.358	1.349	1.381
18	Fe_{sorb}	1.441	1.399	1.715
66	N	0.268	0.316	0.089

Table 5- 4 NBO charges of reactant, intermediate product, and product configurations for indirect electron transfer pathway.

Atom No.	Atom	Reactant	Intermediate Product	Product
1	$Fe_{cluster}$	1.061	1.054	1.074
7	$Fe_{cluster}$	1.073	1.078	1.064
8	$Fe_{cluster}$	1.070	1.054	1.028
17	Fe_{diss}	1.069	1.036	1.016
18	Fe_{sorb}	0.973	0.987	1.181
64	N	0.307	0.365	0.261

Figure 5- 1 Configurations (optimized structure) of reactants, intermediate product, and products used in simulation of electron transfer process between Fe(II) and NO^- in homogeneous system: (a) reactants; (b) intermediate product; (c) products.

Oxygen: Nitrogen: Iron: Hydrogen:

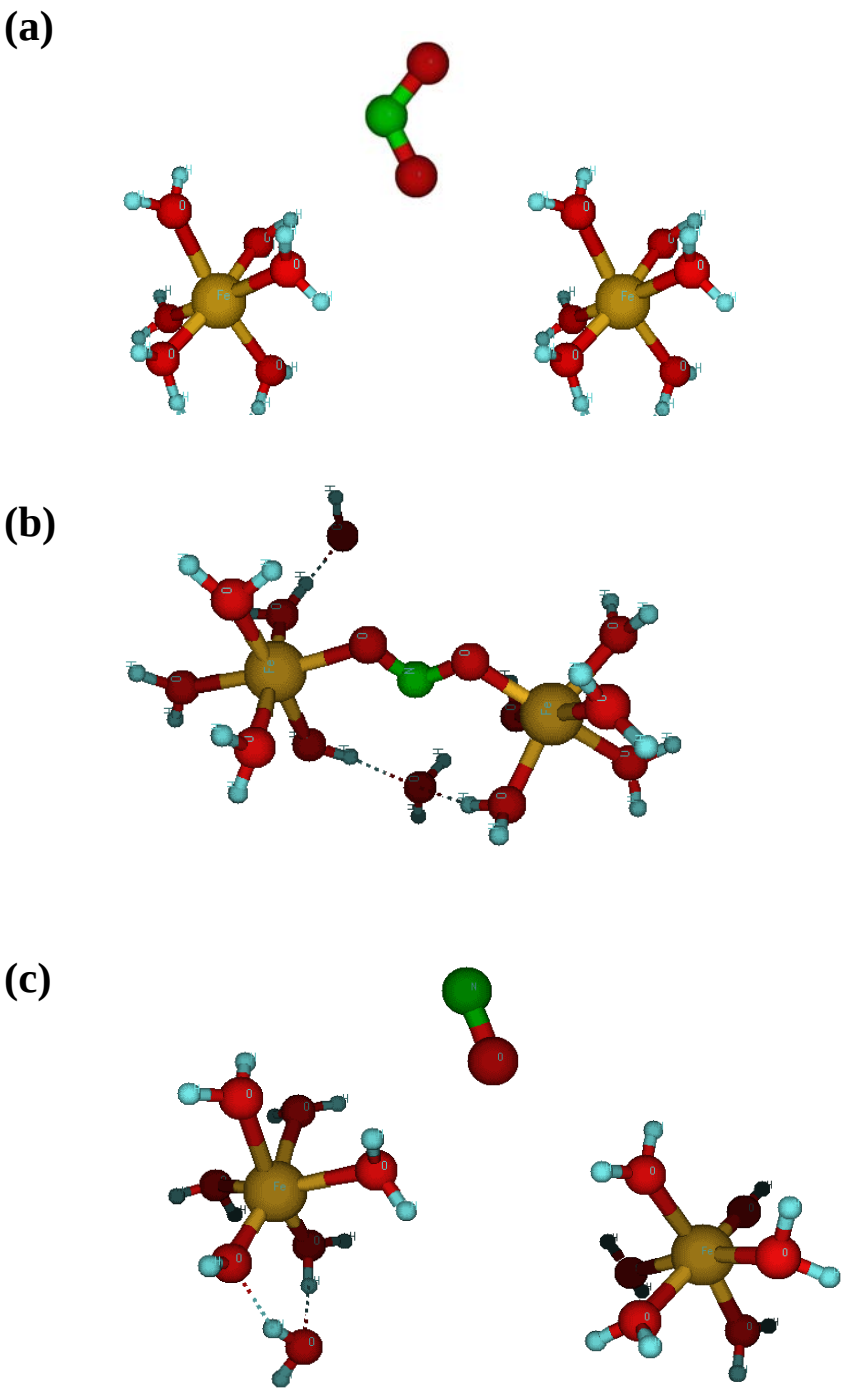

Figure 5- 2 Configurations (optimized structure) of reactants, intermediate product, and products used in simulation of *direct* electron transfer process between Fe(II) and NO^- in heterogeneous system: (a) reactants; (b) intermediate product; (c) products.

Oxygen: Nitrogen: Iron: Hydrogen:

(a)

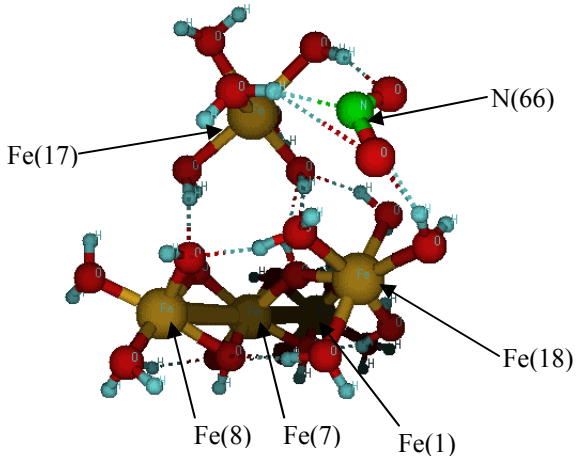

(b)

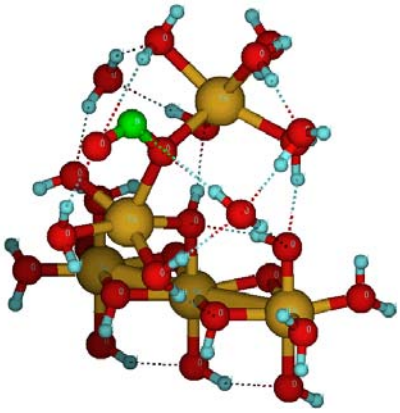

(c)

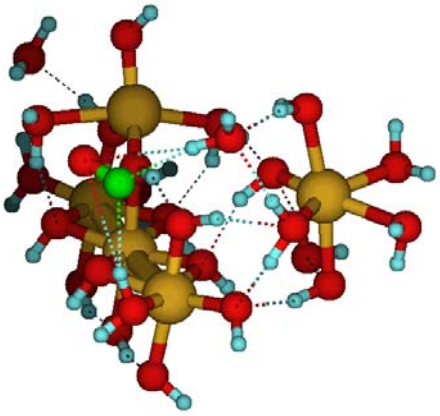

Figure 5- 3 Configurations (optimized structure) of reactants, intermediate product, and products used in simulation of *indirect* electron transfer process between Fe(II) and NO^- in heterogeneous system: (a) reactants; (b) intermediate product; (c) products.

Oxygen: Nitrogen: Iron: Hydrogen:

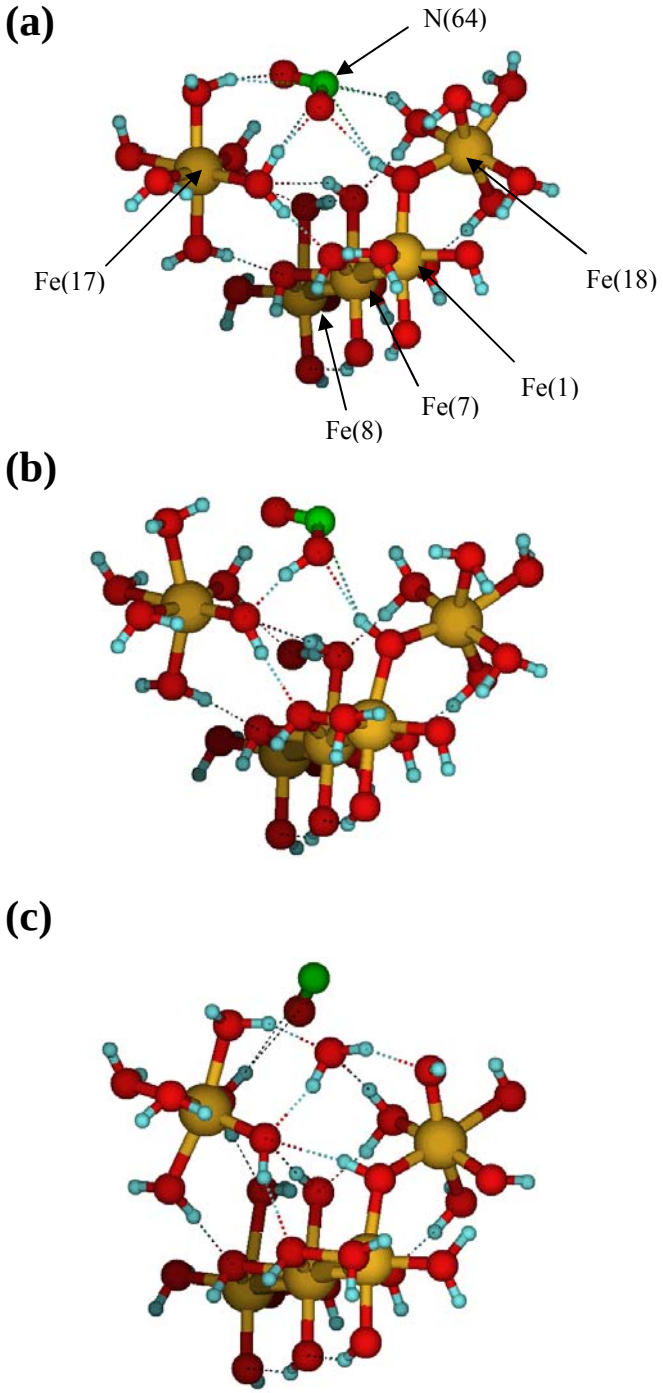

Chapter 6 Conclusions

6.1 Conclusions

This research dealt with the heterogeneous oxidation of Fe(II) by nitrite, arsenate, and uranium using HFO as the catalytical solid phase in a strictly anoxic environment. Reaction stoichiometries and rate laws were derived and reaction mechanisms were proposed based on the experimental observations. A quantum mechanical study was conducted to model the reaction pathways, derive thermodynamic data, and determine the distribution of electron density for reactant molecules in the Fe(II)/HFO/nitrite system. Fast reactions were observed for Fe(II)/HFO/U(VI) and Fe(II)/HFO/NO_2^- . Although no significant reaction was observed between Fe(II) and arsenate for the range of pH and solid concentrations that were tested, the results were included in an appendix of this dissertation to make this information available to other researchers. Based on our wet chemistry observations on Fe(II)/NO_2^- redox reaction, we proposed indirect and direct electron transfer pathways as the main electron transfer mechanisms for between Fe(II) and NO_2^- at the mineral-water interface. Models were set up to simulate these two pathways and quantum mechanical calculations were carried out to provide thermodynamic data of reactant components on the pathway and charges on Fe(II), Fe(III) and N atoms. Based on our observations on Fe(II)/NO_2^- and Fe(II)/U(VI) redox reaction in the presence of HFO and the results from quantum mechanical study, the following conclusions were made.

1) Reduction of nitrite and uranium with Fe(II) at pH 6.8 was catalyzed by the presence of HFO. Reaction was not observed during the experimental timeframe in the absence of the solid phase.

2) The rates of Fe(II)/NO_2^- and Fe(II)/U(VI) heterogeneous redox reaction at pH 6.8 were first-order in both $Fe(II)_{diss}$ and total oxidant concentrations, consistent with the rate equation,

$$rate = -k_{obs} \cdot [Fe(II)_{diss}] \cdot [oxidant]$$

3) The reaction rate constants k_{obs} were proportional to the concentration of solid-bound Fe(II) for Fe(II)/Fe(III) molar ratio < 0.02, resulting in the overall rate equation:

$$rate = - k_{overall} \cdot [Fe(II)_{diss}] \cdot [Fe(II)_{solid\text{-}bound}] \cdot [oxidant]$$

4) Consumed Fe(II)/consumed NO_2^- ratio is about 2 for Fe(II)/NO_2^- experiments, implying that this is a two electron transfer process. However, the stoichiometric ratio for consumed Fe(II)/consumed U(VI) was about one when "U(VI)" was extracted using 1M $NaHCO_3$ and the stoichiometric ratio was about two when extracting with H_3PO_4. These and additional results indicated that the overall Fe(II)/U(VI) reaction over hours to days could be a one electron transfer process followed by eventual disproportionation of U(V). Alternately, the higher phosphoric acid extractable U(VI) could be due to occlusion of U(VI) within the unextracted HFO phase, thus more U(VI) could be extracted with phosphoric acid at pH 1.5 compared with bicarbonate extraction.

5) Solid-bound Fe(II) density was increased by a factor of 3-5 after the addition of U(VI) into Fe(II)/HFO solution compared with Fe(II)/HFO solution without U(VI). The significant increase in solid-bound Fe(II) could be due to the increased concentration of sorption sites resulting from the sorption and reductive precipitation of U(VI) and oxidative precipitation of Fe(II). This finding, along with the observations from other researchers of electron migration at the Fe(II)-Fe(III) (oxyhydr)oxide interface, indicates that the Fe(II)/HFO system is complicated and significantly different than other adsorbent/adsorbate interactions .

6) Solid-bound Fe(II) was conservative after depletion of oxidants, i.e. nitrite and uranium. The immediate predecessor to this work (Park & Dempsey, 2005) was the first wet chemistry evidence of the migration of "Fe(II)" into the bulk Fe(III) (oxyhydr)oxide phase, and those

findings are supported by data from the experimental systems that are reported in this dissertation.

7) The initial increase and then decrease of solid-bound Fe(II) in Fe(II)/HFO/NO_2^- reaction was similar to that previously observed in a Fe(II)/HFO system without any oxidant present. The change in solid-bound Fe(II) in the first 2-4 hr could be attributed to reduced surface area due to partial conversion from HFO to goethite. However, in the presence of uranium, solid-bound Fe(II) increased and remained at higher concentration during the rest of the experiment.
8) The redox reactions in the Fe(II)/HFO/oxidant system were slower for solid-bound Fe(II) density (mol Fe(II)/mol Fe(III)) >0.020~0.026. This result was also consistent with the Park and Dempsey (26) observation of decreased reaction rate at >0.022 Fe(II)/Fe(III) in the Fe(II)/HFO/O_2 system.
9) The reaction rate constants were higher for Fe(II)/HFO/U(VI) than for Fe(II)/HFO/nitrite$^-$. This could be due to the high affinity of U(VI) for the HFO surface (i.e., U(VI) was >98% sorbed while nitrite was ~100% dissolved). Sorption of U(VI) could provide a shorter pathway for the electron-transfer process.
10) Simulation of electron transfer pathways using quantum mechanical calculations concluded that direct electron transfer pathway of Fe(II)/NO_2^- reaction is thermodynamically more preferable than indirect electron transfer pathway. In direct pathway, the electron transfer occurred through the formation of inner sphere quaternary surface complex, ≡Fe – O – Fe – ONO – Fe. Whereas indirect pathway was modeled as outer sphere electron transfer with electron donor and acceptor separated at different sorption sites on Fe(III) (oxy)hydroxide surface.
11) Although results of quantum mechanical calculation did not support indirect mechanism of electron transfer, indirect mechanism remains as one possible electron transfer mechanism supported by wet chemistry evidence and considering that we used simplified models for

description of the Fe(III) (oxyhydr)oxide interface with water and for the location and reactivity of solid-bound Fe(II).

12) Catalytical effect of solid-bound Fe(II) on Fe(II)/As(V) reaction using HFO as the solid phase was not observed in our study. The inertness of redox reaction between As(V) and Fe(II) could be due to the requirement of two-electron transfer for As(V) reduction to As(III), whereas it is possible for O_2, nitrite, and uranyl to undergo one electron transfer with Fe(II) in the presence of HFO.

6.2 Recommendations for Future Study

We observed a significant increase in solid-bound Fe(II) after the addition of U(VI) in Fe(II)/HFO solution and evidence of electron migration into the bulk Fe(III) phase. The result of this study indicated that HFO is a meta-stable solid phase. The addition of uranium, or other metal ions into Fe(II)/HFO solution could lead to dynamic interaction between Fe(II) and metal ions and between Fe(II) and Fe(III) (oxyhydr)oxides. Further investigation with analytical techniques such as XANES and EXAFS could provide more detailed information about identities, distribution, compositions and configurations of surface complexes and surface mineral species that form on ferric oxides due to reaction between Fe(II) and U(VI).

Until recently U(V) was ignored due to its instability and rare occurrence in uranium minerals. However, U(V) could play a important role as a intermediate product in uranium reduction kinetics and deserves more discussion for study of the migration and transformation of uranium species in soils and groundwater.

We used quantum mechanical calculation and Fe(II)-Fe(III) (oxyhydr)oxide model to simulate anode/cathode electron transfer mechanism (indirect electron transfer pathway). However, we used simplified a Fe(III) (oxyhydr)oxide configuration in the calculation.

Furthermore, sorption of Fe(II) ions at separate sites a few atoms apart on the surface might not be representative for the high Fe(III)/Fe(II) ratio commonly found in natural water or sediments. This could have resulted in the slightly positive reaction energy calculated for the indirect electron transfer pathway which was supported by our wet chemistry evidence. Density functional theory (DFT) calculation on periodic Fe(III) (oxyhydr)oxide structure using Vienna Ab Initio Simulation Package (VASP) that can provide more complex simulation on indirect electron transfer pathway could be the alternate tool to study this mechanism.

Decreases in heterogeneous reaction rates were observed at high surface coverage of Fe(II) using NO_2^- and U(VI) as oxidants, consistent with previous studies using U(VI) and O_2 as oxidants (25, 26). Whether this observation could occur for all potential oxidants at high Fe(II) surface coverage or is only limited to NO_2^-, O_2 and U(VI) as oxidants in Fe(II)/Fe(III) (oxyhydr)oxide system shall be further investigated. Additional studies using analytical techniques and wet chemistry are needed to characterize phase transformation and crystallization of Fe(III) (oxyhydr)oxide catalyzed by Fe(II) or oxidants including but not limited to NO_2^-, U(VI), and O_2, in order to determine the effect of the transformation of this dynamic solid phase on the electron transfer process occurring at the mineral-water interface.

Appendix A: Kinetic Modeling Procedures

Fe(II)/HFO/NO_2^-

For Fe(II)/NO_2^- redox reaction, assuming two moles of Fe(II) were oxidized for every mole of NO_2^- reduced as shown in Eq.(1) in section 2.3.1:

$$2\ Fe^{2+} + NO_2^- + 5/2\ H_2O \rightarrow 2\ FeOOH + 1/2\ N_2O + 3\ H^+ \quad (1)$$

, the rate of Fe(II) oxidation can be descried as the following second oredr rate expression:

$$d[Fe(II)]/dt = - k_{obs}[Fe(II)_{diss}]\ [NO_2^-] \quad (2)$$

If x represents the disappearance in nitrite, the reactant concentrations can be calculated as:

$$[Fe(II)_{diss}] = [Fe(II)_{diss}]_o - 2x \quad (3)$$

$$[NO_2^-] = [NO_2^-]_o - x \quad (4)$$

When $[Fe(II)_{diss}]$ and $[NO_2^-]$ in Eq. (2) are replaced by (3) and (4), Eq. (3) can be expressed as:

$$dx / dt = k_{obs}([Fe(II)_{diss}]_o - 2x)([NO_2^-]_o - x) \quad (5)$$

Integration of Eq. (5) for bountary conditions (0,0) and (x, t) yields the following equation:

$$k_{obs}t = \frac{1}{[Fe(II)_{diss}]_o - 2[NO_2^-]_o} \ln \frac{[NO_2^-]_o([Fe(II)_{diss}]_o - 2x)}{[Fe(II)_{diss}]_o([NO_2^-]_o - x)} \quad (6)$$

A trendline is derived on a plot of $k_{obs} \cdot t$ versus time and the slope of the trendline represents the rate constant, k_{obs}, for the 2nd order rate equation. The following figure shows the result in experiment 14 of Table 2-1. In this experiment, $k_{obs} = 1.38 \times 10^{-5}\ \mu M^{-1}\ min^{-1}$.

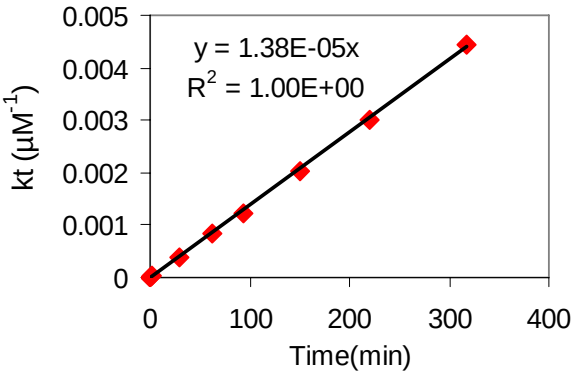

After *x* in Eq.(6) is solved using the derived k_{obs} , modeled Fe(II) and NO_2^- concentrations can be calculated by Eq.(3) and Eq.(4) and the result is shown in the following figure.

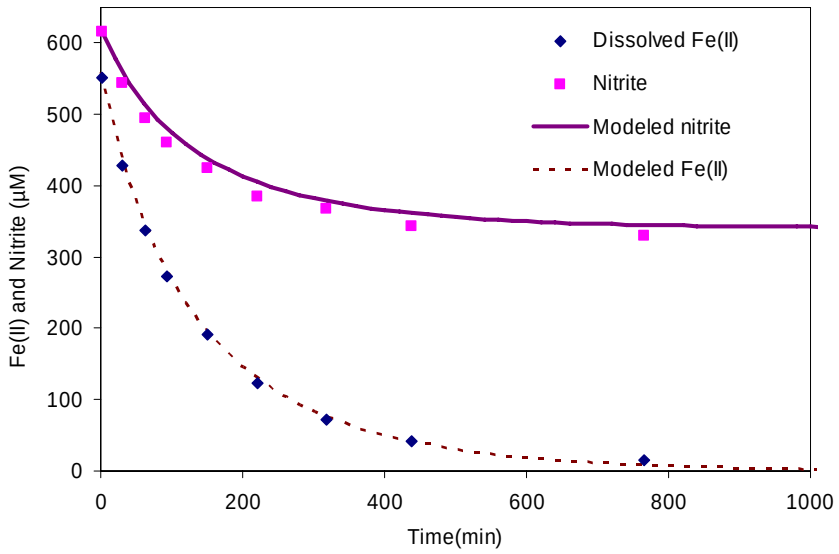

Fe(II)/HFO/UO_2^{2+}

First order rate law

The first order rate equation of UO_2^{2+} reduction is:

$$d[U(VI)]/dt = - k_{obs\text{-}1}[U(VI)] \quad \text{.....(7)}$$

integration of Eq.(7) yield the following equation:

$$\ln([U(VI)] / [U(VI)]_o) = -k_{obs\text{-}1} \cdot t \quad \text{.....(8)}$$

where $k_{obs\text{-}1}$ is first order rate constant of UO_2^{2+} reduction. A trendline is derived on a plot of $\ln([U(VI)] / [U(VI)]_o)$ versus time and the slope of the trendline represent the rate constant, $k_{obs\text{-}1}$. Result of Exp. 6 in Table 3-1 is shown in the following figure as a example.

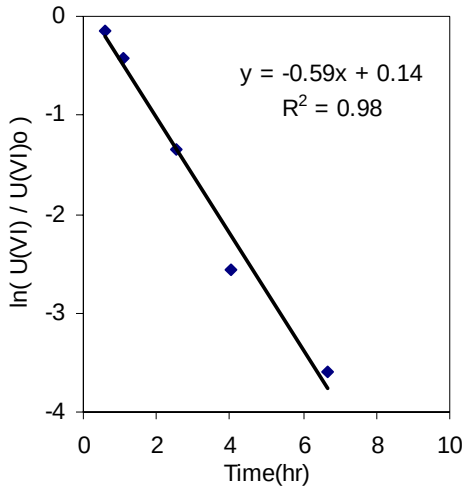

Modeled UO_2^{2+} concentrations can be calculated by Eq.8 with derived $k_{obs\text{-}1}$ and $[U(VI)]_o$ and result is shown in the following figure.

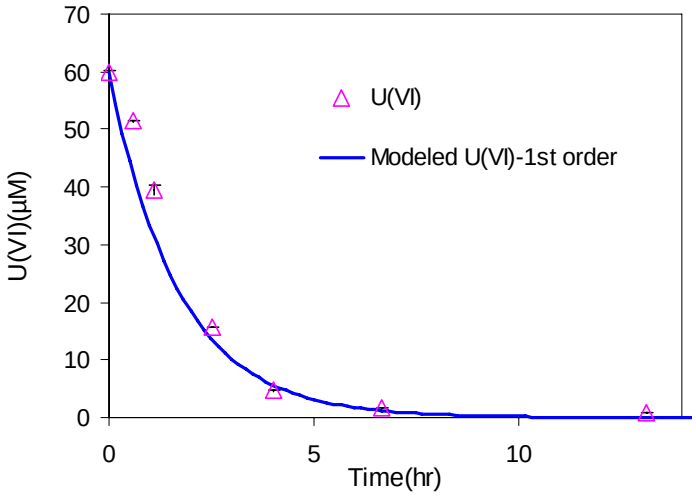

Second order rate law

The Fe(II)/UO_2^{2+} redox reaction can be modeled with second-order rate law. The reactant concenrations in a one-electron-transfer reaction are defined as:

$$[Fe(II)_{diss}] = [Fe(II)_{diss}]_o - x \quad \text{.....(7)}$$

$$[U(VI)] = [U(VI)]_o - x \quad \text{.....(8)}$$

x represents the amount of Fe(II) and U(VI) removed in the reaction.

The second-order rate equation for UO_2^{2+} reduction is:

$$d[U(VI)]/dt = - k_{obs\text{-}2} \cdot [U(VI)] \cdot [Fe(II)_{diss}] \quad \text{.....(9)}$$

Eq.(9) can be transformed to:

$$dx / dt = k_{obs\text{-}2} \cdot ([U(VI)]_o - x)\ ([Fe(II)_{diss}]_o - x) \quad \text{.....(10)}$$

Integration of Eq. (10) for bountary conditions (0,0) and (*x*, t) yields the following equation:

$$k_{obs-2}t = \frac{1}{[Fe(II)_{diss}]_o - [U(VI)]_o} \ln \frac{[U(VI)]_o([Fe(II)_{diss}]_o - x)}{[Fe(II)_{diss}]_o([U(VI)]_o - x)} \quad \text{.....(11)}$$

A trendline is derived on a plot of $k_{obs\text{-}2} \cdot t$ versus time and the slope of the trendline represents the rate constant, $k_{obs\text{-}2}$, for the 2nd order rate equation. The following figure shows the result in experiment 6 of Table 3-1. In this experiment, $k_{obs\text{-}2} = 0.00528\ \mu M^{-1}\ min^{-1}$.

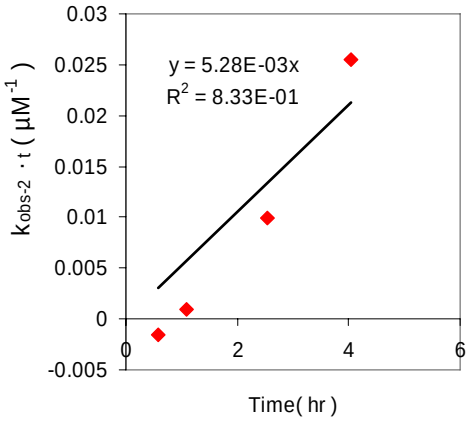

x can be calculated with initial Fe(II), U(VI) concentrations and the derived k_{obs-2} at each time interval. The predictive Fe(II) and U(VI) concentrations can be calculated with Eq. (7) and (8) and the result is plot in the following figure.

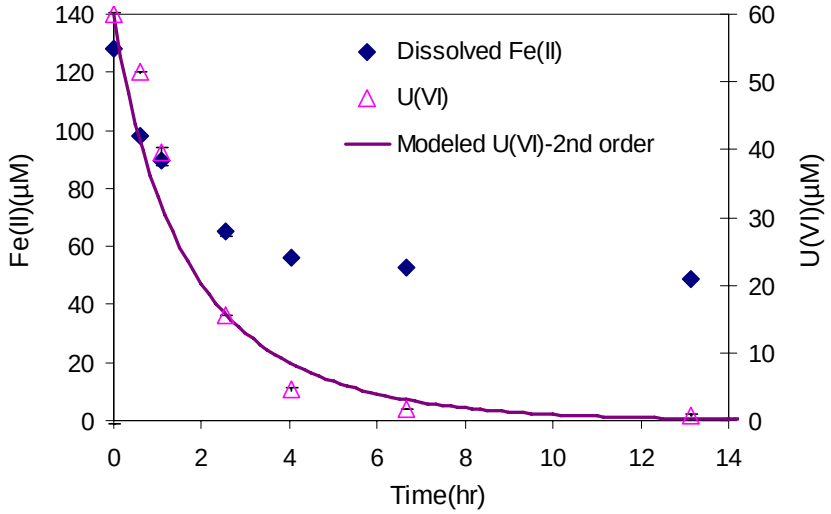

Appendix B: A Study of Fe(II)/HFO/As(V) Reaction

Introduction

Environmental incidents linked to arsenic poisoning have been reported in many countries including Argentina, Bangladesh, Chile, Chile, China, India, Taiwan and the United States (112). Elevated levels of arsenic in groundwater could be due to weathering, dissolution, and hydrothermal activities of arsenic minerals (16, 18) and numerous anthropogenic inputs including mining and smelting activities (17) and arsenate pesticides (113). Chronic ingestion of inorganic arsenic has been established as the cause of various skin alternations and internal cancers including bladder, kidney, liver, lung and skin cancers (114).

Because redox potential of As(V)/As(III) couple falls within the ranges that are most commonly observed in aquifers, soils, and sediments with various water contents (115), redox potential and pH are two key factors that affect arsenic speciation and solubility, and thereby control it's toxicity, mobility, and bioavailability in groundwater systems (116, 117). Arsenate [As(V)] (as $H_2AsO_4^-$ or $HAsO_4^{2-}$) is the predominant As species in oxidized waters, whereas arsenite [As(III)] (as H_3AsO_3 or $H_2AsO_3^-$) is stable relative to As(V) under reducing conditions (118). However, due to the slow kinetics of As(V)-As(III) transformation, both arsenate and arsenite species are commonly found in either reduced or oxidized environments (119). Arsenite is 25-60 times more toxic and is more mobile in the water environments than arsenate species (120).

Iron oxides, especially poorly crystalline hydrous ferric oxide, have a strong binding affinity for both arsenate and arsenite (121-127). Oxyanions including arsenate and arsenite show

decreasing adsorption onto iron oxides with increasing pH due to repulsive forces between the negatively charged arsenic oxyanions and negatively charged Fe-oxide surfaces (112, 119, 128).

The reactions of arsenic with Fe(II) in the presence of hydrous ferric oxide have not been fully studied. Pedersen et al. (23) investigated the fate of arsenic during transformation of iron oxides in the presence of Fe(II) at 25ºC and pH6.5. They observed a decrease of sorbed arsenic during the transformation of HFO into lepidocrocite and goethite at low Fe(II) concentrations and into goethite and magnetite at higher Fe(II) concentrations. They concluded that arsenic became more strongly bound to the new Fe-oxide phases during the recrystallization process and could not be recovered by their extraction method. Less than 1% of the total As was released into the aqueous phase and was identified as arsenite in their experiment.

Materials and Methods

The experimental setup and procedure is similar to Fe(II)/Fe(III)/U(VI) system described in section 3.2.4. The concentration of As(V) is determined on samples filtered through 0.2μm membrane filters by the modified molybdenum blue colorimetric method (129, 130). Ammonium molybdate forms a blue As-Mo complex with As(V) and the colored solution obey Beer's Law. The sample or the standard solutions are mixed with color reagent at a volume ratio of 0.84:0.16 and 40 minutes are allowed for color development. The absorbance is then measured with a Shimadzu UN-1601 spectrophotometer at 865nm. As(III) is oxidized to As(V) by reaction with excess iodate (HIO_3) under acidic condition before the addition of molybdenum blue color reagent. The difference of As(V) concentration after and before iodate oxidation procedure is considered As(III) concentration. Sorbed As is determined by 5N NaOH extraction of the sample followed by filtration and molybdenum blue measurement.

Results and Discussion

Although the reduction of As(V) to As(III) and oxidation of Fe(II) is thermodynamically favorable, the result of our experiment showed that in an anoxic environment there was no significant reduction of arsenate and oxidation of Fe(II) without the presence of ferric oxide in five days as shown in Figure B-1. When we introduced HFO as the solid phase in our system, there was still no measurable reaction between Fe(II) and As(V) at pH6.8 and a Fe(III) concentration of 2.5mM in 4 days as shown in Figure B-2. In contrast to nitrite, which stays in the dissolved form while being reduced by Fe(II), over 99 percent of As is associated with 2.5mM HFO. In order to explore the influence of As(V)/Fe(II) coverage on HFO and dissolved As(V) concentration on the kinetics of the Fe(II)/As(V) redox reaction, the experiment was repeated with the same experimental conditions except a lower HFO content of 0.5mM Fe(III). The lower solid concentration results in a two-fold increase in As surface density on HFO and a substantial increase of dissolved As(V) concentration from 0% to 60% of the total As. However, no significant reaction has been observed as shown in Figure B-3. In another experiment with the same experimental conditions except at a lower pH of 4.0 and a HFO concentration of 2.5mM Fe(III), most of the As(V) are associated with ferric oxide and on the contrary most of the Fe(II) are soluble as shown in Figure B-4. Again, no reaction between Fe(II) and As(V) was observed.

The results of our experiments seem to be consist with hypothesis (1) and (3) listed in section 1.2. In experiment at pH6.8 with 2.5mM HFO, there was no presence of dissolved As(V), whereas in experiment at pH 4 with 2.5mM HFO, there was no $Fe(II)_{sorb}$ to trigger the redox reaction. It's also possible the fast kinetics of the heterogeneous oxidation of Fe(II) and the reduction of either O_2, nitrite and uranyl results from the availability of the one-electron transfer for these oxidizing agents, whereas in the case of arsenic, the inertness of redox reaction between As(V) and Fe(II) could be due to the requirement of two-electron transfer for As(V) reduction to As(III).

Figure B-1 There was no significant reduction of arsenate and oxidation of Fe(II) without the presence of ferric oxide in five days (data after 30 hours not shown)

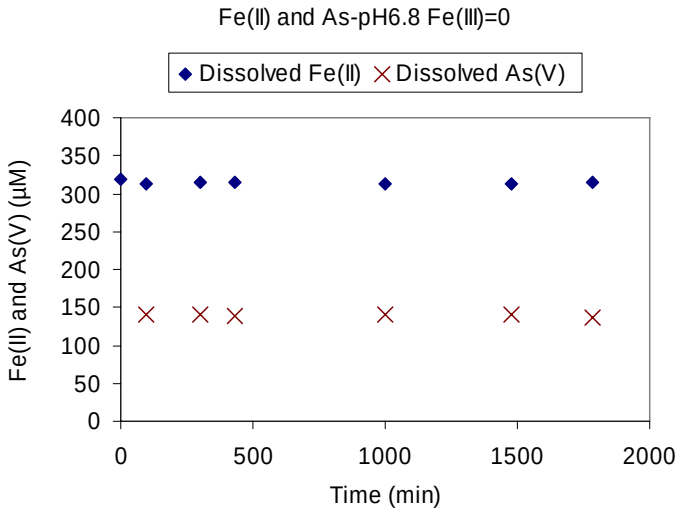

Figure B-2 There was no measurable reaction between Fe(II) and As(V) at pH 6.8 and a Fe(III) concentration of 2.5 mM.

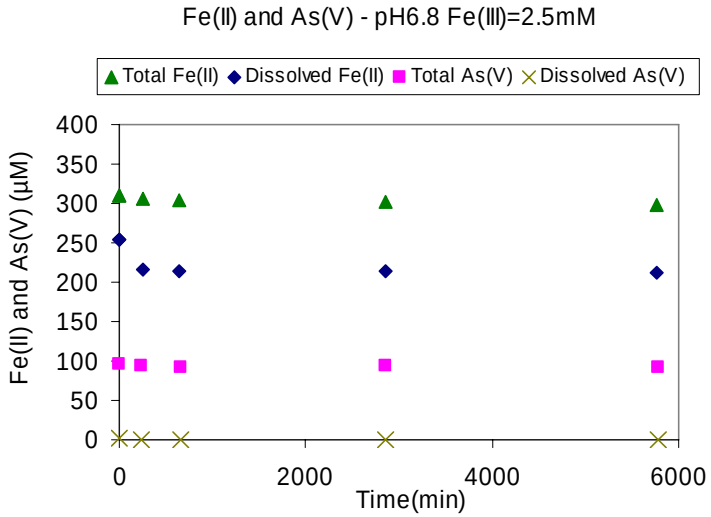

Figure B-3 There was no significant reaction between Fe(II) and As(V) at pH 6.8 and a solid concentration of 0.5 mM Fe(III).

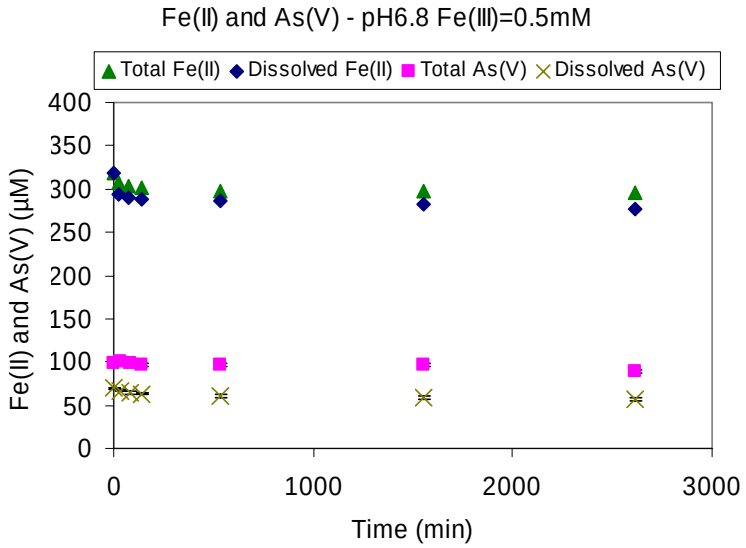

Figure B-4 There was no significant reaction between Fe(II) and As(V) at pH 4.0 and a solid concentration of 2.5 mM Fe(III).

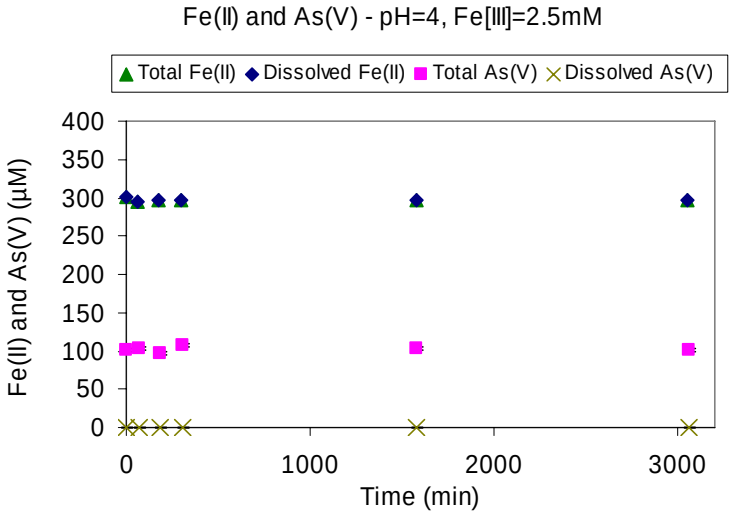

Appendix C: NBO Population Analysis Output

Table C-1 NBO output for reactants, intermediate product and product of direct electron transfer mechanism.

No.	Atom	Reactant			Intermediate Product			Product		
		natural charge	core	valence	natural charge	core	valence	natural charge	core	valence
1	Fe	1.617	17.997	6.245	1.590	17.997	6.270	1.581	17.997	6.282
2	O	-1.057	2.000	7.039	-1.048	2.000	7.030	-1.087	2.000	7.071
3	O	-1.073	2.000	7.058	-1.073	2.000	7.059	-1.104	2.000	7.086
4	O	-1.072	2.000	7.055	-1.080	2.000	7.060	-1.082	2.000	7.066
5	O	-1.082	2.000	7.071	-1.055	2.000	7.044	-1.025	2.000	7.013
6	H	0.500	0.000	0.494	0.507	0.000	0.488	0.519	0.000	0.476
7	Fe	1.616	17.997	6.234	1.611	17.997	6.236	1.598	17.997	6.259
8	Fe	1.583	17.996	6.273	1.593	17.996	6.269	1.582	17.996	6.274
9	O	-1.035	2.000	7.017	-1.037	2.000	7.018	-1.051	2.000	7.035
10	O	-0.948	2.000	6.932	-0.936	2.000	6.920	-1.077	2.000	7.064
11	O	-1.056	2.000	7.039	-1.060	2.000	7.044	-1.043	2.000	7.025
12	O	-1.050	2.000	7.037	-1.037	2.000	7.024	-1.024	2.000	7.012
13	O	-0.930	2.000	6.914	-0.928	2.000	6.912	-0.930	2.000	6.914
14	O	-1.067	2.000	7.053	-1.050	2.000	7.036	-1.075	2.000	7.061
15	O	-1.110	2.000	7.098	-1.117	2.000	7.105	-1.011	2.000	6.996
16	H	0.495	0.000	0.500	0.501	0.000	0.494	0.491	0.000	0.505
17	Fe	1.358	17.998	6.576	1.349	17.997	6.576	1.381	17.998	6.550
18	Fe	1.441	17.998	6.499	1.399	17.997	6.517	1.715	17.994	6.191
19	H	0.476	0.000	0.519	0.487	0.000	0.509	0.497	0.000	0.498
20	H	0.488	0.000	0.507	0.488	0.000	0.507	0.512	0.000	0.483
21	O	-0.947	2.000	6.931	-0.937	2.000	6.921	-0.967	2.000	6.952
22	O	-0.944	2.000	6.928	-0.945	2.000	6.929	-0.933	2.000	6.916
23	H	0.473	0.000	0.524	0.504	0.000	0.493	0.518	0.000	0.478
24	O	-0.976	2.000	6.960	-1.025	2.000	7.009	-1.064	2.000	7.052
25	O	-1.027	2.000	7.013	-1.017	2.000	7.003	-0.994	2.000	6.981
26	O	-1.013	2.000	6.998	-1.156	2.000	7.141	-1.056	2.000	7.043
27	O	-1.039	2.000	7.025	-1.049	2.000	7.037	-1.011	2.000	6.999
28	O	-1.028	2.000	7.015	-1.062	2.000	7.050	-0.971	2.000	6.954
29	O	-1.006	2.000	6.990	-1.000	2.000	6.987	-0.998	2.000	6.988
30	O	-1.150	2.000	7.132	-1.172	2.000	7.158	-1.091	2.000	7.075
31	H	0.529	0.000	0.467	0.530	0.000	0.467	0.518	0.000	0.478
32	H	0.530	0.000	0.468	0.517	0.000	0.477	0.524	0.000	0.469
33	H	0.493	0.000	0.499	0.503	0.000	0.491	0.457	0.000	0.538
34	H	0.520	0.000	0.478	0.507	0.000	0.490	0.519	0.000	0.477
35	H	0.515	0.000	0.480	0.513	0.000	0.485	0.514	0.000	0.484
36	H	0.506	0.000	0.493	0.516	0.000	0.480	0.514	0.000	0.485
37	H	0.507	0.000	0.485	0.496	0.000	0.499	0.521	0.000	0.474

No.	Atom	Reactant			Intermediate Product			Product		
		natural charge	core	valence	natural charge	core	valence	natural charge	core	valence
38	H	0.499	0.000	0.498	0.516	0.000	0.477	0.531	0.000	0.462
39	H	0.512	0.000	0.484	0.521	0.000	0.477	0.523	0.000	0.474
40	H	0.515	0.000	0.478	0.531	0.000	0.466	0.518	0.000	0.480
41	H	0.527	0.000	0.467	0.522	0.000	0.476	0.527	0.000	0.470
42	H	0.524	0.000	0.470	0.522	0.000	0.471	0.524	0.000	0.474
43	H	0.509	0.000	0.485	0.522	0.000	0.472	0.534	0.000	0.460
44	H	0.504	0.000	0.489	0.507	0.000	0.488	0.523	0.000	0.475
45	H	0.516	0.000	0.479	0.493	0.000	0.503	0.500	0.000	0.492
46	H	0.506	0.000	0.489	0.505	0.000	0.489	0.499	0.000	0.500
47	H	0.485	0.000	0.509	0.513	0.000	0.483	0.511	0.000	0.484
48	H	0.490	0.000	0.504	0.517	0.000	0.482	0.521	0.000	0.476
49	H	0.523	0.000	0.475	0.521	0.000	0.473	0.505	0.000	0.489
50	H	0.510	0.000	0.488	0.497	0.000	0.501	0.494	0.000	0.504
51	O	-1.022	2.000	7.008	-1.017	2.000	7.007	-1.011	2.000	6.994
52	O	-1.185	2.000	7.172	-0.994	2.000	6.980	-1.006	2.000	6.991
53	O	-0.976	2.000	6.960	-0.991	2.000	6.977	-1.001	2.000	6.990
54	O	-0.527	2.000	6.513	-0.378	2.000	6.362	-0.173	2.000	6.143
55	O	-0.461	2.000	6.445	-0.670	2.000	6.649	-1.184	2.000	7.171
56	H	0.522	0.000	0.475	0.525	0.000	0.473	0.490	0.000	0.507
57	H	0.541	0.000	0.454	0.540	0.000	0.456	0.515	0.000	0.478
58	H	0.470	0.000	0.529	0.470	0.000	0.529	0.468	0.000	0.530
59	H	0.497	0.000	0.499	0.491	0.000	0.505	0.501	0.000	0.494
60	H	0.505	0.000	0.492	0.498	0.000	0.500	0.500	0.000	0.497
61	H	0.541	0.000	0.454	0.533	0.000	0.462	0.537	0.000	0.459
62	H	0.527	0.000	0.469	0.530	0.000	0.466	0.528	0.000	0.470
63	H	0.528	0.000	0.468	0.535	0.000	0.463	0.542	0.000	0.454
64	H	0.544	0.000	0.451	0.541	0.000	0.455	0.537	0.000	0.460
65	H	0.526	0.000	0.470	0.523	0.000	0.474	0.521	0.000	0.475
66	N	0.268	2.000	4.660	0.316	2.000	4.616	0.089	2.000	4.859
67	O	-1.008	2.000	6.992	-1.009	2.000	6.999	-0.986	2.000	6.976
68	H	0.515	0.000	0.476	0.520	0.000	0.475	0.508	0.000	0.488
69	H	0.520	0.000	0.478	0.509	0.000	0.490	0.511	0.000	0.488
70	O	-1.020	2.000	7.007	-0.973	2.000	6.961	-1.011	2.000	6.997
71	H	0.511	0.000	0.487	0.496	0.000	0.501	0.517	0.000	0.478
72	H	0.523	0.000	0.470	0.489	0.000	0.509	0.528	0.000	0.465

Table C-2 NBO output for reactants, intermediate product and product of indirect electron transfer mechanism.

No	Atom	Reactant			Intermediate Product			Product		
		natural charge	core	valence	natural charge	core	valence	natural charge	core	valence
1	Fe	1.061	17.995	6.830	1.054	17.995	6.835	1.074	17.995	6.823
2	O	-0.934	2.000	6.919	-0.928	2.000	6.912	-0.918	2.000	6.902
3	O	-0.976	2.000	6.958	-0.967	2.000	6.949	-0.908	2.000	6.889
4	O	-0.913	2.000	6.899	-0.913	2.000	6.899	-0.914	2.000	6.900
5	O	-0.952	2.000	6.940	-0.932	2.000	6.921	-0.927	2.000	6.916
6	H	0.519	0.000	0.477	0.519	0.000	0.476	0.519	0.000	0.477
7	Fe	1.073	17.995	6.814	1.078	17.995	6.810	1.064	17.995	6.824
8	Fe	1.070	17.995	6.834	1.054	17.995	6.848	1.028	17.995	6.873
9	O	-0.935	2.000	6.919	-0.934	2.000	6.918	-0.929	2.000	6.913
10	O	-0.887	2.000	6.871	-0.886	2.000	6.870	-0.880	2.000	6.864
11	O	-0.889	2.000	6.872	-0.889	2.000	6.872	-0.886	2.000	6.869
12	O	-0.911	2.000	6.899	-0.920	2.000	6.908	-0.920	2.000	6.908
13	O	-0.950	2.000	6.937	-0.938	2.000	6.925	-0.938	2.000	6.925
14	O	-0.936	2.000	6.924	-0.930	2.000	6.918	-0.926	2.000	6.914
15	O	-0.981	2.000	6.970	-0.979	2.000	6.968	-0.977	2.000	6.966
16	H	0.508	0.000	0.488	0.508	0.000	0.488	0.506	0.000	0.490
17	Fe	1.069	17.998	6.891	1.036	17.997	6.926	1.016	17.997	6.945
18	Fe	0.973	17.997	6.982	0.987	17.997	6.969	1.181	17.996	6.742
19	H	0.508	0.000	0.487	0.507	0.000	0.488	0.510	0.000	0.486
20	H	0.516	0.000	0.481	0.511	0.000	0.485	0.515	0.000	0.482
21	O	-0.979	2.000	6.966	-0.975	2.000	6.962	-0.922	2.000	6.910
22	O	-0.881	2.000	6.865	-0.882	2.000	6.866	-0.872	2.000	6.856
23	H	-0.921	2.000	6.908	-0.954	2.000	6.941	-0.937	2.000	6.924
24	O	-0.997	2.000	6.986	-1.097	2.000	7.086	-1.112	2.000	7.102
25	O	-0.963	2.000	6.950	-0.937	2.000	6.923	-0.953	2.000	6.940
26	O	-0.951	2.000	6.938	-0.955	2.000	6.941	-0.922	2.000	6.909
27	O	-0.947	2.000	6.935	-0.950	2.000	6.938	-1.030	2.000	7.021
28	O	-0.993	2.000	6.981	-0.998	2.000	6.987	-0.943	2.000	6.929
29	O	-1.005	2.000	6.993	-1.015	2.000	7.004	-1.020	2.000	7.009
30	O	0.523	0.000	0.474	0.524	0.000	0.472	0.518	0.000	0.477
31	H	0.524	0.000	0.472	0.525	0.000	0.471	0.526	0.000	0.469
32	H	0.518	0.000	0.480	0.515	0.000	0.484	0.510	0.000	0.488
33	H	0.528	0.000	0.469	0.528	0.000	0.469	0.527	0.000	0.469
34	H	0.515	0.000	0.483	0.514	0.000	0.484	0.508	0.000	0.490
35	H	0.513	0.000	0.478	0.521	0.000	0.477	0.535	0.000	0.461
36	H	0.513	0.000	0.484	0.522	0.000	0.475	0.510	0.000	0.487
37	H	0.534	0.000	0.460	0.515	0.000	0.480	0.511	0.000	0.486
38	H	0.516	0.000	0.478	0.507	0.000	0.485	0.499	0.000	0.500
39	H	0.501	0.000	0.495	0.492	0.000	0.504	0.510	0.000	0.485

No	Atom	Reactants			Intermediate Product			Product		
		natural charge	core	valence	natural charge	core	valence	natural charge	core	valence
40	H	0.515	0.000	0.482	0.513	0.000	0.485	0.508	0.000	0.488
41	H	0.535	0.000	0.461	0.535	0.000	0.460	0.534	0.000	0.461
42	H	0.507	0.000	0.491	0.506	0.000	0.491	0.509	0.000	0.489
43	H	0.507	0.000	0.488	0.501	0.000	0.496	0.515	0.000	0.480
44	H	0.525	0.000	0.469	0.526	0.000	0.468	0.525	0.000	0.470
45	H	0.521	0.000	0.475	0.512	0.000	0.486	0.510	0.000	0.486
46	H	0.532	0.000	0.462	0.534	0.000	0.460	0.534	0.000	0.461
47	H	0.515	0.000	0.483	0.514	0.000	0.484	0.511	0.000	0.487
48	H	0.531	0.000	0.464	0.528	0.000	0.467	0.529	0.000	0.466
49	H	-0.984	2.000	6.972	-0.976	2.000	6.964	-0.973	2.000	6.961
50	H	-0.979	2.000	6.968	-0.974	2.000	6.962	-0.973	2.000	6.962
51	O	-0.962	2.000	6.949	-0.959	2.000	6.945	-0.956	2.000	6.943
52	O	-0.513	2.000	6.498	-0.390	2.000	6.372	-0.241	2.000	6.209
53	O	-0.529	2.000	6.514	-0.543	2.000	6.529	-0.982	2.000	6.970
54	O	0.534	0.000	0.463	0.533	0.000	0.463	0.535	0.000	0.462
55	O	0.551	0.000	0.445	0.550	0.000	0.445	0.551	0.000	0.445
56	H	0.482	0.000	0.515	0.481	0.000	0.517	0.480	0.000	0.518
57	H	0.501	0.000	0.497	0.503	0.000	0.495	0.504	0.000	0.493
58	H	0.499	0.000	0.499	0.495	0.000	0.503	0.504	0.000	0.494
59	H	0.536	0.000	0.459	0.535	0.000	0.460	0.537	0.000	0.461
60	H	0.538	0.000	0.457	0.538	0.000	0.458	0.547	0.000	0.449
61	H	0.538	0.000	0.457	0.538	0.000	0.457	0.542	0.000	0.453
62	H	0.510	0.000	0.487	0.508	0.000	0.489	0.537	0.000	0.461
63	H	0.483	0.000	0.515	0.480	0.000	0.518	0.479	0.000	0.519
64	H	0.307	2.000	4.624	0.365	2.000	4.574	0.261	2.000	4.692
65	H	-0.919	2.000	6.905	-0.918	2.000	6.904	-0.901	2.000	6.887
66	N	0.525	0.000	0.473	0.526	0.000	0.472	0.526	0.000	0.469
67	O	0.516	0.000	0.481	0.516	0.000	0.482	0.510	0.000	0.488
68	H	-0.923	2.000	6.910	-0.936	2.000	6.923	-0.928	2.000	6.915
69	H	0.527	0.000	0.470	0.526	0.000	0.471	0.525	0.000	0.473
70	O	0.524	0.000	0.474	0.521	0.000	0.477	0.516	0.000	0.482
71	H	0.465	0.000	0.531	0.471	0.000	0.524	0.485	0.000	0.510
72	H	0.503	0.000	0.495	0.503	0.000	0.494	0.508	0.000	0.489

REFERENCES

1. Stumm, W.; Sulzberger, B., The cycling of iron in natural environments: Considerations based on laboratory studies of heterogeneous redox processes. *Geochimica et Cosmochimica Acta* **1992,** 56, (8), 3233-3257.
2. Charlet, L.; Silvester, E.; Liger, E., N-compound reduction and actinide immobilisation in surficial fluids by Fe(II): the surface $\equiv Fe^{III}OFe^{II}OH^{o}$ species, as major reductant. *Chemical Geology* **1998,** 151, (1-4), 85-93.
3. Amonette, J. E.; Workman, D. J.; Kennedy, D. W.; Fruchter, J. S.; Gorby, Y. A., Dechlorination of carbon tetrachloride by Fe(II) associated with goethite. *Environ. Sci. Technol.* **2000,** 34, (21), 4606-4613.
4. Suthersan, S. S., *Remediation Engineering Design Concepts*. CRC Press LLC: Boca Raton, 1996; p 200.
5. Elsner, M.; Schwarzenbach, R. P.; Kellerhals, T.; Luzi, S.; Zwank, L.; Angst, W.; Haderlein, S. B., Mechanisms and products of surface-mediated reductive dehalogenation of carbon tetrachloride by Fe(II) on goethite. *Environ. Sci. Technol.* **2004,** 38, (7), 2058-2066.
6. Gregory, K. B.; Larese-Casanova, P.; Parkin, G. F.; Scherer, M. M., Abiotic transformation of hexahydro-1,3,5-trinitro-1,3,5-triazine by Fe^{II} bound to magnetite. *Environ. Sci. Technol.* **2004,** 38, (5), 1408-1414.
7. Jeon, B. H.; Dempsey, B. A.; Burgos, W. D.; Barnett, M. O.; Roden, E. E., Chemical reduction of U(VI) by Fe(II) at the solid-water interface using natural and synthetic Fe(III) oxides. *Environmental Science & Technology* **2005,** 39, (15), 5642-5649.
8. Sorensen, J.; Thorling, L., Stimulation by lepidocrocite (r-FeOOH) of Fe(II)-dependent nitrite reduction. *Geochimica et Cosmochimica Acta* **1991,** 55, (5), 1289-1294.
9. Dodge, C. J.; Francis, A. J.; Gillow, J. B.; Halada, G. P.; Eng, C.; Clayton, C. R., Association of uranium with iron oxides typically formed on corroding steel surfaces. *Environmental Science & Technology* **2002,** 36, (16), 3504-3511.
10. Lammel, G.; Grassl, H., Greenhouse effect of NOx. *Environmental Science and Pollution Research* **1995,** 2, (1), 40-45.
11. IPCC, *Climate change 2007: The physical scientific basis. contribution of working Group I to the fourth assessment report of the Intergovernmental Panel on climate change*. Cambridge University Press: Cambridge, United Kingdom and New York, NY, USA, 2007.
12. Van Cleemput, O.; Baert, L., Nitrite stability influenced by iron compounds. *Soil Biology and Biochemistry* **1983,** 15, (2), 137-140.
13. VanCleemput, O.; Samater, A. H., Nitrite in soils: Accumulation and role in the formation of gaseous N compounds. *Fertilizer Research* **1996,** 45, (1), 81-89.
14. Venterea, R. T.; Rolston, D. E., Mechanisms and kinetics of nitric and nitrous oxide production during nitrification in agricultural soil. *Global Change Biology* **2000,** 6, (3), 303-316.
15. Sorg, T. J., Methods for Removing Uranium from Drinking-Water. *Journal American Water Works Association* **1988,** 80, (7), 105-111.
16. Tanaka, T., Distribution of arsenic in the natural environment with emphasis on rocks and soils. *Applied Organometallic Chemistry* **1988,** 2, (4), 283-295.

17. Li, X. D.; Thornton, I., Arsenic, Antimony and Bismuth in Soil and Pasture Herbage in Some Old Metalliferous Mining Areas in England. *Environmental Geochemistry and Health* **1993,** 15, (2-3), 135-144.
18. Welch, A. H.; Lico, M. S.; Hughes, J. L., Arsenic in Ground-Water of the Western United-States. *Ground Water* **1988,** 26, (3), 333-347.
19. O'Loughlin, E. J.; Kelly, S. D.; Cook, R. E.; Csencsits, R.; Kemner, K. M., Reduction of Uranium(VI) by mixed iron(II/iron(III) hydroxide (green rust): Formation of UO2 manoparticies. *Environmental Science & Technology* **2003,** 37, (4), 721-727.
20. Liger, E.; Charlet, L.; Van Cappellen, P., Surface catalysis of uranium(VI) reduction by iron(II). *Geochimica Et Cosmochimica Acta* **1999,** 63, (19-20), 2939-2955.
21. Johnston, R. B.; Singer, P. C., Redox reactions in the Fe-As-O2 system. *Chemosphere* **2007,** 69, (4), 517-525.
22. Tai, Y.-L.; Dempsey, B. A., Nitrite reduction with hydrous ferric oxide and Fe(II): Stoichiometry, rate, and mechanism. *Water Research* **2009,** 43, (2), 546-552.
23. Pedersen, H. D.; Postma, D.; Jakobsen, R., Release of arsenic associated with the reduction and transformation of iron oxides. *Geochimica Et Cosmochimica Acta* **2006,** 70, (16), 4116-4129.
24. Scott, T. B.; Allen, G. C.; Heard, P. J.; Randell, M. G., Reduction of U(VI) to U(IV) on the surface of magnetite. *Geochimica Et Cosmochimica Acta* **2005,** 69, (24), 5639-5646.
25. Jang, J.-H.; Dempsey, B. A.; Burgos, W. D., Reduction of U(VI) by Fe(II) in the presence of hydrous ferric oxide and hematite: Effects of solid transformation, surface coverage, and humic acid. *Water Research* **2008,** 42, (8-9), 2269-2277.
26. Park, B.; Dempsey, B. A., Heterogeneous oxidation of Fe(II) on ferric oxide at neutral pH and a low partial pressure of O_2. *Environ. Sci. Technol.* **2005,** 39, (17), 6494-6500.
27. Jeon, B.-H.; Dempsey, B., A. ; Royer, R., A. ; Burgos, W., D. , Low-temperature oxygen trap for maintaining strict anoxic conditions. *Journal of Environmental Engineering* **2004,** 130, (11), 1407-1410.
28. Rosso, K. M.; Smith, D. M. A.; Dupuis, M., An ab initio model of electron transport in hematite (alpha-Fe_2O_3) basal planes. *Journal of Chemical Physics* **2003,** 118, (14), 6455-6466.
29. Williams, A. G. B.; Scherer, M. M., Spectroscopic evidence for Fe(II)-Fe(III) electron transfer at the iron oxide-water interface. *Environ. Sci. Technol.* **2004,** 38, (18), 4782-4790.
30. Kerisit, S.; Rosso, K. M., Kinetic Monte Carlo model of charge transport in hematite (alpha-Fe_2O_3). *The Journal of Chemical Physics* **2007,** 127, (12), 124706-10.
31. Venterea, R. T.; Rolston, D. E., Nitric and nitrous oxide emissions following fertilizer application to agricultural soil: Biotic and abiotic mechanisms and kinetics. *Journal of Geophysical Research-Atmospheres* **2000,** 105, (D12), 15117-15129.
32. Venterea, R. T., Nitrite-driven nitrous oxide production under aerobic soil conditions: kinetics and biochemical controls. *Global Change Biology* **2007,** 13, (8), 1798-1809.
33. Zachara, J. M.; Kukkadapu, R. K.; Fredrickson, J. K.; Gorby, Y. A.; Smith, S. C., Biomineralization of poorly crystalline Fe(III) oxides by dissimilatory metal reducing bacteria (DMRB). *Geomicrobiology Journal* **2002,** 19, 179-207.
34. Cornell, R. M.; Schwertmann, U., *The Iron Oxides: Structure, Properties, Reactions, Occurences and Uses*. 2nd ed.; Wiley-VCH: Weinheim, Germany, 2003.
35. Dzombak, D. A.; Morel, F. M. M., Surface Complexation Modeling-Hydrous Ferric Oxide. *John Wiley & Sons, Inc.* **1990**.
36. Jeon, B. H.; Dempsey, B. A.; Burgos, W. D., Kinetics and mechanisms for reactions of Fe(II) with iron(III) oxides. *Environ. Sci. Technol.* **2003,** 37, (15), 3309-3315.

37. Grenthe, I.; Stumm, W.; Laaksuharju, M.; Nilsson, A. C.; Wikberg, P., Redox potentials and redox reactions in deep groundwater systems. *Chemical Geology* **1992,** 98, (1-2), 131-150.
38. Dempsey, B. A.; Roscoe, H. C.; Ames, R.; Hedin, R.; Jeon, B.-H., Ferrous oxidation chemistry in passive abiotic systems for the treatment of mine drainage. *Geochemistry: Exploration, Environment, Analysis* **2001,** 1, 81-88.
39. Sung, W.; Morgan, J. J., Kinetics and product of ferrous iron oxygenation in aqueous systems. *Environ. Sci. Technol.* **1980,** 14, 561-568.
40. Strathmann, T. J.; Stone, A. T., Mineral surface catalysis of reactions between Fe^{II} and oxime carbamate pesticides. *Geochimica et Cosmochimica Acta* **2003,** 67, (15), 2775-2791.
41. Pecher, K.; Haderlein, S. B.; Schwarzenbach, R. P., Reduction of polyhalogenated methanes by surface-bound Fe(II) in aqueous suspensions of iron oxides. *Environ. Sci. Technol.* **2002,** 36, (8), 1734-1741.
42. Shao, H.; Butler, E. C., The influence of iron and sulfur mineral fractions on carbon tetrachloride transformation in model anaerobic soils and sediments. *Chemosphere* **2007,** 68, (10), 1807-1813.
43. Luther, G. W. I., The frontier-molecular-orbital theory approach in geochemical processes. In *Aquatic Chemical Kinetics*, Stumm, W., Ed. Wiley-Inter-Science: New York, 1990.
44. Wehrli, B., Redox reaction of metal ions at mineral surfaces. In *Aquatic Chemical Kinetics*, Stumm, W., Ed. Wiley-Inter-Science: New York, 1990; pp 311-336.
45. APHA; AWWA; WEF, *Standard methods for the examination of water and wastewater, 21th edition* American Public Health Association Washington, DC, 2005.
46. Perrin, D. D.; Dempsey, B., *Buffers for pH and Metal Ion Control*. Chapman and Hall: London, U.K., 1974.
47. Tamura;, H.; Goto;, K.; Nagayama;, M., Spectrophotometric determination of iron(II) with 1,10-phenanthroline in the presence of large amount of iron(II). *Talanta* **1974,** 21, 314-318.
48. Jang, J.-H.; Dempsey, B. A.; Catchen, G. L.; Burgos, W. D., Effects of Zn(II), Cu(II), Mn(II), Fe(II), NO_3^-, or SO_4^{2-} at pH 6.5 and 8.5 on transformations of hydrous ferric oxide (HFO) as evidenced by Mossbauer spectroscopy. *Colloids and Surfaces A: Physicochemical and Engineering Aspects* **2003,** 221, (1-3), 55-68.
49. Larese-Casanova, P.; Scherer, M. M., Fe(II) sorption on hematite: New insights based on spectroscopic measurements. *Environ. Sci. Technol.* **2007,** 41, (2), 471-477.
50. Barnett, M. O.; Jardine, P. M.; Brooks, S. C.; Selim, H. M., Adsorption and transport of uranium(VI) in subsurface media. *Soil Science Society of America Journal* **2000,** 64, (3), 908-917.
51. Riley, R. G.; Zachara, J. M.; Wobber, F. J. *Chemical Contaminants on DOE lands and selection of contaminant mixtures for subsurface research*; Department of Energy: 1992.
52. Hsi, C. K. D.; Langmuir, D., Adsorption of Uranyl onto Ferric Oxyhydroxides - Application of the Surface Complexation Site-Binding Model. *Geochimica Et Cosmochimica Acta* **1985,** 49, (9), 1931-1941.
53. Waite, T. D.; Davis, J. A.; Payne, T. E.; Waychunas, G. A.; Xu, N., Uranium(VI) adsorption to ferrihydrite: Application of a surface complexation model. *Geochimica et Cosmochimica Acta* **1994,** 58, (24), 5465-5478.
54. Bargar, J. R.; Reitmeyer, R.; Lenhart, J. J.; Davis, J. A., Characterization of U(VI)-carbonato ternary complexes on hematite: EXAFS and electrophoretic mobility measurements. *Geochimica et Cosmochimica Acta* **2000,** 64, (16), 2737-2749.
55. Ho, C. H.; Miller, N. H., Adsorption of uranyl species from bicarbonate solution onto hematite particles. *Journal of Colloid and Interface Science* **1986,** 110, (1), 165-171.
56. Duff, M. C.; Amrhein, C., Method for the separation of uranium(IV) and (VI) oxidation states in natural waters. *Journal of Chromatography A* **1996,** 743, (2), 335-340.

57. Wazne, M.; Korfiatis, G. P.; Meng, X. G., Carbonate effects on hexavalent uranium adsorption by iron oxyhydroxide. *Environmental Science & Technology* **2003,** 37, (16), 3619-3624.
58. Renshaw, J. C.; Butchins, L. J. C.; Livens, F. R.; May, I.; Charnock, J. M.; Lloyd, J. R., Bioreduction of uranium: Environmental implications of a pentavalent intermediate. *Environmental Science & Technology* **2005,** 39, (15), 5657-5660.
59. Charlet, L.; Silvester, E.; Liger, E., N-compound reduction and actinide immobilisation in surficial fluids by Fe(II): the surface [6-point triple bond; length half of m-dash]FeIIIOFeIIOH[deg] species, as major reductant. *Chemical Geology* **1998,** 151, (1-4), 85-93.
60. Elsner, M.; Schwarzenbach, R. P.; Haderlein, S. B., Reactivity of Fe(II)-bearing minerals toward reductive transformation of organic contaminants. *Environ. Sci. Technol.* **2004,** 38, (3), 799-807.
61. Klausen, J.; Trober, S. P.; Haderlein, S. B.; Schwarzenbach, R. P., Reduction of substituted nitrobenzenes by Fe(II) in aqueous mineral suspensio. *Environ. Sci. Technol.* **1995,** 29, (9), 2396-2404.
62. Jeon, B. H.; Kelly, S. D.; Kemner, K. M.; Barnett, M. O.; Burgos, W. D.; Dempsey, B. A.; Roden, E. E., Microbial reduction of U(VI) at the solid-water interface. *Environmental Science & Technology* **2004,** 38, (21), 5649-5655.
63. Senko, J. M.; Kelly, S. D.; Dohnalkova, A. C.; McDonough, J. T.; Kemner, K. M.; Burgos, W. D., The effect of U(VI) bioreduction kinetics on subsequent reoxidation of biogenic U(IV). *Geochimica et Cosmochimica Acta* **2007,** 71, (19), 4644-4654.
64. Alowitz, M. J.; Scherer, M. M., Kinetics of nitrate, nitrite, and Cr(VI) reduction by iron metal. *Environmental Science & Technology* **2002,** 36, (3), 299-306.
65. Sowder, A. G.; Clark, S. B.; Fjeld, R. A., The effect of sample matrix quenching on the measurement of trace uranium concentrations in aqueous solutions using kinetic phosphorimetry. *Journal of Radioanalytical and Nuclear Chemistry* **1998,** 234, (1-2), 257-260.
66. Elias, D. A.; Senko, J. M.; Krumholz, L. R., A procedure for quantitation of total oxidized uranium for bioremediation studies. *Journal of Microbiological Methods* **2003,** 53, (3), 343-353.
67. Wehrli, B.; Sulzberger, B.; Stumm, W., Redox processes catalyzed by hydrous oxide surfaces. *Chemical Geology* **1989,** 78, (3-4), 167-179.
68. Boyanov, M. I.; O'Loughlin, E. J.; Roden, E. E.; Fein, J. B.; Kemner, K. M., Adsorption of Fe(II) and U(VI) to carboxyl-functionalized microspheres: The influence of speciation on uranyl reduction studied by titration and XAFS. *Geochimica et Cosmochimica Acta* **2007,** 71, (8), 1898-1912.
69. Fredrickson, J. K.; Zachara, J. M.; Kennedy, D. W.; Duff, M. C.; Gorby, Y. A.; Li, S.-m. W.; Krupka, K. M., Reduction of U(VI) in goethite ([alpha]-FeOOH) suspensions by a dissimilatory metal-reducing bacterium. *Geochimica et Cosmochimica Acta* **2000,** 64, (18), 3085-3098.
70. Jenne, E. A., Trace element sorption by sediments and soils—Sites and processes. In *Molybdenum in the Environment* K.K., C. W. R. a. P., Ed. Marcel Dekker Inc.: New York, 1977; pp 425-553.
71. Bruno, J.; De Pablo, J.; Duro, L.; Figuerola, E., Experimental study and modeling of the U(VI)-Fe(OH)3 surface precipitation/coprecipitation equilibria. *Geochimica et Cosmochimica Acta* **1995,** 59, (20), 4113-4123.
72. Duff, M. C.; Coughlin, J. U.; Hunter, D. B., Uranium co-precipitation with iron oxide minerals. *Geochimica et Cosmochimica Acta* **2002,** 66, (20), 3533-3547.

73. US, E. P. A., Technology Screening Guide for Radioactively Contaminated Sites In 1996; Vol. EPA/402-R-96-017.
74. Langmuir, D., Uranium solution-mineral equilibria at low temperatures with applications to sedimentary ore deposits. *Geochimica et Cosmochimica Acta* **1978,** 42, (6, Part 1), 547-569.
75. Gorby, Y. A.; Lovley, D. R., Enzymatic Uranium Precipitation. *Environmental Science & Technology* **1992,** 26, (1), 205-207.
76. Lovley, D. R.; Phillips, E. J. P.; Gorby, Y. A.; Landa, E. R., Microbial Reduction of Uranium. *Nature* **1991,** 350, (6317), 413-416.
77. Pedersen, H. D.; Postma, D.; Jakobsen, R.; Larsen, O., Fast transformation of iron oxyhydroxides by the catalytic action of aqueous Fe(II). *Geochimica Et Cosmochimica Acta* **2005,** 69, (16), 3967-3977.
78. Weidler, P. G.; Stanjek, H., The effect of dry heating of synthetic 2-line and 6-line ferrihydrite: II. Surface area, porosity and fractal dimension. *Clay Minerals* **1998,** 33, (2), 277-284.
79. Burleson, D. J.; Penn, R. L., Two-Step Growth of Goethite from Ferrihydrite. *Langmuir* **2005,** 22, (1), 402-409.
80. Kukkadapu, R. K.; Zachara, J. M.; Fredrickson, J. K.; Smith, S. C.; Dohnalkova, A. C.; Russell, C. K., Transformation of 2-line ferrihydrite to 6-line ferrihydrite under oxic and anoxic conditions. *American Mineralogist* **2003,** 88, (11-12), 1903-1914.
81. Smith, S. C.; Douglas, M.; Moore, D. A.; Kukkadapu, R. K.; Arey, B. W., Uranium Extraction From Laboratory-Synthesized, Uranium-Doped Hydrous Ferric Oxides. *Environmental Science & Technology* **2009,** 43, (7), 2341-2347.
82. Ikeda, A.; Hennig, C.; Tsushima, S.; Takao, K.; Ikeda, Y.; Scheinost, A. C.; Bernhard, G., Comparative study of uranyl(VI) and -(V) carbonato complexes in an aqueous solution. *Inorganic Chemistry* **2007,** 46, (10), 4212-4219.
83. Burns, P. C.; Ewing, R. C.; Hawthorne, F. C., The crystal chemistry of hexavalent uranium: Polyhedron geometries, bond-valence parameters, and polymerization of polyhedra. *Canadian Mineralogist* **1997,** 35, 1551-1570.
84. Burns, P. C.; Finch, R. J., Wyartite: Crystallographic evidence for the first pentavalent-uranium mineral. *American Mineralogist* **1999,** 84, (9), 1456-1460.
85. Ilton, E. S.; Haiduc, A.; Cahill, C. L.; Felmy, A. R., Mica surfaces stabilize pentavalent uranium. *Inorganic Chemistry* **2005,** 44, (9), 2986-2988.
86. Grenthe, I.; Fuger, J.; Konings, R. J. M.; Lemire, R. J.; Muller, A. B.; Nguyen-Trung, C.; Wanner, H., *Chemical Thermodynamics of Uranium*. OECD: 1992.
87. Heal, H. G., Some Observations on the Electrochemisty of Uranium. *Transactions of the Faraday Society* **1949,** 45, (1), 1-11.
88. Ekstrom, A., Kinetics and Mechanism of Disproportionation of Uranium(V). *Inorganic Chemistry* **1974,** 13, (9), 2237-2241.
89. Graves, C. R.; Kiplinger, J. L., Pentavalent uranium chemistry-synthetic pursuit of a rare oxidation state. *Chemical Communications* **2009**, (26), 3831-3853.
90. Morris, D. E., Redox Energetics and Kinetics of Uranyl Coordination Complexes in Aqueous Solution. *Inorganic Chemistry* **2002,** 41, (13), 3542-3547.
91. Steele, H.; Taylor, R. J., A Theoretical Study of the Inner-Sphere Disproportionation Reaction Mechanism of the Pentavalent Actinyl Ions. *Inorganic Chemistry* **2007,** 46, (16), 6311-6318.
92. Wander, M. C. F.; Kerisit, S.; Rosso, K. M.; Schoonen, M. A. A., Kinetics of triscarbonato uranyl reduction by aqueous ferrous iron: A theoretical study. *Journal of Physical Chemistry A* **2006,** 110, (31), 9691-9701.
93. Weidler, P. G. Oberflächen synthetischer Eisenoxide. Technical University, münchen, 1995.

94. Stanjek, H.; Weidler, P. G., The Effect of Dry Heating on the Chemistry, Surface-Area, and Oxalate Solubility of Synthetic 2-Line and 6-Line Ferrihydrites. *Clay Minerals* **1992,** 27, (4), 397-412.
95. Mason, C. F. V.; Turney, W. R. J. R.; Thomson, B. M.; Lu, N.; Longmire, P. A.; Chisholm-Brause, C. J., Carbonate Leaching of Uranium from Contaminated Soils. *Environmental Science & Technology* **1997,** 31, (10), 2707-2711.
96. Cohen, D., Preparation and Spectrum of Uranium(V) Ions in Aqueous Solutions. *Journal of Inorganic & Nuclear Chemistry* **1970,** 32, (11), 3525-&.
97. Mizuguchi, K.; Park, Y. Y.; Tomiyasu, H.; Ikeda, Y., Electrochemical and Spectroelectrochemical Studies on Uranyl Carbonato and Aqua Complexes. *Journal of Nuclear Science and Technology* **1993,** 30, (6), 542-548.
98. Arland, S., Solution Chemistry and Kinetics of Ionic Reaction. In *The Chemistry of the Actinide Elements*, Katz, J. J.; Seaborg, G. T.; Morss, L. R., Eds. Chapman and Hall: London, 1986; pp 1480-1546.
99. Fiedor, J. N.; Bostick, W. D.; Jarabek, R. J.; Farrell, J., Understanding the Mechanism of Uranium Removal from Groundwater by Zero-Valent Iron Using X-ray Photoelectron Spectroscopy. *Environmental Science & Technology* **1998,** 32, (10), 1466-1473.
100. Guilbert, S.; Guittet, M. J.; Barré, N.; Gautier-Soyer, M.; Trocellier, P.; Gosset, D.; Andriambololona, Z., Dissolution of UO2 in Boom clay water in oxidizing conditions: an XPS study. *Journal of Nuclear Materials* **2000,** 282, (1), 75-82.
101. Allen, G. C.; Crofts, J. A.; Curtis, M. T.; Tucker, P. M.; Chadwick, D.; Hampson, P. J., X-Ray Photoelectron-Spectroscopy of Some Uranium Oxide Phases. *Journal of the Chemical Society-Dalton Transactions* **1974**, (12), 1296-1301.
102. Allen, G. C.; Holmes, N. R., Mixed-Valency Behavior in Some Uranium-Oxides Studies by X-Ray Photoelectron-Spectroscopy. *Canadian Journal of Applied Spectroscopy* **1993,** 38, (5), 124-130.
103. Ilton, E. S.; Haiduc, A.; Moses, C. O.; Heald, S. M.; Elbert, D. C.; Veblen, D. R., Heterogeneous reduction of uranyl by micas: Crystal chemical and solution controls. *Geochimica et Cosmochimica Acta* **2004,** 68, (11), 2417-2435.
104. Van den Berghe, S.; Miserque, F.; Gouder, T.; Gaudreau, B.; Verwerft, M., X-ray photoelectron spectroscopy on uranium oxides: a comparison between bulk and thin layers. *Journal of Nuclear Materials* **2001,** 294, (1-2), 168-174.
105. Bera, S.; Sali, S. K.; Sampath, S.; Narasimhan, S. V.; Venugopal, V., Oxidation state of uranium: an XPS study of alkali and alkaline earth uranates. *Journal of Nuclear Materials* **1998,** 255, (1), 26-33.
106. Paul, K. W.; Kubicki, J. D.; Sparks, D. L., Quantum Chemical Calculations of Sulfate Adsorption at the Al- and Fe-(Hydr)oxide-H2O Interface-Estimation of Gibbs Free Energies. *Environ. Sci. Technol.* **2006,** 40, (24), 7717-7724.
107. Frisch, M. J. e. a., *Gaussian 03*. Gaussian, Inc.: Pittsburgh, 2004.
108. Lee, C. T.; Yang, W. T.; Parr, R. G., Development of the Colle-Salvetti Correlation-Energy Formula into a Functional of the Electron-Density. *Physical Review B* **1988,** 37, (2), 785-789.
109. Becke, A. D., Density-Functional Thermochemistry .3. the Role of Exact Exchange. *Journal of Chemical Physics* **1993,** 98, (7), 5648-5652.
110. Jang, J.-H.; Dempsey, B. A.; Burgos, W. D., Solubility of Hematite Revisited: Effects of Hydration. *Environmental Science & Technology* **2007,** 41, (21), 7303-7308.
111. Davis, J. A.; Leckie, J. O., Surface Ionization and Complexation at Oxide-Water Interface .2. Surface Properties of Amorphous Iron Oxyhydroxide and Adsorption of Metal-Ions. *Journal of Colloid and Interface Science* **1978,** 67, (1), 90-107.

112. Smedley, P. L.; Kinniburgh, D. G., A review of the source, behaviour and distribution of arsenic in natural waters. *Applied Geochemistry* **2002,** 17, (5), 517-568.
113. Renshaw, C. E.; Bostick, B. C.; Feng, X. H.; Wong, C. K.; Winston, E. S.; Karimi, R.; Folt, C. L.; Chen, C. Y., Impact of land disturbance on the fate of arsenical pesticides. *Journal of Environmental Quality* **2006,** 35, (1), 61-67.
114. Smith, A. H.; Goycolea, M.; Haque, R.; Biggs, M. L., Marked increase in bladder and lung cancer mortality in a region of Northern Chile due to arsenic in drinking water. *American Journal of Epidemiology* **1998,** 147, (7), 660-669.
115. Inskeep, W. P.; McDermott, T. R.; Fendorf, S., Arsenic(V)/(III) cycling in soils and natural waters:Chemical and microbiological processes. In *Environmental chemistry of arsenic*, Frankenberger, W. T., Ed. Marcel Dekker: New York, 2002; pp 183-215.
116. Deuel, L. E.; Swoboda, A. R., Arsenic Solubility in a Reduced Environment. *Soil Science Society of America Proceedings* **1972,** 36, (2), 276-&.
117. Brannon, J. M.; Patrick, W. H., Fixation, Transformation, and Mobilization of Arsenic in Sediments. *Environmental Science & Technology* **1987,** 21, (5), 450-459.
118. Masscheleyn, P. H.; Delaune, R. D.; Patrick, W. H., Effect of Redox Potential and Ph on Arsenic Speciation and Solubility in a Contaminated Soil. *Environmental Science & Technology* **1991,** 25, (8), 1414-1419.
119. Raven, K. P.; Jain, A.; Loeppert, R. H., Arsenite and arsenate adsorption on ferrihydrite: Kinetics, equilibrium, and adsorption envelopes. *Environmental Science & Technology* **1998,** 32, (3), 344-349.
120. Korte, N. E.; Fernando, Q., A Review of Arsenic(Iii) in Groundwater. *Critical Reviews in Environmental Control* **1991,** 21, (1), 1-39.
121. Livesey, N. T.; Huang, P. M., Adsorption of Arsenate by Soils and Its Relation to Selected Chemical-Properties and Anions. *Soil Science* **1981,** 131, (2), 88-94.
122. Pierce, M. L.; Moore, C. B., Adsorption of Arsenite and Arsenate on Amorphous Iron Hydroxide. *Water Research* **1982,** 16, (7), 1247-1253.
123. Hsia, T. H.; Lo, S. L.; Lin, C. F., As(V) adsorption on amorphous iron oxide: Triple layer modelling. *Chemosphere* **1992,** 25, (12), 1825-1837.
124. Fuller, C. C.; Davis, J. A.; Waychunas, G. A., Surface-Chemistry of Ferrihydrite .2. Kinetics of Arsenate Adsorption and Coprecipitation. *Geochimica Et Cosmochimica Acta* **1993,** 57, (10), 2271-2282.
125. Jain, A.; Raven, K. P.; Loeppert, R. H., Arsenite and arsenate adsorption on ferrihydrite: Surface charge reduction and net OH- release stoichiometry. *Environmental Science & Technology* **1999,** 33, (8), 1179-1184.
126. Mok, W. M.; Wai, C. M., Distribution and Mobilization of Arsenic Species in the Creeks around the Blackbird Mining District, Idaho. *Water Research* **1989,** 23, (1), 7-13.
127. Manaka, M., Amount of amorphous materials in relationship to arsenic, antimony, and bismuth concentrations in a brown forest soil. *Geoderma* **2006,** 136, (1-2), 75-86.
128. Bowell, R. J., Sorption of arsenic by iron oxides and oxyhydroxides in soils. *Applied Geochemistry* **1994,** 9, (3), 279-286.
129. Balistrieri, L. S.; Murray, J. W.; Paul, B., The Geochemical Cycling of Trace-Elements in a Biogenic Meromictic Lake. *Geochimica Et Cosmochimica Acta* **1994,** 58, (19), 3993-4008.
130. Langner, H. W.; Inskeep, W. P., Microbial reduction of arsenate in the presence of ferrihydrite. *Environmental Science & Technology* **2000,** 34, (15), 3131-3136.

VITA

YUAN-LIANG (DANIEL) TAI

EDUCATION

Ph.D., Environmental Engineering, 2009
The Pennsylvania State University, University Park, U.S.A.
"Kinetic and Mechanistic Study of the Abiotic Oxidation of Fe(II) Catalyzed at the Ferric (Oxyhydr)oxide and Solution Interface"
M.S., Environmental Engineering, 1991
The Pennsylvania State University, University Park, U.S.A.
"Physical and Chemical Characterization of Street Dust and Dirt from Urban Areas."
B.S., Civil Engineering, 1985
National Chiao Tung University, Hsinchu, Taiwan

PROFESSIONAL CAREER

Girder Engineering Consultant, Co. Ltd., Taipei, Taiwan (Feb. 2000 to July 2004)
Techwood Engineering Consultant, Co. Ltd., Taipei, Taiwan (March 1996 to Feb. 2000)
Champion Env. Protection Indus., Co. Ltd., Kaohsiung, Taiwan (March 1994 to March 1996)
Montgomery Watson, Havens and Emerson Division, New Jersey, U.S.A. (May 1991 to Feb. 1994)
Army of the Republic of China (July 1985to May 1987)

PROFESSIONAL LICENSE

Engineer-in-Training, Pennsylvania
Registered Air Pollution Control Engineer, Taiwan
Registered Solid Waste Management Engineer, Taiwan
Registered Quality Control and Assurance Engineer, Taiwan

PUBLICATIONS AND PRESENTATIONS

Tai, Y.-L. and Dempsey, B. A. (2009) Nitrite reduction with hydrous ferric oxide and Fe(II): Stoichiometry, rate, and mechanism. *Water Research* 43(2), 546-552

Dempsey, B. A., **Tai, Y. L.**, and Harrison, S. G. (1993) Mobilization and removal of contaminants associated with urban dust and dirt. *Water Science and Technology* 28(3-5), 225-230.

Tai, Y.L. and Dempsey, B.A., Fe(II)/HFO reactions with O_2, nitrite, and uranyl at pH 6.8. American Chemical Society National Meeting, Salt Lake City, UT, March 22-26, 2009

Tai, Y.L. and **Dempsey, B.A.**, Mechanistic Study of the Heterogeneous Oxidation of Fe(II) by Nitrite. Geological Society of American Annual Meeting and Exposition, Philadelphia, PA, October 22–25, 2006